PHARMACOLOGICAL APPROACH FOR INHIBITION OF NEOINTIMAL HYPERPLASIA ASSOCIATED WITH ARTERIOVENOUS HEMODIALYSIS GRAFT STENOSIS

by

Sun Hyung Kwon

A dissertation submitted to the faculty of
The University of Utah
in partial fulfillment of the requirements for the degree of

Doctor of Philosophy

Department of Pharmacology and Toxicology

The University of Utah

August 2014

The University of Utah Graduate School

STATEMENT OF DISSERTATION APPROVAL

The dissertation of **Sun Hyung Kwon**

has been approved by the following supervisory committee members:

Donald Blumenthal	, Chair	**07/09/13** Date Approved
Alfred Cheung	, Member	**07/09/13** Date Approved
Andrea Bild	, Member	**07/09/13** Date Approved
Philip Moos	, Member	**07/09/13** Date Approved
Yan-Ting Shiu	, Member	**07/09/13** Date Approved

and by **William Crowley** , Chair/Dean of

the Department/College/School of **Pharmacology and Toxicology**

and by David B. Kieda, Dean of The Graduate School.

ABSTRACT

Venous neointimal hyperplasia (NH) leading to stenosis, thrombosis, and failure of hemodialysis arteriovenous grafts (AVG) is an important clinical problem that has no effective treatment for prevention. Many factors contribute to venous NH development; however, the underlying mechanisms are incompletely understood.

The objectives are: i) to evaluate the effects of sunitinib on suppressing NH-promoting events in vivo, and on attenuating venous NH formation in an ex vivo perfused culture system; ii) to investigate the genomic responses underlying the pathophysiology of venous NH in a porcine AVG stenosis model; iii) to assess the genomic responses of porcine venous endothelial cells exposed to physiological or pathophysiological hemodynamic shear stress.

In a porcine AVG model, elevated expression of platelet-derived growth factor (PDGF), vascular endothelial growth factor (VEGF), and their cognate receptors was seen at the venous anastomosis within 2 weeks after AVG placement. Sunitinib exhibited antiproliferative and antimigratory properties against vascular smooth muscle cells and endothelial cells (EC), which was supported by changes in the phosphorylation state or expression of the signaling proteins involved. Sunitinib also significantly attenuated the formation of venous NH in vein segments exposed to nonphysiological flow in an ex vivo culture model.

We investigated the genomic changes underlying the NH-prone and NH-resistant vein regions in a porcine AVG stenosis model to identify potential therapeutic targets to inhibit NH. Using microarray, gene expression changes in these two distinct regions were examined 5 and 14 days following graft placement. In the NH-prone region, genes related to regulation of cell proliferation were most enriched among the significantly up-regulated genes at day 5, while up-regulated genes associated with osteo/chondrogenic vascular remodeling were most enriched at day 14. At both time periods, genes related to muscle phenotype were significantly down-regulated.

Lastly, shear stress-responsive genes in porcine venous ECs exposed to physiologically low or pathologically high shear stress for a prolonged period were studied. We found that shear stress can induce a variety of cellular processes in ECs which may contribute to venous NH development.

Our findings demonstrate the utility of an ex vivo perfused vein model to investigate NH-preventive pharmacotherapies, such as sunitinib. Our gene expression studies also provide insight into improved understanding of the molecular mechanisms that may be implicated in the development of venous NH.

TABLE OF CONTENTS

LIST OF FIGURES

LIST OF TABLES

ACKNOWLEDGEMENTS

First and foremost, I would like to express my sincere gratefulness to my advisors and mentors, Dr. Donald Blumenthal and Dr. Alfred Cheung, for their invaluable guidance, motivation, and support throughout my graduate studies. Emphatic thanks to my dissertation committee members, Dr. Yan-Ting Shiu, Dr. Andrea Bild, and Dr. Philip Moos, for supporting my research and providing insightful advice. Special thanks go to Dr. Li Li and Dr. Christi Terry who have helped me develop my interests in the field of vascular biology and who have made this dissertation possible. Dr. Li Li's work contributed to Figures 2.1 through 2.5 in Chapter 2. I would also like to thank Mr. Brett Milash for providing technical assistance and scientific ideas on the microarray projects.

Thanks to all of my colleagues in the Cheung research group (Huan, Yuxia, Ilya, Will, Dan, and Mary). It has been an honor and great pleasure working with a wonderful team of animal surgeons, a molecular biologist, a pharmaceutical scientist, and a bioengineer. I would also like to thank my fellow graduate students in the Department of Pharmacology and Toxicology for sharing research ideas and experience that helped my research move forward.

I sincerely thank Pastor Han and other members of the Korean Presbyterian Church of Utah. My wholehearted thanks go to my family and our beautiful daughter, Sarah, whose love and support led me to this day.

CHAPTER 1

NEOINTIMAL HYPERPLASIA ASSOCIATED WITH HEMODIALYSIS ARTERIOVENOUS GRAFT STENOSIS

1.1 Overview of Hemodialysis Vascular Access Modalities

1.1.1 The three principal forms of hemodialysis vascular access

As the prevalent end-stage renal disease (ESRD) population continues to show linear growth, the hemodialysis population also rapidly increases every year in the United States, with the number of patients requiring hemodialysis reaching nearly 384,000 at the end of 2010 (1). For these patients, hemodialysis is the major mode of renal replacement therapy before kidney transplantation is available. When initiating chronic hemodialysis, successful creation of a well-functioning vascular access is first required prior to treatment initiation. Currently, there are three principal forms of hemodialysis vascular access; the native arteriovenous fistula (AVF), the synthetic arteriovenous graft (AVG), and the central venous catheter (also called central venous line), each of which possesses its own merits and drawbacks as a vascular access. Selection and placement of an appropriate vascular access should be individualized and advance planning is essential because permanent vascular accesses can take weeks to months to establish. Vascular accesses are also prone to dysfunction and failure, leading to morbidity and hospitalization of hemodialysis patients. More than 20% of all hospitalizations in the hemodialysis population and up

to 50% of the first year hemodialysis costs are associated with vascular access complications (2).

Central venous catheters, most often placed in the neck or chest, are primarily used as a temporary vascular access when the kidney disease is quickly progressed and the time to achieve a more permanent vascular access (i.e., AVG or AVF) is insufficient. In 2010 in the United States, over 80% of incident hemodialysis patients with no pre-ESRD nephrologist care initiated hemodialysis treatment with venous catheters alone as their vascular access, while 18% started treatment with catheters together with either maturing or functional AVF or AVG. Among patients who have had pre-ESRD nephrologist care for more than 12 months before hemodialysis initiation, the percentage of catheter use alone dropped to 41% and nearly 60% of patients had maturing or functional AVF or AVG (1). While venous catheters could be used long-term in some patients with difficult to develop functional AVF or AVG, they are highly prone to infection and other complications, such as narrowing of the veins in which they are placed, and therefore are not a suitable permanent vascular access for the majority of patients (3).

Hemodialysis AVG and AVF are created by surgically connecting the artery and the vein, most frequently in the forearm, and the blood flows directly from the artery into the vein. Shunting of the arterial circulation thus provides adequate extracorporeal blood flow rates for effective dialysis, and once functional, these conduits can be used for long-term treatment. While AVG uses synthetic or biological materials as a graft, AVF provides direct connection between the native artery and the vein allowing the vein itself to mature into a thickened and dilated vessel suitable for repeated dialysis. Once established, AVF is universally recognized as the preferred choice of permanent vascular access because it has the least long-term complications and greatest

functional longevity, as compared to AVG or venous catheters (4). In order to maximize the use of AVF, National Kidney Foundation Dialysis Outcome Quality Initiative (DOQI) Clinical Practice Guidelines now strongly recommend that options for AVF placement be considered first in incident hemodialysis patients with adequate vascular anatomy, followed by prosthetic AVG if AVF placement is not possible (4). These guidelines also indicate that venous catheters should be avoided for hemodialysis and be used only if other vascular access options are not available (4). In accordance with these guidelines, the prevalence of AVG has steadily decreased in the United States in the last decade, while cases of AVF placement have increased significantly, with the national AVF placement rate exceeding 60% in prevalent hemodialysis patients as of April, 2012 (5, 6).

After creation, however, an AVF typically requires several months to mature into a sustainable vascular access, and a substantial proportion of AVF fail to properly develop within the expected time frame. Inadequate maturation, early thrombosis, and failure of first and subsequent cannulations all lead to unfunctional primary AVF failure (7). The primary failure rate of AVF reported in the current literature varies from 20% and up to 60%, depending on the study design and fistula patient population examined by each study (8-11). Early AVF failures may result in multiple attempts to construct a functional AVF, often leading to undesirable consequences such as exhaustion of vascular sites, patient intolerance, and the necessity of using a temporary venous catheter for a prolonged period. AVF are also subject to secondary failure in which failure occurs after the AVF has met dialysis suitability, and consequently, the conduit is permanently abandoned (12). Efforts to resolve such obstacles associated with AVF maturation and to improve AVF

functional longevity have been the subject of intensive research in recent years.

1.1.2 AVG is still an important vascular access modality

The alternative permanent vascular access modality to AVF is connecting the artery and the vein via a prosthetic AVG. Selection of a synthetic or biological graft material may take technical suitability, vascular surgeon's experience, and cost into consideration (4). A fluorocarbon polymer polytetrafluoroethylene (PTFE) and its derivative, expanded PTFE (ePTFE), have been the prosthetic graft materials of choice, but other synthetic and biological materials such as polyurethane or bovine heterografts are also currently available with similar reported outcomes (4). Although AVG is now only preferably indicated for patients with failed AVF, for patients lacking suitable vessels to construct AVF, and for pediatric patients who have difficulty tolerating multiple venipuncture associated with AVF (13). However, AVG has several advantages over AVF in terms of reliably providing high blood flow rates and large surface area for cannulation, and the capacity to be used shortly after implantation (10). Hence, AVG is continuously being used in a significant number of hemodialysis patients. Unfortunately, the major drawback of AVG and the predominant reason for its acknowledged inferiority to AVF is that AVG is prone to developing stenosis, the abnormal narrowing of the blood vessel, followed by thrombosis and eventual occlusion of the conduit. This pathophysiology leads to the poor primary patency rate of AVG: approximately 50% and 25% at 1 and 2 years after placement, respectively (11, 14-16). AVG are also susceptible to technical failure that usually occurs within the first 30 days of placement, which are associated with inadequate graft configurations, poor surgical performance, and pre-existing patient

comorbidities (4).

Nevertheless, currently AVG in hemodialysis patients is an indispensable access method, serving as one of the two available permanent vascular access modalities. Those unique merits of AVG over AVF have attracted researchers to study the mechanisms of AVG failure caused by stenosis and investigations into means of intervention to prevent stenosis. Currently, AVG stenosis and associated thrombosis are treated with routine radiologic and surgical procedures to restore graft patency. Angioplasty and stent placement are performed on stenosed and clotted grafts in conjunction with pharmacomechanical thrombolytic measures. When such interventions fail, surgical revision and thrombectomy of the graft is done to eliminate lesions before the placement of a new graft at a new anatomical location (17-19). Radiologic and surgical approaches, however, often cause injury to the native vessels, which predispose grafts to restenosis, and are inefficient in treating recurrent stenosis as new lesions can rapidly emerge over time (10, 17). Instead, attempts to pharmacologically prevent and/or treat AVG stenosis have become the most promising realm of investigation. Pharmacological approaches, however, require intensive and extensive research into the pathophysiology as thorough understanding of the underlying mechanisms resulting in AVG stenosis must precede selection of potentially effective therapeutic agent(s) to attenuate cellular and molecular events associated with the pathogenesis. In this chapter, the pathophysiology associated with the ePTFE grafts is reviewed specifically, although AVG stenosis using other graft materials may display similar pathophysiology to ePTFE grafts (4).

1.2 Pathophysiology of AVG Stenosis

1.2.1 Histological and biochemical properties of stenotic lesions

The blood vessel wall consists of three distinct compartments: the (tunica) intima, the media, and the adventitia. AVG stenosis most frequently develops around the graft-venous anastomosis (hereafter referred to as the venous anastomosis) and adjacent vein regions, between the graft and the outflow vein, and less frequently at the graft-arterial anastomosis (arterial anastomosis). Aggressive neointimal hyperplasia (NH), defined as the abnormal growth and thickening of the neointima (inner-most layer of the blood vessel wall), is known as the most important cause of the majority of stenosis and thrombosis associated with AVG (10, 15, 16, 20, 21). Roy-Chaudhury et al. demonstrated that histological and biochemical evaluation of human AVG stenotic tissues obtained from the venous anastomosis during an AVG surgical revision displayed hyperplastic lesions comprised of smooth muscle alpha-actin-staining cells, most likely smooth muscle cells (SMC) and/or myofibroblasts (adventitial fibroblasts that have transformed into an active contractile phenotype) derived from the media and/or the adventitia, and excessively deposited extracellular matrix (ECM) components (22). In addition, active macrophages and other cells of the immune system like T-cells were recruited to the synthetic graft material, and neo-microvascularization (angiogenesis) within the neointima and adventitia was observed (22). In these human specimens, various growth factors, including platelet-derived growth factor (PDGF), vascular endothelial growth factor (VEGF), and basic fibroblast growth factor (bFGF), were also overly expressed (22), suggesting that such growth factor-mediated stimulation of cellular proliferation, migration and ECM protein accumulation may play pivotal roles in the formation of

the NH lesions. Various pathogenic factors that may contribute to the pathophysiology of AVG stenosis and NH development are discussed further in section **1.3**.

1.2.2 Large animal models to study AVG stenosis

Due to the limitations of utilizing human specimens to study AVG stenosis pathophysiology, large animal AVG models (e.g., swine and canine) that can recapitulate the pathophysiology of AVG stenosis and subsequent graft failure in humans have been developed previously. In particular, swine have long been considered an excellent biomedical model to study a variety of human diseases due to their similarity in size, physiology, organ development, and disease progression to humans. In addition, the cardiovascular anatomy of swine is analogous to humans; therefore, swine have been used popularly in vascular research (23, 24). One of the first pig models of AVG stenosis described in the literature was by Rotmans et al., in which an ePTFE graft was placed between the common carotid artery and the internal jugular vein bilaterally in the neck of Landrace pigs (24). Kelly et al. also reported a similar pig AVG stenosis model in which the graft was placed between the femoral artery and the femoral vein (20). In these studies, the pig models rapidly developed thick NH lesions predominantly in the venous outflow tracts of AVG within a few weeks after the graft placement, and only minimal NH was observed at the arterial anastomoses. Consequently, the graft blood flow rate dramatically decreased in the patent grafts, eventually resulting in thrombotic AVG failure (20, 24). The histogenesis of porcine NH lesions was characterized by most of the key features described above by Roy-Chaudhury et al. in human AVG NH specimens, thus closely resembling the pathophysiology of human AVG stenosis (22).

These pig models of AVG stenosis and thrombosis have been widely adopted by us and others since then, especially for pharmacological and toxicological studies of potential antihyperplastic drugs and delivery of such drugs, although the detailed surgical methods to implant the graft may have varied from the original studies. In addition to pigs, dogs have also provided good experimental models for studying the pathophysiology of AVG stenosis. McLennan et al. and Masaki et al. reported the use of a canine AVG model in which the NH lesions formed at the arterial and venous anastomoses resembled the hyperplastic lesions in humans (25, 26). Despite the benefits of using whole animals, however, generation of a controlled pathologic environment and elucidation of its effects on NH development is often difficult to achieve in animal models due to the complexity of in vivo systems. Hence, such in vivo studies may be complemented by utilizing in vitro and ex vivo models described below in section **1.2.3**.

1.2.3 In vitro and ex vivo model systems to study AVG stenosis

Because using animal models to study the pathophysiology of AVG stenosis and NH development are relatively costly and time-consuming, isolated in vitro cell cultures and ex vivo organ culture models of explanted blood vessels have been widely adopted. Monolayer and/or co-cultured vascular SMCs and endothelial cells (EC) have provided convenient tools to study the cellular characteristics under a controlled pathologic environment, as well as to rapidly assess responses to potentially effective therapies. Organ culture models are excellent experimental systems with a major advantage of using intact vessels, thus maintaining the native vessel wall architecture and intercellular and cell-matrix interactions (27, 28). Many studies have reported the

induction of neointima formation in explanted vein segments obtained from humans and from animals by applying a variety of controlled pathologic cues, such as high serum concentration, aberrant hemodynamics, or elevated oxygen tension under either static or perfused culture conditions (27, 29-34). The behavior of cultured vein segments in response to such stimuli closely mimics the hyperplasia development underlying vein graft stenosis in vivo in that highly proliferative smooth muscle cells and/or myofibroblasts directed towards the intima primarily constitute the hyperplastic lesions (31, 33). With our current knowledge, it is not clear how each pathologic stimulus induces a hyperplasia-prone state ex vivo, or whether the kinetics of NH development is similar to in vivo situations. In any case, ex vivo organ culture models serve as a valuable experimental system for investigation into the etiology and amelioration of NH associated with AVG stenosis.

1.3 The Pathogenic Contributors of Venous NH Development

1.3.1 Differential NH susceptibility between the arterial and the venous anastomoses

Anatomically, NH predominantly forms in the susceptible “shoulder” and the “cushion” regions of the venous anastomosis in human specimens obtained from failed ePTFE AVG and in a porcine model of AVG stenosis (10). To date, the etiology of NH development selectively at the venous anastomosis is not clearly understood, although numerous studies postulate that multiple pathogenic factors specific to the venous anastomosis may contribute to the venous NH formation. During AVG placement surgeries, damage to the protective adventitia and endothelium in the

native vessels occurs. Normally, an intact endothelial layer lining the lumen produces nitric oxide (NO) and prostacyclins that inhibit aggregation and adhesion of platelets to the vessel wall (35). Injury to the adventitia can also be detrimental as damaged vasa vasorum in the adventitia can lead to tissue hypoxia and trigger downstream events leading to increased inflammation, cellular proliferation, and migration (36, 37). However, surgical trauma and subsequent wound healing activities upon graft placement are experienced by both the artery and the vein. In addition, local inflammatory responses caused by the presence of foreign graft material (bio-incompatibility) may be another common pathogenic feature in both vascular types (15, 20, 22).

It is conceivable, however, that cells of the artery and the vein may possess inherent differences in terms of responding differentially to such pathogenic stimuli, contributing at least partially to the differential susceptibility to NH formation. In support of this, Li et al. demonstrated that arterial and venous SMCs display distinct proliferation profiles in response to each of the three PDGF isoforms, one of the key SMC mitogens abundantly expressed in NH lesions (38-40). This study also noted that the expression of certain PDGF receptors during quiescence was different between the arterial and venous SMCs. Li et al. also demonstrated the differential sensitivity of the arterial and venous SMCs to a PDGF receptor-inhibitor, imatinib, in that the venous SMCs were more sensitive to the drug's effects (41).

Moreover, the venous anastomosis harbors pathogenic factors less frequently observed at the arterial anastomosis. Upon graft placement, the arterial circulation is shunted into the venous system, abruptly exposing the vein to arterial-level high blood flow rates and blood pressure. Following this, the compliance mismatch between the stiff graft material and the native vein

causes the vein to stretch and dilate (10, 42, 43). This dramatic change in the vessel geometry generates a variety of mechanical stresses at the venous anastomosis: abnormally high and/or low fluid wall shear stress (WSS), increased circumferential wall stress, and disturbed and/or turbulent flow patterns (44-47). The correlation between such aberrant hemodynamic forces and venous remodeling has been reported in the literature. Gusic et al. showed that unphysiologically low WSS applied to explanted porcine vein segments induced hyperplasia formation in a perfused organ culture system (31). Thickening of the medial layer was observed when the explanted vein segments were exposed to elevated pressure beyond its normal physiological range (31). In a study by Budu-Grajdeanu et al., localized turbulent blood flow was suggested to stimulate the SMC production of growth factors known to promote NH formation in the context of venous NH (48). High WSS can also damage and denude the venous endothelium, exposing SMCs and the connective tissue to greater hemodynamic forces and circulating coagulation factors, leading to thrombosis and pathologic reactions (44, 45).

The arterial anastomosis may also experience hemodynamic stresses as the inflow current appears to generate disturbed flow patterns at certain locations within the arterial anastomosis, but to a much lesser extent than the venous anastomosis (49). Unlike the veins, arteries by nature have much thicker elastic muscle structures and display quite different mechanical properties. Hence, the higher propensity of the venous anastomosis to develop NH is likely, at least in part, due to the greater hemodynamic and geometric changes seen at the venous anastomosis, compared to the arterial anastomosis. In an in vivo system like the porcine AVG stenosis model, examining the individual contributions of each pathogenic factor separately to NH

formation is difficult; therefore, a simpler model system is needed to characterize the key factors that render differential NH susceptibility between the arterial and venous anastomoses.

1.3.2 Cellular and molecular mechanisms underlying NH formation

Our current knowledge of the cellular and molecular mechanisms by which venous NH initiates and expands is far from complete. The NH lesions are highly cellularized with abnormally deposited ECM proteins and neo-microvessels that progress over time. Hence, pathogenic factors discussed in the above section **1.3.1** are thought to trigger a cascade of cellular and molecular events leading to the production and release of mediators that stimulate proliferation, migration, neo-microvascularization, inflammatory responses, and ECM remodeling. At the molecular level, the specific mechanisms provoking these events have not been investigated extensively, although a few studies have used genomic and proteomic approaches to provide an indication of the genes, proteins, and cellular signaling pathways uniquely modulated in NH lesions (50-52). In fact, NH can develop not only in the context of AVG stenosis but also in many arterial diseases (e.g., atherosclerosis, arterial balloon injury) and in other vein graft conduits, and the cellular compositions of arterial and venous NH do not appear to be significantly different from each other. The mechanisms of NH development have been more extensively studied in arterial NH; therefore, it is reasonable to review what is known from studies of arterial NH. A pathogenic cue, such as an injury, inflammation, and other forms of stress associated with arterial diseases, activates the adhering platelets and the vessel wall to secrete PDGF and other cytokines that stimulate arterial SMCs, ECs, and cells of the immune system. SMCs, in response, are stimulated to undergo

phenotypic transition from a quiescent contractile type to a synthetic (proliferative) type, likely involving gene expression changes that modulate the SMC phenotype (53, 54). PDGF also acts as a chemoattractant that promotes phenotypically modified SMCs to migrate into the intima (55). Activated SMCs, ECs, and immune cells recruited to the site of pathogenesis produce components of the ECM as well as enzymes that participate in ECM remodeling (53, 56, 57). These series of events are thought to promote the development of arterial NH lesion formation. It appears that venous NH development in vein grafts undergoes rather similar cellular processes to that of arterial NH, although initial pathogenic cues may be different from that of arterial diseases.

1.3.3 Investigation of global events underlying NH development

Identification of cellular pathways, or even more specifically, genes, their protein products, and other cellular components, that may be important in the early development of venous NH is expected to facilitate our understanding of the complex AVG stenosis etiology. Besides the well-accepted growth factor pathways activated by PDGF, VEGF, and other growth promoters, many studies have been conducted that hypothesized involvement of a variety of different pathways underlying NH formation. For instance, Sanders et al. showed that proinflammatory soluble epoxide hydrolases (sEH) are overly expressed in venous NH lesions in a porcine AVG model, and proposed a role for sEH in NH histogenesis (58). Jiang et al. suggested that monocyte chemoattractant protein-1 (MCP-1) and CC chemokine receptor 2 (CCR2) signaling in concert with certain physical stimulus plays a dominant role in vein graft NH development (59). It was also reported that hypoxia inducible factor-1α (HIF-1α) may increase the expression of matrix

metalloproteinases (MMP) -2 and -9 and their tissue inhibitors in myofibroblasts, thereby leading to vein graft remodeling (60, 61). These studies emphasize the potential importance of specific pathways and their components, but a global view of cellular and molecular changes associated with the venous NH pathophysiology are lacking.

In this respect, global transcription and proteomic profiling studies could provide a powerful means to explore all differentially regulated molecular events in NH. Misra et al. adopted a proteomic analysis with isotope-coded affinity tag (ICAT) to identify all differentially expressed proteins in stenotic tissues removed from a pig AVG model, and found that expression of α-fetoprotein, fetuin-A, macrophage migration inhibitory factor (MIF), pyruvate dehydrogenase E1 component, lactoferrin, and decorin were meaningfully modulated in NH lesions (51). Another study using the same techniques showed that a disintegrin and metalloproteinase thrombospondin-1 (ADAMTS-1) was significantly up-regulated in thrombosed human hemodialysis grafts (50). Currently, there are no published studies that have explored the global gene expression profiles of venous NH of AVG stenosis. However, high-throughput gene expression microarrays have been used to identify transcription profiles in arterial NH formation. For example, one study used gene expression microarrays and identified a set of genes associated with SMC and mesenchymal stromal cell proliferation and migration, inflammatory cytokines, ECM components, and muscle contraction to be significantly modulated in rat balloon-injured carotid artery neointima (62). Studies like these primarily provide preliminary data for potential biological targets and may require further investigation aimed at interfering with altered molecular events in NH.

1.4 Pharmacological Interventions to Prevent or Treat AVG Stenosis

Efforts to attenuate NH development in arterial diseases and in vein grafts using a pharmacological approach have been an active area of research. Numerous broad spectrum antihyperplastic agents have been tested using in vitro and in in vivo vascular hyperplasia models. Strategies that have been examined for efficacy include use of small molecule drugs, antisense or decoy oligonucleotides, gene transfer, and cell-based therapies (10). Among these various strategies, our laboratory has focused on the use of small molecule therapies to attenuate AVG NH formation because these drugs have delivery and manufacturing advantages over biological reagents, and are less likely to cause immunologic reactions in vivo. Moreover, a variety of technologies to locally deliver these drugs to the site of action that circumvents any problems of systemic treatment can be applied, i.e., placement of a drug-eluting stent, direct coating of the graft with drugs, or implantation of a perivascular drug depot. For example, Lee et al. reported the use of paclitaxel-coated ePTFE grafts in pig AVG models and demonstrated that paclitaxel, a drug used to treat cancers, was effective in inhibiting NH formation and improving the AVG survival (63, 64). The same drug was shown effective when used in a polymer-based sustained drug depot placed perivascularly at the anastomoses in a canine AVG model by Masaki et al. (26). Like paclitaxel that stabilizes mitotic microtubules and thus inhibits cell division, other small molecule drugs that have been explored previously act through mechanisms that suppress many of the cellular events occurring in NH lesions, such as cellular proliferation and migration, inflammation, angiogenesis, and thrombosis. Rapamycin (sirolimus) is an antiproliferative and anti-inflammatory agent clinically used to prevent rejection associated with organ transplantation (65). It has been

employed in coronary artery stents to prevent restenosis after angioplasty (66). Previously in our laboratory, we showed that administration of rapamycin-laden polymer gel was effective in reducing venous NH formation when evaluated in a porcine AVG model (67). Drugs with such mechanisms of action may indeed be promising therapeutic candidates; however, not all of the efforts have been successful. Dipyridamole is an antiplatelet agent that also inhibits SMC proliferation (68), and one clinical study suggested that daily dipyridamole administration with aspirin modestly decreased the incidence of PTFE graft occlusion in dialysis patients, although dipyridamole-mediated NH inhibition was not directly proved (69). However, a study by Kuji et al. found that local sustained delivery of dipyridamole in a porcine AVG model was ineffective in attenuating NH lesion formation (70). The in vivo efficacy of dipyridamole against AVG stenosis, as a consequence, remains to be further validated.

Another class of drugs that may have potential as antihyperplastic agents is the receptor tyrosine kinase (RTK) inhibitors. These drugs potently counter the effects of various growth factor ligands at the receptor level, resulting in suppression of the downstream events, including cellular proliferation, migration, and angiogenesis. Targeting growth factor receptors in NH have been demonstrated previously by using specific antibodies against PDGF and bFGF receptors in arterial and AVF NH models (71, 72). Many of the RTK inhibitors were originally used in the treatment of malignant tumors, but their therapeutic potentials could encompass treatment of pathological lesions such as NH that closely resemble the pathophysiology of cancers. Li et al. studied the antiproliferative properties of imatinib, a small molecule RTK inhibitor developed as an antileukemic agent, in an in vitro vascular SMC culture system (41), and Makiyama et al.

demonstrated the antihyperplastic effects of imatinib in a rat NH model of balloon injury (73). To date, there are at least twelve clinically used RTK inhibitors, including monoclonal antibodies against RTK (74), many of which target more than one type of tyrosine kinase (74, 75). In Chapter 2, we investigated a broad spectrum RTK inhibitor, sunitinib, which primarily targets all receptors of the PDGF and VEGF, for its potential as an antihyperplasia therapy (75, 76). In the clinic, sunitinib has been used to treat imatinib-resistant gastrointestinal cancers and renal stromal cell cancers. Its well-established antiproliferative and antiangiogenic properties in cancer cells might be utilized to attenuate hyperplasia development, including venous AVG NH (77-79).

Inhibitors of sEH are experimental drugs that have gained recent attention as potential antihyperplastic agents. They have been shown in animal models to exhibit antihypertensive and antivascular remodeling effects in cardiovascular diseases (80, 81), and possess potent anti-inflammatory activities by potentiating the protective properties of epoxyeicosatrienoic acids (EETs) against inflammation. Sanders et al. demonstrated the intense expression of proinflammatory sEH in venous anastomosis tissues in a porcine AVG model, and suggested the possibility of sEH inhibitors as a novel therapeutic approach against AVG stenosis.

Despite the availability of the above-listed pharmacological treatments with diverse mechanisms to potentially inhibit NH, currently there are no clinically effective therapies to prevent AVG stenosis. Yet it is not clear why such successful antihyperplastic drugs in model systems failed to exhibit efficacy in humans, but it is conceivable that our current understanding of the properties of those drugs tested as well as of the molecular mechanisms underlying NH development is incomplete. Moreover, inappropriate selection of in vitro or in vivo model systems

that may or may not properly mimic the clinical conditions of humans also cannot be ruled out. Future studies, therefore, may require advanced knowledge in these aspects in order to characterize and develop successful antihyperplasia therapies.

1.5 Summary and Objectives

Despite the technological advances, AVG vascular access dysfunction still remains an expensive, uncontrolled clinical problem for a large portion of the hemodialysis population. Our past and current efforts to better understand the complex pathophysiology associated with AVG stenosis have indeed led us to the improved knowledge of the mechanisms by which stenosis develops, thus enabling us to devise potential therapeutic strategies against the condition. Yet the problem is far from completely resolved and elucidation of the final solution awaits further laboratory and clinical studies.

The objectives of this thesis work are: i) to evaluate the pharmacological effects of a RTK inhibitor, sunitinib, on suppressing NH-promoting events in vitro, and on attenuating venous NH formation in an ex vivo perfusion system; ii) to investigate the global genomic responses underlying the pathophysiology of venous NH formation in a pig AVG stenosis model; iii) to assess the genomic responses of porcine venous endothelial cells exposed to aberrant hemodynamic stress.

1.6 References

1. United States Renal Data System, USRDS 2012 Annual Data Report: Atlas of Chronic Kidney Disease and End-Stage Renal Disease in the Unites States, National Institutes of Health, National Institute of Diabetes and Digestive and Kidney Diseases, Bethesda, MD, 2012.

2. Lok CE, Bhola C, Croxford R, Richardson RM. Reducing vascular access morbidity: comparative trial of two vascular access monitoring strategies. *Nephrol Dial Transplant* 18: 1174-1180, 2003.

3. Marr KA, Sexton DJ, Conlon PJ, Corey GR, Schwab SJ, Kirkland KB. Catheter-related bacteremia and outcome of attempted catheter salvage in patients undergoing hemodialysis. *Ann Intern Med* 127: 275-280, 1997.

4. National Kidney Foundation. KDOQI Clinical Practice Guidelines and Clinical Practice Recommendations for 2006 Updates: Hemodialysis Adequacy, Peritoneal Dialysis Adequacy and Vascular Access. *Am J Kidney Dis* 48: S1-S322 (suppl 1), 2006.

5. Lok CE. Fistula First Initiative: Advantages and Pitfalls. *Clin J Am Soc Nephrol* 2: 1043-1053, 2007.

6. Vassalotti JA, Jennings WC, Beathard GA, Neumann M, Caponi S, Fox CH, Spergel LM; Fistula First Breakthrough Initiative Community Education Committee. Fistula first breakthrough initiative: targeting catheter last in fistula first. *Semin Dial* 25: 303-310, 2012.

7. Schinstock CA, Albright RC, Williams AW, Dillon JJ, Bergstralh EJ, Jenson BM, McCarthy JT, Nath KA. Outcomes of arteriovenous fistula creation after the Fistula First Initiative. *Clin J Am Soc Nephrol* 6: 1996-2002, 2011.

8. Allon M, Robbin ML. Increasing arteriovenous fistulas in hemodialysis patients: problems and solutions. *Kidney Int* 62: 1109-1124, 2002.

9. Dember LM, Beck GJ, Allon M, Delmez JA, Dixon BS, Greenberg A, Himmelfarb J, Vazquez MA, Gassman JJ, Greene T, Radeva MK, Braden GL, Ikizler TA, Rocco MV, Davidson IJ, Kaufman JS, Meyers CM, Kusek JW, Feldman HI; Dialysis Access Consortium Study Group. Effect of clopidogrel on early failure of arteriovenous fistulasfor hemodialysis: a randomized controlled trial. *JAMA* 299: 2164-2171, 2008.

10. Li L. Terry CM, Shiu YT, Cheung AK. Neointimal hyperplasia associated with synthetic hemodialysis grafts. *Kidney Int* 74: 1247-1261, 2008.

11. Schwab SJ, Harrington JT, Singh A, Roher R, Shohaib SA, Perrone RD, Meyer K, Beasley D. Vascular access for hemodialysis. *Kidney Int* 55: 2078-2090, 1999.

12. Huijbregts HJ, Bots ML, Wittens CH, Schrama YC, Moll FL, Blankestijn PJ; CIMINO study group. Hemodialysis arteriovenous fistula patency revisited: results of a prospective, multicenter initiative. *Clin J Am Soc Nephrol* 3: 714-719, 2008.

13. Akoh JA. Prosthetic arteriovenous grafts for hemodialysis. *J Vasc Access* 10: 137-147, 2009.

14. United States Renal Data System, USRDS 2004 Annual Data Report: Atlas of Chronic Kidney Disease and End-Stage Renal Disease in the Unites States, National Institutes of Health, National Institute of Diabetes and Digestive and Kidney Diseases, Bethesda, MD, 2004.

15. Li L, Terry CM, Blumenthal DK, Kuji T, Masaki T, Kwan BC, Zhuplatov I, Leypoldt JK, Cheung AK. Cellular and morphological changes during neointimal hyperplasia development in a porcine arteriovenous graft model. *Nephrol Dial Transplant* 21: 3139-3146, 2007.

16. Roy-Chaudhury P, Kelly BS, Melhem M, Zhang J, Li J, Desai P, Munda R, Heffelfinger SC. Vascular access in hemodialysis: issues, management, and emerging concepts. *Cardiol Clin* 23: 249-273, 2005.

17. Beathard GA. Percutaneous transvenous angioplasty in the treatment of vascular access stenosis. *Kidney Int* 42: 1390-1397, 1992.

18. Miller PE, Carlton D, Deierhoi MH, Redden DT, Allon M. Natural history of arteriovenous grafts in hemodialysis patients. *Am J Kidney Dis* 36: 68-74, 2000.

19. Lilly RZ, Carlton D, Barker J, Saddekni S, Hamrick K, Oser R, Westfall AO, Allon M. Predictors of arteriovenous graft patency after radiologic intervention in hemodialysis patients. *Am J Kidney Dis* 37: 945-953, 2001.

20. Kelly BS, Heffelfinger SC, Whiting JF, Miller MA, Reaves A, Armstrong J, Narayana A, Roy-Chaudhury P. Aggressive venous neointimal hyperplasia in a pig model of arteriovenous graft stenosis. *Kidney Int* 62: 2272-2280, 2002.

21. Roy-Chaudhury P, Sukhatme VP, Cheung AK. Hemodialysis vascular access dysfunction: a cellular and molecular viewpoint. *J Am Soc Nephrol* 17: 1112-1127, 2006.

22. Roy-Chaudhury P, Kelly BS, Miller MA, Reaves A, Armstrong J, Nanayakkara N, Heffelfinger SC. Venous neointimal hyperplasia in polytetrafluoroethylene dialysis grafts. *Kidney Int* 59: 2325-2334, 2001.

23. Lunney JK. Advances in swine biomedical model genomics. *Int J Biol Sci* 3: 179-184, 2007.

24. Rotmans JI, Velema E, Verhagen HJ, Blankensteijn JD, Kastelein JJ, de Kleijn DP, Yo M, Pasterkamp G, Stroes ES. Rapid, arteriovenous graft failure due to intimal hyperplasia. *J Surg Res* 113: 161-171, 2003.

25. McLennan G, Trerotola SO, Forney M, Jellison B, Dreesen RG, Tennery J. Short-term patency and safety of an expanded polytetrafluoroethylene encapsulated endoluminal device at the venous anastomosis of a canine arteriovenous graft model. *J Vasc Interv Radiol* 12: 227-234, 2001.

26. Masaki T, Rathi R, Zentner G, Leypoldt JK, Mohammad SF, Burns GL, Li L, Zhuplatov S, Chirananthavat T, Kim SJ, Kern S, Holman J, Kim SW, Cheung AK. Inhibition of neointimal hyperplasia in vascular grafts by sustained perivascular delivery of paclitaxel. *Kidney Int* 66: 2061-2069, 2004.

27. Porter KE, Varty K, Jones L, Bell PR, London NJ. Human saphenous vein organ culture: a useful model of intimal hyperplasia? *Eur J Vasc Endovasc Surg* 11: 48-58, 1996.

28. Wilson YG, Davies AH, Southgate K, Currie IC, Sheffield E, Baird RN, Lamont PM, Angelini GD. Vein quality influences neointimal hyperplasia in an organ culture model of human saphenous vein. *Eur J Vasc Endovasc Surg* 13: 557-562, 1997.

29. Soyombo AA, Thurston VJ, Newby AC. Endothelial control of vascular smooth muscle proliferation in an organ culture of human saphenous vein. *Eur Heart J* 14 (Suppl. 1): 201-206, 1993.

30. Soyombo AA, Angelini GD, Newby AC. Neointima formation is promoted by surgical preparation and inhibited by cyclic nucleotides in human saphenous vein organ cultures. *J Thorac Cardiovasc Surg* 109: 2-12, 1995.

31. Gusic RJ, Myung R, Petko M, Gaynor JW, Gooch KJ. Shear stress and pressure modulate saphenous vein remodeling ex vivo. *J. Biomech* 38: 1760-1769, 2005.

32. Gusic RJ, Petko M, Myung R, William Gaynor J, Gooch KJ. Mechanical properties of native and ex vivo remodeled porcine saphenous veins. *J Biomech* 38: 1770-1779, 2005.

33. Joddar B, Shaffer RJ, Reen RK, Gooch KJ. Arterial pO_2 stimulates intimal hyperplasia and serum stimulates inward eutrophic remodeling in porcine saphenous veins cultured ex vivo. *Biomech Model Mechanobiol* 10: 161-175, 2011.

34. Semsroth S, Stigler RG, Bernecker OY, Ruttmann-Ulmer E, Troppmair J, Macfelda K, Bonatti JO, Laufer G. Everolimus attenuates neointimal hyperplasia in cultured human saphenous vein grafts. *Eur J Cardiothorac Surg* 35: 515-520, 2009.

35. Radomski MW, Palmer RM, Moncada S. The anti-aggregating properties of vascular endothelium: interactions between prostacyclin and nitric oxide. *Br J Pharmacol* 92: 639-646, 1987.

36. Martin JF, Booth RF, Moncada S. Arterial wall hypoxia following thrombosis of the vasa vasorum is an initial lesion in atherosclerosis. *Eur J Clin Invest* 21: 355-359, 1991.

37. Gössl M, Versari D, Lerman LO, Chade AR, Beighley PE, Erbel R, Ritman EL. Low vasa vasorum densities correlate with inflammation and subintimal thickening: potential role in location--determination of atherogenesis. *Atherosclerosis* 206: 362-368, 2009.

38. Li L, Blumenthal DK, Terry CM, He Y, Carlson ML, Cheung AK. PDGF-induced proliferation in human arterial and venous smooth muscle cells: molecular basis for differential effects of PDGF isoforms. *J Cell Biochem* 112: 289-298, 2011.

39. Heldin CH, Westermark B. Mechanism of action and in vivo role of platelet-derived growth factor. *Physiol Rev* 79: 1283-1316, 1999.

40. Raines EW. PDGF and cardiovascular disease. *Cytokine Growth Factor Rev* 15: 237-254, 2004.

41. Li L, Blumenthal DK, Masaki T, Terry CM, Cheung AK. Differential effects of imatinib on PDGF-induced proliferation and PDGF receptor signaling in human arterial and venous smooth muscle cells. *J Cell Biochem* 99: 1553-1563, 2006.

42. Ballyk PD, Walsh C, Butany J, Ojha M. Compliance mismatch may promote graft-artery intimal hyperplasia by altering suture-line stresses. *J Biomech* 31: 229-237, 1998.

43. Hofer M, Rappitsch G, Perktold K, Trubel W, Schima H. Numerical study of wall mechanics and fluid dynamics in end-to-side anastomoses and correlation to intimal hyperplasia. *J Biomech* 29: 1297-1308, 1996.

44. Haruguchi H, Teraoka S. Intimal hyperplasia and hemodynamic factors in arterial bypass and arteriovenous grafts: a review. *J Artif Organs* 6: 227-235, 2003.

45. Sivanesan S, How TV, Black RA, Bakran A. Flow patterns in the radiocephalic arteriovenous fistula: an in vitro study. *J Biomech* 32: 915-925, 1999.

46. Fung YC. Biomechanics: Mechanical Properties of Living Tissues. 2. Springer-Verlag; New York: 1993.

47. Manos TA, Sokolis DP, Giagini AT, Davos CH, Kakisis JD, Kritharis EP, Stergiopulos N, Karayannacos PE, Tsangaris S. Local hemodynamics and intimal hyperplasia at the venous side of a porcine arteriovenous shunt. *IEEE Trans Inf Technol Biomed* 14: 681-690, 2010.

48. Budu-Grajdeanu P, Schugart RC, Friedman A, Valentine C, Agarwal AK, Rovin BH. A mathematical model of venous neointimal hyperplasia formation. *Theor Biol Med Model* 5: 2, 2008.

49. Loth F, Fischer PF, Bassiouny HS. Blood flow in end-to-side anastomoses. *Annu Rev Fluid Mech* 40: 367-393, 2008.

50. Misra S, Lee N, Fu AA, Raghavakaimal S, Mandrekar J, Bjarnason H, McKusick MA, Iruela-Arispe L, Mukhopadhyay D. Increased expression of a disintegrin and metalloproteinase thrombospondin 1 in thrombosed hemodialysis grafts. *J Vasc Interv Radiol* 19: 111-119, 2008.

51. Misra S, Fu AA, Puggioni A, Glockner JF, McKusick MA, Bjarnason H, Mukhopadhyay D. Proteomic profiling in early venous stenosis formation in a porcine model of hemodialysis graft. *J Vasc Interv Radiol* 20: 241-251, 2009.

52. Misra S, Shergill U, Yang B, Janardhanan R, Misra KD. Increased expression of HIF-1alpha, VEGF-A and its receptors, MMP-2, TIMP-1, and ADAMTS-1 at the venous stenosis of arteriovenous fistula in a mouse model with renal insufficiency. *J Vasc Interv Radiol* 21: 1255-1261, 2010.

53. Newby AC, Zaltsman AB. Molecular mechanisms in intimal hyperplasia. *J Pathol* 190: 300-309, 2000.

54. Thyberg J. Phenotypic modulation of smooth muscle cells during formation of neointimal thickenings following vascular injury. *Histol Histopathol* 13: 871-891, 1998.

55. Dardik A, Yamashita A, Aziz F, Asada H, Sumpio BE. Shear stress-stimulated endothelial cells induce smooth muscle cell chemotaxis via platelet-derived growth factor-BB and interleukin-1alpha. *J Vasc Surg* 41: 321-331, 2005.

56. Ang AH, Tachas G, Campbell JH, Bateman JF, Campbell GR. Collagen synthesis by cultured rabbit aortic smooth-muscle cells. Alteration with phenotype. *Biochem J* 265: 461-469, 1990.

57. Thyberg J. Differentiated properties and proliferation of arterial smooth muscle cells in culture. *Int Rev Cytol* 169: 183-265, 1996.

58. Sanders WG, Morisseau C, Hammock BD, Cheung AK, Terry CM. Soluble epoxide hydrolase expression in a porcine model of arteriovenous graft stenosis and anti-inflammatory effects of a soluble epoxide hydrolase inhibitor. *Am J Physiol Cell Physiol* 303: C278-290, 2012.

59. Jiang Z, Yu P, Tao M, Ifantides C, Ozaki CK, Berceli SA. Interplay of CCR2 signaling and local shear force determines vein graft neointimal hyperplasia in vivo. *FEBS Lett* 583: 3536-3540, 2009.

60. Misra S, Fu AA, Rajan DK, Juncos LA, McKusick MA, Bjarnason H, Mukhopadhyay D. Expression of hypoxia inducible factor-1 alpha, macrophage migration inhibition factor, matrix metalloproteinase-2 and -9, and their inhibitors in hemodialysis grafts and arteriovenous fistulas. *J Vasc Interv Radiol* 19: 252-259, 2008.

61. Misra S, Fu AA, Misra KD, Shergill UM, Leof EB, Mukhopadhyay D. Hypoxia-induced phenotypic switch of fibroblasts to myofibroblasts through a matrix metalloproteinase 2/tissue inhibitor of metalloproteinase-mediated pathway: implications for venous neointimal hyperplasia in hemodialysis access. *J Vasc Interv Radiol* 21: 896-902, 2010.

62. Li JM, Zhang X, Nelson PR, Odgren PR, Nelson JD, Vasiliu C, Park J, Morris M, Lian J, Cutler BS, Newburger PE. Temporal evolution of gene expression in rat carotid artery following balloon angioplasty. *J Cell Biochem* 101: 399-410, 2007.

63. Lee BH, Nam HY, Kwon T, Kim SJ, Kwon GY, Jeon HJ, Lim HJ, Lee WK, Park JS, Ko JY, Kim DJ. Paclitaxel-coated expanded polytetrafluoroethylene haemodialysis grafts inhibit neointimal hyperplasia in porcine model of graft stenosis. *Nephrol Dial Transplant* 21: 2432-2438, 2006.

64. Lim HJ, Nam HY, Lee BH, Kim DJ, Ko JY, Park JS. A novel technique for loading of paclitaxel-PLGA nanoparticles onto ePTFE vascular grafts. *Biotechnol Prog* 23: 693-697, 2007.

65. Touzot M, Soulillou JP, Dantal J. Mechanistic target of rapamycin inhibitors in solid organ transplantation: from benchside to clinical use. *Curr Opin Organ Transplant* 17: 626-633, 2012.

66. Abizaid A. Sirolimus-eluting coronary stents: a review. *Vasc Health Risk Manag* 3: 191-201, 2007.

67. Terry CM, Li L, Li H, Zhuplatov I, Blumenthal DK, Kim SE, Owen SC, Kholmovski EG, Fowers KD, Rathi R, Cheung AK. In vivo evaluation of the delivery and efficacy of a sirolimus-laden polymer gel for inhibition of hyperplasia in a porcine model of arteriovenous hemodialysis graft stenosis. *J Control Disease* 160: 459-467, 2012.

68. Himmelfarb J, Couper L. Dipyridamole inhibits PDGF- and bFGF-induced vascular smooth muscle cell proliferation. *Kidney Int* 52: 1671-1677, 1997.

69. Dixon BS, Beck GJ, Vazquez MA, Greenberg A, Delmez JA, Allon M, Dember LM, Himmelfarb J, Gassman JJ, Greene T, Radeva MK, Davidson IJ, Ikizler TA, Braden GL, Fenves AZ, Kaufman JS, Cotton JR Jr, Martin KJ, McNeil JW, Rahman A, Lawson JH, Whiting JF, Hu B, Meyers CM, Kusek JW, Feldman HI; DAC Study Group. Effect of dipyridamole plus aspirin on hemodialysis graft patency. *N Engl J Med* 360: 2191-2201, 2009.

70. Kuji T, Masaki T, Goteti K, Li L, Zhuplatov S, Terry CM, Zhu W, Leypoldt JK, Rathi R, Blumenthal DK, Kern SE, Cheung AK. Efficacy of local dipyridamole therapy in a porcine model of arteriovenous graft stenosis. *Kidney Int* 69: 2179-2185, 2006.

71. Rutherford C, Martin W, Salame M, Carrier M, Anggård E, Ferns G. Substantial inhibition of neo-intimal response to balloon injury in the rat carotid artery using a combination of antibodies to platelet-derived growth factor-BB and basic fibroblast growth factor. *Atherosclerosis* 130: 45-51, 1997.

72. Davies MG, Owens EL, Mason DP, Lea H, Tran PK, Vergel S, Hawkins SA, Hart CE, Clowes AW. Effect of platelet-derived growth factor receptor-alpha and -beta blockade on flow-induced neointimal formation in endothelialized baboon vascular grafts. *Circ Res* 86: 779-786, 2000.

73. Makiyama Y, Toba K, Kato K, Hirono S, Ozawa T, Saigawa T, Minagawa S, Isoda M, Asami F, Ikarashi N, Oda M, Moriyama M, Higashimura M, Kitajima T, Otaki K, Aizawa Y. Imatinib mesilate inhibits neointimal hyperplasia via growth inhibition of vascular smooth muscle cells in a rat model of balloon injury. *Tohoku J Exp Med* 215: 299-306, 2008.

74. Lemmon MA, Schlessinger J. Cell signaling by receptor tyrosine kinases. *Cell* 141: 1117-1134, 2010.

75. Fabian MA, Biggs WH 3rd, Treiber DK, Atteridge CE, Azimioara MD, Benedetti MG, Carter TA, Ciceri P, Edeen PT, Floyd M, Ford JM, Galvin M, Gerlach JL, Grotzfeld RM, Herrgard S, Insko DE, Insko MA, Lai AG, Lélias JM, Mehta SA, Milanov ZV, Velasco AM, Wodicka LM, Patel HK, Zarrinkar PP, Lockhart DJ. A small molecule-kinase interaction map for clinical kinase inhibitors. *Nat Biotechnol* 23: 329-336, 2005.

76. Karaman MW, Herrgard S, Treiber DK, Gallant P, Atteridge CE, Campbell BT, Chan KW, Ciceri P, Davis MI, Edeen PT, Faraoni R, Floyd M, Hunt JP, Lockhart DJ, Milanov ZV, Morrison MJ, Pallares G, Patel HK, Pritchard S, Wodicka LM, Zarrinkar PP. A quantitative analysis of kinase inhibitor selectivity. *Nat Biotechnol* 26: 127-132, 2008.

77. Christensen JG. A preclinical review of sunitinib, a multitargeted receptor tyrosine kinase inhibitor with anti-angiogenic and antitumour activities. *Ann Oncol* 18 (Suppl 10): x3-x10, 2007.

78. Roskoski R Jr. Sunitinib: a VEGF and PDGF receptor protein kinase and angiogenesis inhibitor. *Biochem Biophys Res Commun* 356: 323-328, 2007.

79. Chow LQ, Eckhardt SG. Sunitinib: from rational design to clinical efficacy. *J Clin Oncol* 25: 884-896, 2007.

80. Imig JD, Hammock BD. Soluble epoxide hydrolase as a therapeutic target for cardiovascular diseases. *Nat Rev Drug Discov* 8: 794-805, 2009.

81. Simpkins AN, Rudic RD, Roy S, Tsai HJ, Hammock BD, Imig JD. Soluble epoxide hydrolase inhibition modulates vascular remodeling. *Am J Physiol Heart Circ Physiol* 298: H795-806, 2010.

CHAPTER 2

PERFUSED VEIN CULTURE AS A MODEL SYSTEM TO TEST SUNITINIB AS PHARMACOTHERAPY FOR NEOINTIMAL HYPERPLASIA

2.1 Abstract

Neointimal hyperplasia (NH) is the predominant cause of stenosis in hemodialysis arteriovenous grafts (AVG) but currently, there are no clinically effective pharmacotherapies to prevent NH. We developed an ex vivo perfused vein model where NH develops in a clinically relevant flow environment, and examined the potential for this model to be used to test pharmacotherapies to prevent venous NH. Data from an in vivo porcine AVG stenosis model indicated that growth factors PDGF and VEGF, and their respective cognate receptors PDGFR-α and VEGFR-2, were up-regulated at the graft-venous anastomosis within 2 weeks after AVG placement, with subsequent NH development by 4 weeks. Sunitinib, a broad-spectrum tyrosine kinase inhibitor, was therefore chosen to test in vitro. Sunitinib inhibited PDGF-stimulated proliferation of cultured smooth muscle cells (SMCs) and VEGF-stimulated endothelial cell proliferation in a dose-dependent manner. Migration of PDGF-stimulated SMCs was inhibited at similar concentrations of drug. Additionally, sunitinib inhibited PDGF-induced changes in phosphorylation of MAPK and PI3K/Akt signaling proteins and expression of cell-cycle regulatory

proteins of SMCs in vitro. Significant NH formation was observed in ex vivo cultures of porcine vein segments perfused for 12 days under nonphysiological venous wall shear stress, a key factor postulated to promote NH. Sunitinib (100 nM) inhibited NH formation under these conditions, with the intima-to-lumen area ratio decreasing from 0.45 ± 0.25 in the untreated vessels to 0.04 ± 0.02 ($p < 0.05$). These findings demonstrate the utility of an ex vivo perfused vein model to investigate pharmacotherapies in a clinically relevant pathophysiological flow environment.

2.2 Introduction

Hemodialysis for patients with end-stage renal disease requires a vascular access that can provide high extracorporeal blood flow rates. A well-functioning native arteriovenous fistula (AVF) is the preferred form of vascular access because it has the least long-term complications. AVFs may, however, require months before becoming mature and usable, and up to 60% of native AVFs fail to mature (1, 7, 21, 31). Synthetic arteriovenous grafts (AVGs) made of expanded polytetrafluoroethylene (ePTFE) provide an alternative option. AVGs do not require maturation and can be used within days of creation. However, AVGs are associated with high stenosis rates, followed by thrombosis and occlusion, with 50% and 75% failure at 1 and 2 years after implantation, respectively (20, 37). Currently, AVG stenosis is treated by angioplasty, but the vascular wall injury associated with this procedure predisposes to restenosis (21).

Neointimal hyperplasia (NH) accounts for practically all stenotic lesions in AVGs (14, 21). Histologically, NH consists of proliferating smooth muscle cells (SMCs) and myofibroblasts, mostly derived from the medial and the adventitial layers of the vessel wall (14, 18, 20, 23, 25, 29, 35).

While the compositions of arterial and venous NH lesions do not appear to be significantly different from each other, in most circumstances, progressive NH occurs at the graft-venous anastomosis (hereafter referred to as venous anastomosis) and less frequently at the graft-arterial anastomosis (arterial anastomosis) of AVG (2, 14, 21). It is thought that the venous anastomosis is more susceptible to multiple pathogenic factors that may potentiate NH formation, such as nonphysiological hemodynamics, damage to the protective adventitia and endothelium, and enhanced inflammation. In addition, the AVG shunts arterial blood flow directly into the vein, exposing the vein to high blood pressures and pulsatile and/or disturbed flow patterns, resulting in highly aberrant wall shear stress (WSS). The higher propensity of the venous anastomosis to develop NH is likely, at least in part, due to the greater hemodynamic changes seen at the venous anastomosis, compared to the arterial anastomosis.

We have developed an ex vivo perfused organ culture model using explanted whole porcine vein segments. This ex vivo system enables us to recapitulate the pathological hemodynamic parameters occurring at the venous anastomosis in vivo, such as very low or high WSS, and can be utilized to efficiently identify agents that inhibit NH under these and other specific isolated conditions. In addition, whole vessel segments retain the vessel wall architecture as well as cell-cell and cell-extracellular matrix interactions that are more relevant than primary monolayer cell cultures to the in vivo environment.

Currently, there are no drugs used routinely to prevent and/or treat NH, although the combination of aspirin and dipyridamole used prophylactically and sustained over a long period appears to produce a modest effect in retarding AVG failure (8). The early stage of NH

development requires the rapid growth and migration of cells. A rational approach to NH prevention would be the pharmacological inhibition of cell migration and proliferation (15, 20, 23). Potential molecular targets involved in NH formation were investigated in a porcine model of AVG stenosis, and early expression of the platelet-derived growth factor (PDGF) and vascular endothelial growth factor (VEGF) pathways were identified. Because the PDGF and VEGF pathways are both involved in NH, one candidate agent to prevent NH is the antineoplastic drug sunitinib, a multitarget receptor tyrosine kinase (RTK) inhibitor with well-established antiangiogenic and antiproliferative properties. The efficacy of sunitinib in inhibiting growth factor-stimulated proliferation of SMCs and endothelial cells (ECs), and the associated intracellular events, was examined in vitro and in the ex vivo perfused vein model. The results of the in vitro and ex vivo experiments demonstrate the utility of sunitinib as a pharmacological inhibitor of NH and the value of the ex vivo organ culture system for evaluating other potential NH-preventative agents.

2.3 Materials and Methods

2.3.1 Materials

All cell and organ culture reagents were purchased from Cascade Biologics (Portland, OR) except for fetal calf serum (FCS), which was purchased from Atlanta Biologicals (Lawrenceville, GA). Sunitinib maleate was provided by Pfizer Inc. (New York, NY). Recombinant human platelet-derived growth factor-BB (PDGF-BB) and human vascular endothelial growth factor 165 ($VEGF_{165}$) were purchased from R&D Systems (Minneapolis, MN). Antibodies against PDGF-B chain, VEGF, PDGFR-α, and VEGFR-2, were purchased from Thermo Scientific (Fremont, CA).

Antibodies against von Willebrand Factor (vWF) and Ki-67 were purchased from DAKO Pharmaceuticals (Carpinteria, CA). Anti-smooth muscle α-actin antibody was purchased from Sigma (St. Louis, MO) and anti-glyceraldehyde-3-phosphate dehydrogenase (GAPDH) antibody was purchased from Abcam (Cambridge, MA). Secondary antibodies conjugated to horseradish peroxidase (HRP) were purchased from Santa Cruz Biotechnology (Santa Cruz, CA). All other antibodies were obtained from Cell Signaling Technologies (Danvers, MA). Precast polyacrylamide gels for electrophoresis, nitrocellulose membranes, and Immun-star^{TM} HRP chemiluminescent kit were purchased from Bio-Rad Laboratories (Hercules, CA). Complete Mini-Protease Inhibitor Cocktail was obtained from Roche Applied Science (Indianapolis, IN). Bicinchoninic acid (BCA) protein assay kit was purchased from Pierce Chemical (Rockford, IL).

2.3.2 Porcine model of AVG stenosis

All animal procedures were performed in accordance with a protocol that was approved by the Institutional Animal Care and Use Committees (IACUCs) at the Veterans Affairs Salt Lake City Health Care System and the University of Utah. The porcine model of AVG stenosis has been well-established and employed routinely in our laboratory (16, 27, 33). Anesthetized female Yorkshire cross domestic pigs (Sigma Livestock, Salt Lake City, UT) weighing 30 to 35 kg were used for the implantation of a spiral-reinforced ePTFE graft (C. R. Bard, Murray Hill, NJ) unilaterally between the common carotid artery (CCA) and the ipsilateral external jugular vein (EJV).

Animals were sedated prior to surgery with a cocktail consisting of ketamine (4 mg/kg), telazol (4 mg/kg), and xylazine (4 mg/kg), and isoflurane inhalation was used for anesthesia during surgery. The graft (spiral-reinforced, 7 cm in length and 6 mm in internal diameter), cut at an angle of 55° at both ends, was attached to the CCA and EJV such that the graft loop lies in the cranial direction, creating both arterial and venous end-to-side anastomoses. Sodium heparin was administered intravenously during the surgery. Oral aspirin (Pharmaceutical Formulations, Edison, NJ), clopidogrel (Bristol-Myers Squibb, New York, NY) and enrofloxacin (Bayer, Pittsburgh PA) were administered peri-operatively. The animal was euthanized at the indicated time points. The AVG and adjoining blood vessels were retrieved en bloc for histology/immunohistochemistry (IHC) and morphometric studies as described below. A total of 23 pigs were used to study the time course of NH development, angiogenesis, and proliferation (see Figure 2.1 legend for the number of animals at each specific time point).

2.3.3 Histology and morphometry in a porcine AVG model

Grafted EJV segments (1-2 cm in length) at the vein-graft junction were harvested at various time points after the AVG implantation. Explanted EJV segments were perfusion-fixed in 10% neutral-buffered formalin to maintain the in vivo geometry and then immersed in formalin for 24 to 48 h. Paraffin-embedded 5 μm thick tissue cross-sections from the center of the venous anastomosis, where the ePTFE graft and the vein wall comprise approximately the same proportion in the tissue section (20), were stained with elastic Van Gieson's stain (Accustain Elastic Stain, Sigma), examined under light microscopy, and digitally photographed using the QImaging

system (Surrey, BC, Canada). The external and the internal elastic laminae were visualized. The surface areas of the NH (defined as the tissue area between the venous lumen and the internal elastic lamina), the media and the graft were quantified separately using ImageJ 1.45 software (http://rsb.info.nih.gov/ij/). The NH index was calculated as the ratio of the NH surface area to the combined surface area of the graft and media, which corrects for variations in the angle of the histological sections and thus, the apparent thickness of the vascular wall layers.

Tissue sections from the same anastomotic region were immunostained for the endothelial marker, vWF, to identify ECs. Neovascularization was fairly homogenous within each region. Direct microscopic manual counting of the neovessel densities in the NH and the adventitia in a given image field was performed separately by three independent observers at a magnification of x 20. The final counts included small lumens surrounded by vWF-positive cells and single or clusters of vWF-positive cells. We selected the most vascularized areas at a low magnification (x 5) and counted the representative areas at a higher magnification (x 20).

Tissue sections from the same anastomotic region were also immunostained for the nuclear proliferation marker, Ki-67, present in the neointima and the adventitia separately. The number of Ki-67-positive nuclei and the number of total nuclei stained with hematoxylin in a given image field were counted by three independent observers at a magnification of x 20. The proliferation index (PI) was calculated as the number of Ki-67-positive nuclei divided by the total number of nuclei x 100.

To determine the expression of VEGF, VEGFR-2, PDGF-B, PDGFR-α in the NH lesions, tissue sections from the same anastomotic region were subjected to IHC using the respective

antibodies.

2.3.4 Cell culture

Primary human aortic smooth muscle cells (HASMC), human saphenous vein smooth muscle cells (HVSMC), and human umbilical vein endothelial cells (HUVEC) were obtained from Cambrex (Chicago, IL). SMCs were identified by positive staining with anti-smooth muscle α-actin. The endothelial phenotype of HUVECs was confirmed by positive anti-factor VIII staining. Cells were maintained in their respective basal media supplemented with 10% or 2% FCS, respectively, additional growth factors, and antibiotics (gentamicin/amphotericin B) in a humidified 37 °C incubator with 5% CO_2 and 95% ambient air. Fresh culture media was supplied every 2 to 3 days. For all experiments, both HASMCs and HVSMCs from three different donors and cells at passage 3 to 7 were used. SMCs were cultured to approximately 70 to 80% confluence and HUVECs to 90% confluence, and then rendered quiescent before each experiment as described below.

2.3.5 In vitro proliferation and migration assays

For proliferation assays, SMCs and HUVECs were seeded on 96-well microtiter plates at a density of $5x10^3$ cells/well and cultured to the desired confluence. Before each experiment, cells were rendered quiescent by incubating for 24 h with their respective basal media containing 0.5% FCS but no additional growth factors. These cells were then pretreated with various concentrations of sunitinib (1 to 1,000 nM) for 1 h, followed by stimulation with either PDGF-BB (50 ng/ml) or $VEGF_{165}$ (50 ng/ml) for SMCs and ECs, respectively. After 48 h, DNA synthesis was assessed by 5-bromo-2'-deoxyuridine (BrdU) incorporation (Cell Proliferation ELISA, Roche

Applied Science). In brief, BrdU labeling solution was added to the culture medium for 12 to 24 h before the cells were fixed for 30 min. Cells were then incubated for 90 min with peroxidase-conjugated anti-BrdU antibody. BrdU-antibody complexes were detected by a colorimetric reaction with the substrate (3,3',5,5'-tetramethylbenzidine), and the optical density read at 450 nm in a microplate reader (Multiskan Ascent, Thermo Electron Corporation, San Jose, CA). At least six replicate experiments were analyzed for each sunitinib concentration for both SMCs and ECs.

SMC migration was assessed using the InnoCyte^{TM} Cell Migration Assay (Calbiochem, San Diego, CA) according to the manufacturer's instructions. In brief, a suspension of $5x10^4$ HASMC was loaded into the well of the upper migration chamber (the insert) which contained media with 0.5% FCS but no additional growth factors. The upper migration chamber was then attached to the lower chamber (the tray). Cells were preincubated with various concentrations of sunitinib added to the media in both the upper and lower chambers for 1 h, and then 50 ng/ml of PDGF-BB was added to the lower chamber. Cells were allowed to migrate through the porous membrane towards the lower chamber for 4 h in a humidified 37 °C tissue culture incubator. Finally, the migrated cells attached at the underneath side of the membrane were dislodged and fluorescence-labeled with Calcein-AM, followed by quantification at 485 nm using a standard fluorescence microplate reader (SpectraMax 250, Molecular Devices, Sunnyvale, CA). At least 3 replicate experiments were analyzed for each sunitinib concentration.

2.3.6 Western blotting

Signal transduction pathways activated by PDGF-BB in HASMCs were explored by examining the phosphorylation of ERK1/2, Akt, p70S6K, and rpS6 using Western blotting. Expression of cell-cycle regulatory proteins cyclin D1, p21, and p27 was also assessed. Quiescent HASMCs were exposed to various concentrations of sunitinib for 1 h, then stimulated with 50 ng/ml of PDGF-BB for 10 min (to determine early changes in protein phosphorylation) and for 24 h (to assess changes in cell-cycle regulatory protein expression). Cells were then washed twice with ice-cold phosphate-buffered saline (PBS) and lysed with lysis buffer (PBS containing 0.6 percent NP-40, 150 mM NaCl, 10 mM HEPES, pH 7.9 with protease inhibitors). Protein concentrations were determined by the BCA protein assay. Cell lysates containing equal amounts of total protein were subjected to SDS-PAGE on precast 4 to 20% gradient polyacrylamide gels (Life Technologies, Grand Island, NY). Following electrophoresis and transfer to nitrocellulose membranes, immunoblots were incubated overnight at 4 °C with primary antibodies specific for the respective proteins or for the phosphorylated form of the proteins. Immunoblots were incubated overnight with primary antibodies specific for the respective proteins or for the phosphorylated form of the proteins. Immunoblot detection was performed using an Immun-star™ HRP Chemiluminescent kit according to the manufacturer's instructions.

2.3.7 Ex vivo perfused vein culture and analysis

Porcine internal jugular vein (IJV) segments were harvested with sterile techniques from female Yorkshire cross domestic pigs weighing at least 30 kg that have been used for AVG model

experiments. In most of the AVG pig studies conducted in our laboratory, only CCA and EJV segments were manipulated and experimentally utilized and IJV typically remains intact. IJV segments harvested this way do not exhibit pre-existing NH lesions and are not expected to be different from IJV collected from unoperated animals.

The ex vivo perfusion system is similar to that described by Gusic et al. (5, 11, 12), with modifications regarding the vessel chamber and the long-term application of laminar flow with various WSS values. Briefly, explanted IJV segments were fixed at their in vivo length (3 to 5 cm) onto stainless steel tubes using surgical sutures, and bathed in a vessel chamber filled with Dulbecco's Modified Eagle Medium (DMEM) supplemented with 30% FCS and antibiotics but no additional growth factors. Vein segments were perfused with the same oxygenated media that was recirculated at a laminar, constant volumetric flow rate to generate specific calculated WSS values inside the vessel. Volumetric flow rate was measured manually through a flow valve positioned immediately downstream of the vessel chamber. Vein segments were cultured for 12 consecutive days with media flowing continuously (N = 6). Fresh media was supplied every 2 to 3 days. Sterile conditions were maintained in the entire system in the 37 °C constant-temperature hood. In sunitinib-treated veins (N = 3), sunitinib was added to the circulating media as well as to the media that filled the vessel chamber on the second day of ex vivo culture in order to allow vessels to recover from explantation procedures, and was added to the fresh replacement media to maintain a constant final drug concentration of 100 nM throughout the entire experiment.

WSS (τ) was calculated using the following equation: $\tau = (4\mu Q)/(\pi r^3)$, where μ is the viscosity of the culture media containing serum (μ = 0.01 Poise), Q is the volumetric flow rate

through the vessel adjusted to generate the desired WSS, and r is the inner radius of the vessel lumen measured at the time of harvest. The WSS inside the vessels was maintained at <1 dyne/cm^2 at the beginning of culture (N = 5), a value that is considered nonphysiologically low for the normal vein. Veins are typically exposed to 1 to 5 dyne/cm^2 under normal conditions. One of the untreated control IJV segments had a small inner radius such that we were unable to generate an initial low WSS value; therefore, this vein segment was subjected to a WSS of >50 dyne/cm^2 which is also nonphysiological for the vein. Because we observed the greatest NH formation in this particular vein segment among all other segments tested, this particular piece of data was included in our study. A total of five animals were used to collect veins for the perfusion experiments.

Explanted IJV segments exposed to the above-described WSS conditions were fixed in 10% neutral buffered formalin at the end of each perfusion experiment. After formalin was directly perfused into the lumen of the vessel through the metal tubes, the entire vessel was immersed in formalin for 24 to 48 h. Paraffin-embedded cross-sections were stained with either hematoxylin/eosin (Poly Scientific, Bay Shore, NY) or Van Gieson's stain. The cross-sectional surface areas of vessel wall regions were determined using planimetry under light microscopy and the Q-Imaging system, and were quantified using ImageJ software. The results were used to calculate the intima-to-media area ratio (I/M) and the intima-to-lumen area ratio (I/L). In IHC, SMCs and/or myofibroblasts were identified by positive staining with anti-smooth muscle α-actin, while proliferating cells were identified by positive staining with anti-Ki-67. ECs were identified by positive staining with anti-vWF. Immunostained proteins were visualized using confocal

microscopy.

Some IJV segments were kept in a static condition for 14 days. After harvest, vein segments of about 1 to 2 cm were cut longitudinally to expose the lumen and pinned up on a sterile mesh, and cultured with DMEM containing 30% FCS in a tissue culture dish. Formalin-fixation, paraffin-embedding, and Van Gieson's stain was performed as described above.

2.3.8 Data analysis

Results are reported as means ± standard deviation (SD). Two-tailed Student's t-test and one-way analysis of variance (ANOVA) with Tukey's post test were performed using GraphPad Prism version 5.00 for Windows (GraphPad Software, San Diego, CA). Statistically significant results are defined as $p < 0.05$. Mean 50% inhibitory concentrations (IC_{50}) were estimated using GraphPad Prism's built-in nonlinear regression (least squares) curve fitting.

2.4 Results

2.4.1 NH in porcine AVG model

In the porcine model of AVG established in our laboratory, significant stenosis is usually present within 4 weeks after the graft placement (16, 20). In the present study, we conducted a time-course analysis to delineate the temporal relationship among NH, angiogenesis, and cell proliferation in tissue sections obtained from the venous anastomosis. Progression of the NH index (Figure 2.1A), calculated as the ratio of the NH area to the combined area of the graft and media, exhibited the same trend as the time-dependent increase in angiogenesis within the NH lesions (Figure 2.1B). Specifically, both NH index and angiogenesis in the NH lesions were

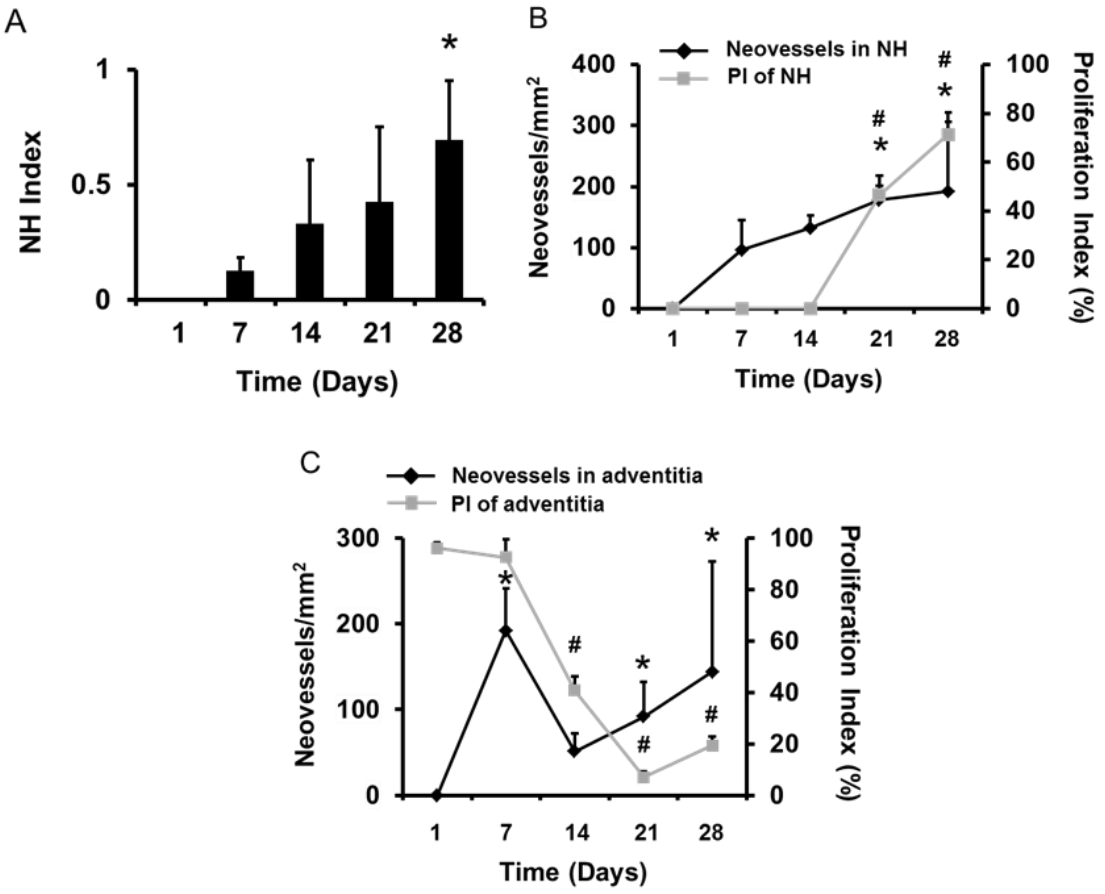

Figure 2.1 Time-course of NH development, neovessel density, and proliferation index (PI) at the venous anastomosis in a porcine AVG model. A. NH index at the venous anastomosis was calculated as the ratio of NH area to the combined area of the graft and media in tissues collected at various time points (N = 2, 3, 3, 7, 5 animals at day 1, 7, 14, 21, and 28, respectively). *$p < 0.05$ vs. Day 1. **B and C.** Anastomotic tissue sections were immunostained to detect neovessels and proliferating cells, using antibodies against vWF and Ki-67, respectively, within the NH **(B)** and the adventitia **(C)**. Proliferation index (PI) was determined by dividing the number of Ki-67-positive nuclei by the total number of nuclei in the image field. N = 4 animals for each time point. *$p < 0.05$ vs. Day 1 for neovessel density; $^{\#}p < 0.001$ vs. Day 1 for PI. For all panels, each data point represents the mean and standard deviation.

increased at postoperative day 7, whereas PI in the NH lesions was significantly increased after day 14. This time lag is consistent with the notion that angiogenesis is essential for further NH development by supplying oxygen and nutrients to proliferating cells. Interestingly, the neovessel density within the adventitia immediately increased after AVG placement, but was followed by a sharp decrease after day 7 (Figure 2.1C). The adventitia showed the highest PI at early time periods, and after day 7 the increase in adventitial PI largely paralleled changes in neovessel density. This temporal profile of proliferating cells in the adventitia was different from that in the NH and is consistent with the notion that an early event in NH development is the transformation and proliferation of adventitial myofibroblasts which subsequently migrate into the NH and contribute to NH formation (18, 35).

2.4.2 Enhanced expression of pro-NH factors in porcine AVG model

Expression of various growth factors, including VEGF, PDGF, and basic fibroblast growth factor (bFGF), are prominent in the venous NH lesions in specimens obtained from patients with failed AVG (29). Our porcine AVG model allows us to investigate whether these mediators of proliferation, migration and angiogenesis, and their cognate receptors are prominently expressed in the venous anastomosis, and thus, can be implicated as potential causal factors in the early development of NH. Figure 2.2 shows that in the NH lesions, VEGF, PDGF-B, and representative isoforms of their main receptors, VEGFR-2, PDGFR-α, respectively, stained intensely at 14 days after AVG placement, compared to the control EJV tissue sections. Moreover, the expression of these growth factor receptors remained high at 28 days postoperatively. These observations are

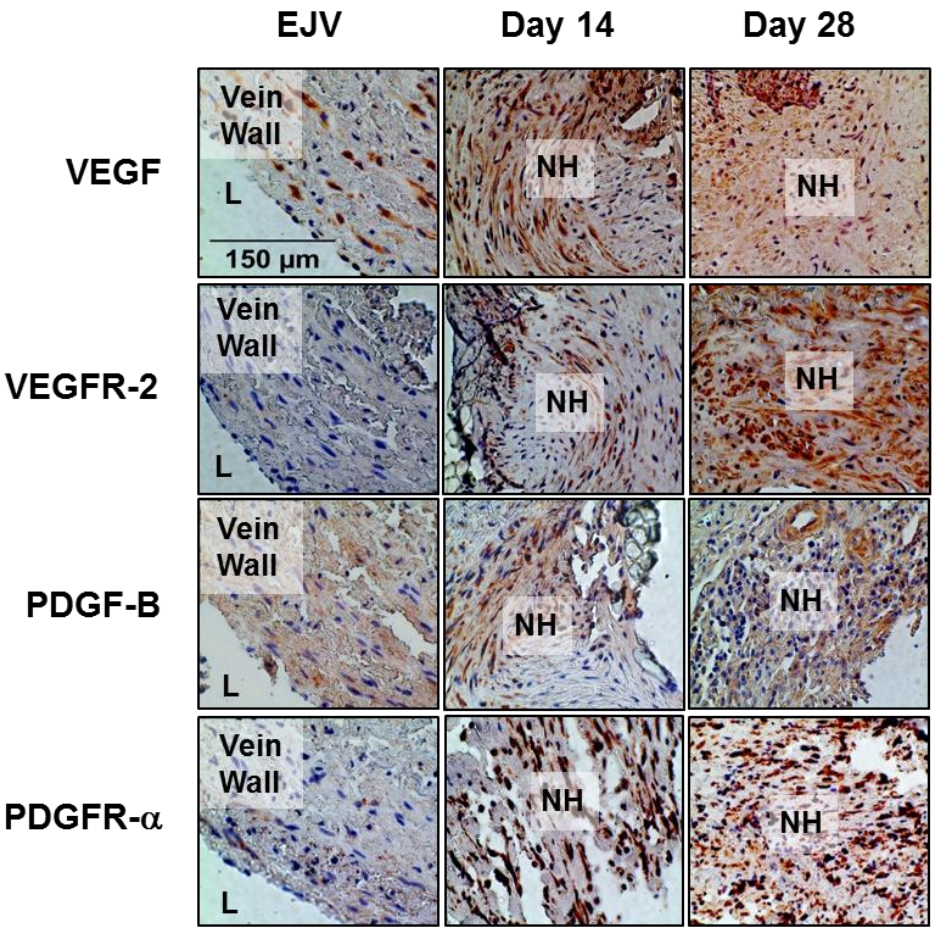

Figure 2.2 Enhanced expression of VEGF, PDGF, and their cognate receptors at the venous anastomosis in a porcine AVG model. Expression of VEGF, VEGFR-2, PDGF-B, and PDGFR-α in fresh external jugular vein (EJV, left column) and in the venous anastomotic tissues at 14 days (middle column) and 28 days (right column) after AVG placement was assessed by immunohistochemistry. Rust brown-color indicates positive staining for the indicated proteins. Blue structures are hematoxylin-stained nuclei. When compared to fresh EJV, venous anastomotic tissues had early (14 days) robust up-regulated expression of these growth factors and their cognate receptors, as well as sustained (28 days) over-expression of both growth factor receptors. Stained sections were assessed at original magnification x 20, and the scale bar in the top left panel applies to all panels in this figure. L = lumen; NH = neointimal hyperplasia.

consistent with the notion that VEGF, PDGF, and their receptors play key roles in both early development and sustained progression of NH. In addition, PDGF is known to activate other growth factor receptors within SMCs, such as epidermal growth factor receptors (EGFRs), resulting in the stimulation of multiple tyrosine kinase pathways (19). These observations provide a rationale to explore pharmacological interventions to prevent and/or treat NH by inhibiting signaling through these growth factor receptors. Accordingly, we examined the effects of sunitinib, a small molecule RTK inhibitor, in cell cultures and in an ex vivo perfused vein model.

2.4.3 Sunitinib inhibits growth factor-induced proliferation of vascular cells

We have previously demonstrated that among the three PDGF isoforms (PDGF-AA, PDGF-AB, and PDGF-BB), PDGF-BB had the greatest potency to stimulate the proliferation of both HASMCs and HVSMCs (19). In the present study, HASMCs and HVSMCs were pretreated with various concentrations of sunitinib for 1 h, and then stimulated with 50 ng/ml of PDGF-BB for 48 h. We found that sunitinib inhibited the PDGF-BB-induced proliferation of SMCs in a dose-dependent manner, with complete inhibition occurring at ~100 nM (Figure 2.3A). The mean IC_{50} was approximately 10 nM for HASMCs and 40 nM for HVSMCs. Sunitinib almost completely inhibited VEGF-induced proliferation of HUVECs at concentrations ≥10 nM (Figure 2.3B), with IC_{50} at approximately 8 nM. Cytotoxicity was not apparent under these conditions, as assessed by morphologic examination, and was manifested only at concentrations >10,000 nM (data not shown). Such high concentrations needed to induce cytotoxicity are consistent with those previously reported by others in other cell types, such as HEK-293 cells, human glioblastoma cell

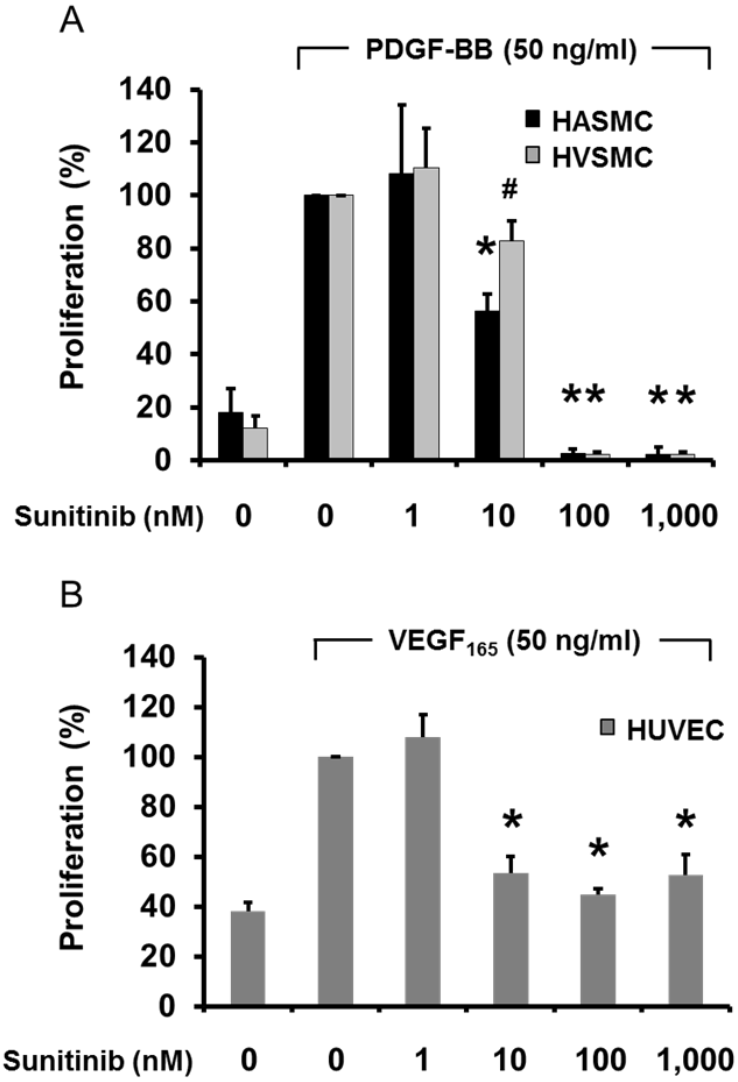

Figure 2.3 Sunitinib inhibits PDGF-BB-induced proliferation of smooth muscle cells and $VEGF_{165}$-induced proliferation of endothelial cells in vitro. A. Human arterial (HASMC) and venous (HVSMC) smooth muscle cells were preincubated with the indicated concentrations of sunitinib for 1 h before exposure to PDGF-BB (50 ng/ml) for 48 h. **B.** Human umbilical vein endothelial cells (HUVECs) were preincubated with the indicated concentrations of sunitinib for 1 h before exposure to $VEGF_{165}$ (50 ng/ml) for 48 h. Proliferation was assessed using the bromodeoxyuridine incorporation assay. At least six replicate experiments were analyzed for each sunitinib concentration. *$p < 0.001$ vs. PDGF-stimulated no-sunitinib control HASMC, PDGF-stimulated no-sunitinib control HVSMC, or VEGF-stimulated no-sunitinib control HUVEC; $^{\#}p < 0.01$ vs. PDGF-stimulated no-sunitinib control HVSMC.

lines, and fetal rat astrocytes (6, 30).

2.4.4 Sunitinib inhibits PDGF-BB-induced migration of vascular SMCs

Because NH initiation and development are attributable in part to the migration of cells, including medial SMCs and presumably adventitial fibroblasts/myofibroblasts, into the growing NH (18, 20, 35), we investigated whether sunitinib also attenuated the migration of HASMCs. Sunitinib inhibited the SMC migration stimulated by 50 ng/ml of PDGF-BB in a dose-dependent manner with approximately 45% inhibition observed at 1 nM (Figure 2.4). Higher concentrations of sunitinib (100 to 1000 nM) did not further inhibit SMC migration.

2.4.5 Effects of sunitinib on signaling and cell-cycle regulatory proteins in vascular SMCs

The effects of sunitinib on the two main PDGF-stimulated signaling pathways in SMCs, the mitogen-activated protein kinase (MAPK) and phosphatidylinositol-3 kinase (PI3K)/Akt pathways, were characterized using phospho-specific antibodies by Western blotting. As previously reported (10, 38), PDGF-BB at 50 ng/ml activated the MAPK and PI3K/Akt pathways, as indicated by the robust phosphorylation of ERK1/2, Akt, p70S6k, and rpS6 (Figure 2.5A). Sunitinib inhibited the phosphorylation of these proteins in a dose-dependent manner. PDGF-induced phosphorylation of ERK1/2 and Akt was almost completely abolished by 100 nM sunitinib, the same concentration that completely inhibited SMC proliferation, as shown in Figure2.3A. Sunitinib also inhibited, in a dose-dependent manner, the effects of PDGF-BB on the expression of the key cell-cycle regulatory proteins cyclin D1, p21, and p27. At 100 nM sunitinib,

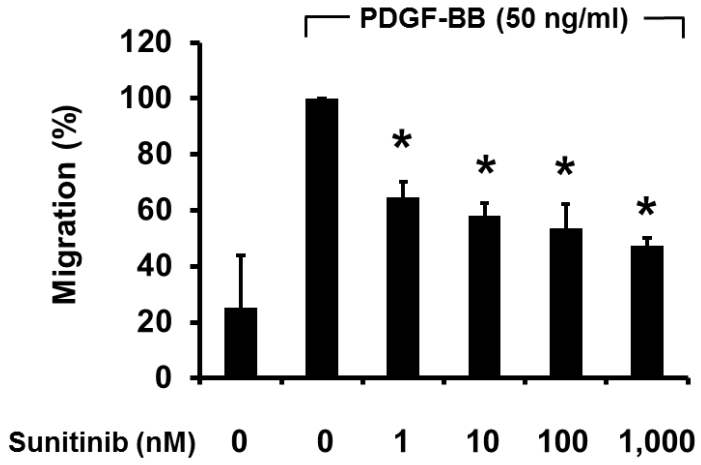

Figure 2.4 Sunitinib inhibits PDGF-BB-induced migration of smooth muscle cells in vitro. HASMCs in a migration-assay chamber were pre-incubated with the indicated concentrations of sunitinib for 1 h, and then stimulated with 50 ng/ml of PDGF-BB. HASMCs were allowed to migrate for 4 h, and the migrated cells were fluorescence-labeled and counted. At least three replicate experiments were analyzed for each sunitinib concentration. *$p < 0.001$ vs. PDGF-stimulated no-sunitinib control.

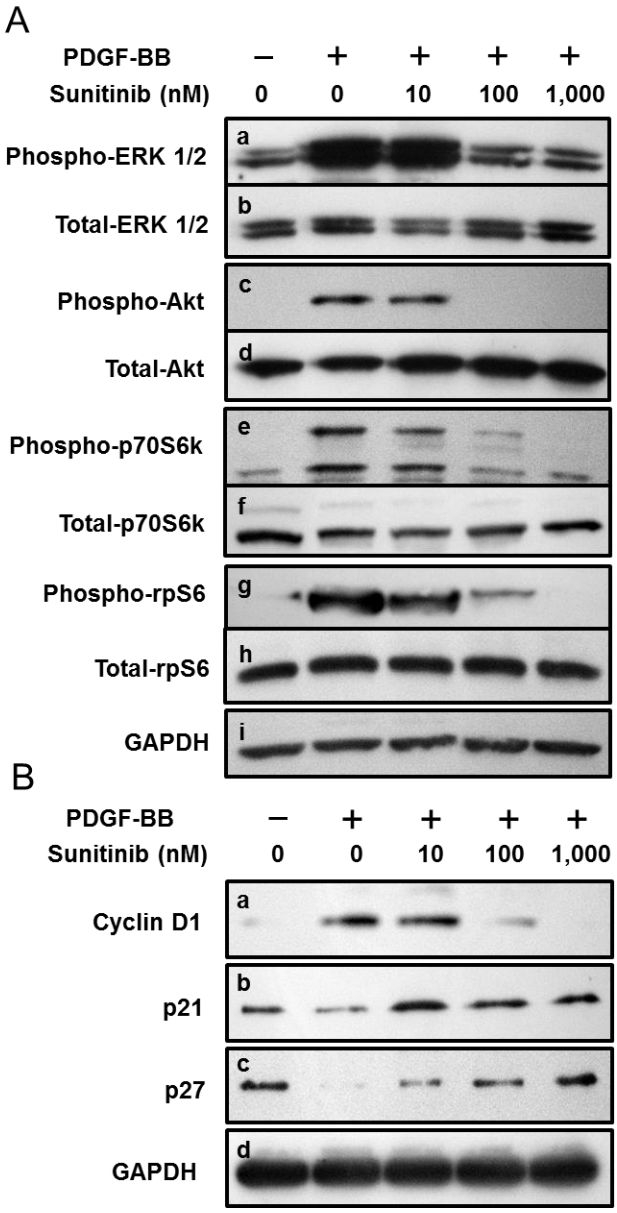

Figure 2.5 Sunitinib inhibits PDGF-BB-induced changes in phosphorylation of MAPK and PI3K/AKT signaling proteins and expression of cell-cycle regulatory proteins of smooth muscle cells in vitro. A. Phosphorylation of the MAPK and the PI3K/Akt pathway after exposure of HASMCs to PDGF-BB for 10 min, in the absence or presence of sunitinib, is shown in panels **a** (ERK1/2), **c** (Akt), **e** (p70S6k), and **g** (rpS6). Levels of total ERK1/2, Akt, p70S6k, and rpS6 proteins are shown in panels **b**, **d**, **f**, and **h**, respectively. **B.** Levels of various cell-cycle regulatory proteins after exposure of HASMCs to PDGF-BB for 24 h, in the absence or presence of sunitinib, are shown in panels **a** (cyclin D1), **b** (p21), and **c** (p27). GAPDH was used as a loading control (panels **i** and **d**).

the PDGF-induced expression of cyclin D1, a cyclin-dependent kinase activator and one of the earliest mitogenic regulators of cell cycle progression, was nearly completely inhibited (Figure 2.5B). In contrast, the expression of p21 and p27, cyclin-dependent kinase inhibitors that function as antimitogenic regulators, were potently decreased by PDGF-BB stimulation, and this effect was reversed by concentrations of sunitinib as low as 10 nM (Figure 2.5B). These observations are consistent with the notion that sunitinib inhibits the action of PDGF-BB by suppressing the expression of promitotic regulatory proteins and enhancing the expression of cell-cycle progression inhibitors.

2.4.6 Sunitinib inhibits venous NH formation in ex vivo perfused vein culture

In these experiments, explanted porcine IJV segments exposed to 30% FCS, but with no additional growth factors, were perfused ex vivo under defined nonphysiological laminar flow conditions for up to 12 days, or kept in static condition as described. All ex vivo cultured vein segments appeared intact and patent after 12 days. However, significant NH formation was seen only in the perfused vein segments examined histologically at 12 days in culture (Figure 2.6). The vein segments in static culture did not develop NH (Supplemental Figure 2.1), suggesting that perfusion is sufficient to induce NH. Van Gieson's staining of elastin fibers of the perfused vein sections displayed an overall healthy elastic lamina. Furthermore, there was only a low level of apoptotic cell death as assessed by the in situ cleaved caspase-3 assay (Supplemental Figure2.2). Cells in the NH lesions appeared disorganized, with elevated levels of proliferation as determined by Ki-67 staining. Positive Ki-67 staining, a measure of proliferation, demonstrates the long-term

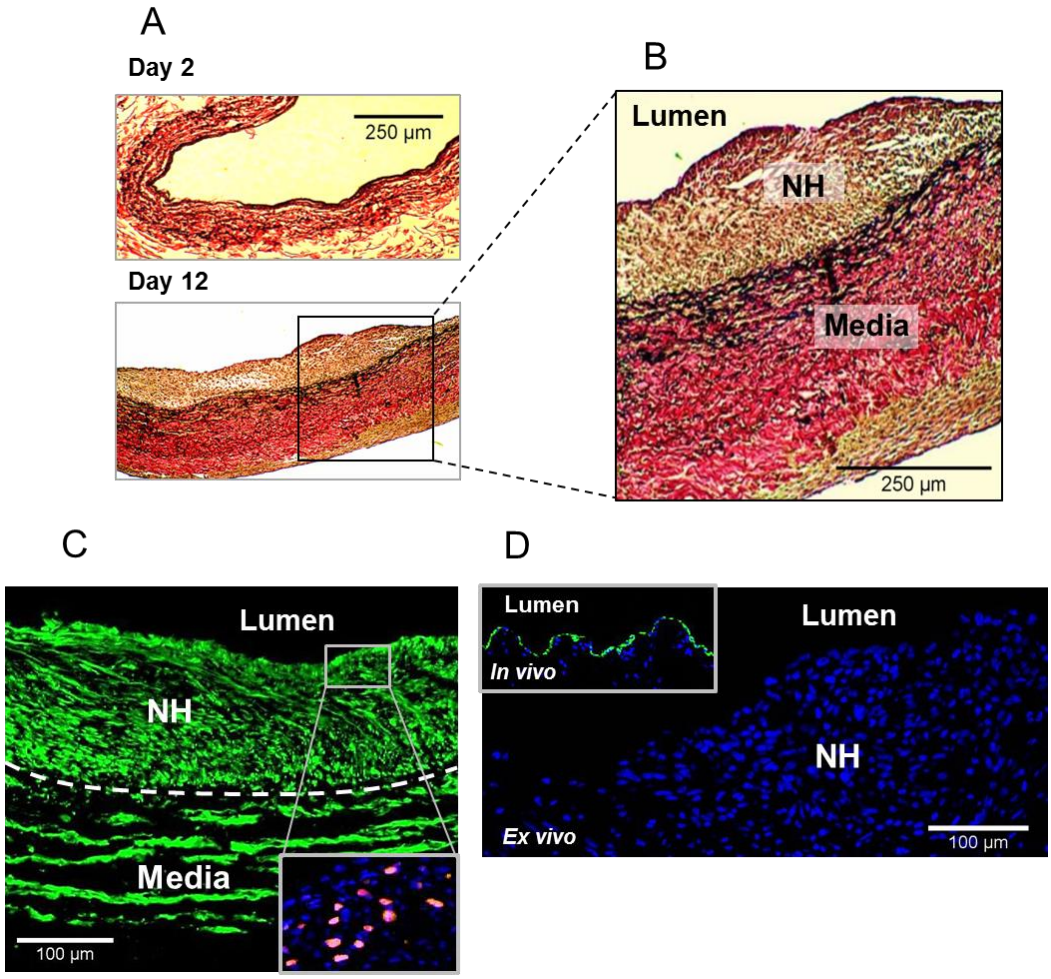

Figure 2.6 NH formation in porcine internal jugular vein (IJV) segments maintained in an ex vivo perfused culture. Porcine IJV segments were exposed to nonphysiological WSS in a perfused culture system for 12 days. N=3. Cross-sections of ex vivo cultured vein were stained with Van Gieson's stain (elastic fibers and nuclei appear black; collagen appears red). Representative cross-sectional views are shown. **A and B.** IJV segment harvested after 2 days of perfused culture shows no NH lesions. Prominent NH lesions were observed after 12 days of perfused culture. **C.** Tissue sections were co-immunostained for smooth muscle α-actin (appearing green) and Ki-67 (appearing pink in the insert) and examined under confocal microscopy at a magnification of x 20. Blue staining denotes cell nuclei and the dashed line demarcates the NH lesion from the media. Cells constituting the lesions co-stained positive for α-actin and Ki-67. **D.** NH lesions formed at the venous anastomosis of an external jugular vein (EJV) in vivo and in ex vivo perfused vein segments were examined for ECs. Tissue sections were assessed at a magnification of x 20. Blue staining denotes cell nuclei. NH lesions formed in EJV 4 weeks after graft implantation had an intact endothelium that stained positive for vWF (appearing green in the insert). NH lesions formed in IJV after 12 days of ex vivo perfused culture were negative for vWF staining.

viability of ex vivo cultured veins. In addition, cells were immunoreactive for smooth muscle α-actin, suggesting that the cells occupying the NH lesions primarily resulted from the migration and proliferation of de-differentiated SMCs and/or transformed myofibroblasts (Figure 2.6C). These histological features are similar to those observed in the NH lesions in our porcine model in vivo. It is important to note, however, that we did not detect an intact endothelium nor any neovessels in the NH lesions (Figure 2.6D). The loss of EC in the venous segment upon ex vivo organ culture was similar to that previously reported by others (5, 11). Notwithstanding the loss of ECs, the key features of NH in our ex vivo model are the same observed in the in vivo model, including proliferation, possible migration, and disorganized appearance of the SMCs. Sunitinib (100 nM) markedly inhibited NH lesion formation in the ex vivo perfused vein segments (Figure 2.7A). The mean I/M area ratio decreased in sunitinib-treated vein segments, as shown in Figure 2.7B (0.38 ± 0.24 vs. 0.13 ± 0.05; N = 3 each; $p < 0.15$) although this difference did not reach statistical significance. The mean I/L area ratio (Figure 2.7B), which takes into consideration variations in the lumen diameters, was significantly decreased (0.45 ± 0.25 vs. 0.04 ± 0.02; N = 3 each; $p < 0.05$). The low level of apoptotic cell death indicates that the inhibitory effect of sunitinib on NH formation was not the result of cell death.

2.5 Discussion

In human specimens retrieved from patients with failed AVGs as well as in tissues obtained from our porcine model of AVG stenosis, angiogenesis has been shown to occur within the NH as well as in the adventitia at the venous anastomosis, accompanied by an increased

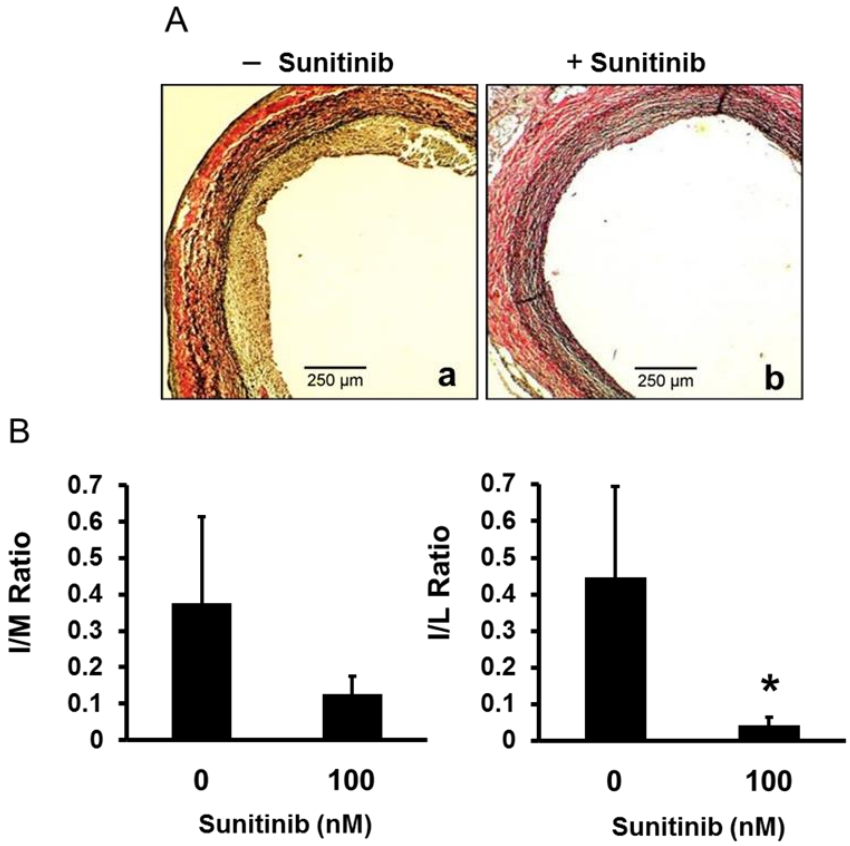

Figure 2.7 Sunitinib inhibits NH formation in porcine internal jugular vein (IJV) segments maintained in an ex vivo perfused culture. A. Representative histological images of the tissue cross-sections (by Van Gieson's stain, x 10) revealed healthy vein walls in both untreated control (panel **a**) and sunitinib (100 nM)-treated vein segments (panel **b**) perfused for 12 days. **B.** The intima-to-media area ratio (I/M ratio) decreased from 0.38 ± 0.24 in the untreated vessels (N = 3) to 0.13 ± 0.05 in the sunitinib-treated vessels (N = 3, $p < 0.15$). The intima-to-lumen area ratio (I/L ratio) decreased from 0.45 ± 0.25 to 0.04 ± 0.02 (*$p < 0.05$).

expression of VEGF and VEGFRs (21, 28, 29, 32). Our in vivo time-course study showed that the density of neovessels within NH lesions gradually increased with NH progression (Figure 2.1). The neovessels likely promote NH development by supplying oxygen and nutrients to the highly proliferative cells, as well as providing a conduit for inflammatory cells that release pro-proliferative and promigratory mediators. Although there was a marked increase in neovessel density in the NH lesions, few Ki-67-positive proliferating cells were observed in the early period (Figure 2.1B). Thus, the mechanism(s) by which early neovessels develop in NH lesions is likely not due to cell proliferation and may result from cell migration. At the same time, an early increase in neovessel density and cell proliferation in the adventitia was observed, followed by an abrupt decrease of both features in that location (Figure 2.1C). While these observations do not prove causality, the strong temporal associations suggest that adventitial angiogenesis and proliferation contribute to subsequent angiogenesis and cell proliferation in the NH lesions. Enhanced adventitial angiogenesis soon after AVG implantation may be the consequence of wound-healing activities following surgical trauma, but the exact underlying mechanism(s) requires further investigation.

It has been proposed that multiple pathogenic factors may contribute to NH development after AVG placement (21). However, the localized nature of NH with strong predisposition to form at the venous anastomosis points toward abnormal blood flow as a crucial pathogenic factor, as shunting of arterial blood flow directly into the vein exposes the vein to an aberrant hemodynamic environment. Previous biomechanics studies have shown that manipulation of certain hemodynamic parameters in the vein, such as hydrostatic pressure or WSS, can induce pathological vessel remodeling, including NH development and wall hypertrophy (11). Here, we

exploited this concept and demonstrated that nonphysiological levels of WSS were associated with NH formation in the explanted porcine vein segments, resembling the lesions observed in vivo. Specifically, we found that the ex vivo NH lesions were comprised primarily of disorganized, proliferating cells that stained positive for smooth muscle α-actin. Importantly, neither untreated nor sunitinib-treated perfused vein segments showed any notable increase in apoptosis, compared to fresh veins or venous anastomotic tissue sections retrieved from our animal model. One difference between the NH lesions in cultured vein (IJV) segments after 12 days of perfusion and the NH at the anastomotic vein (EJV) segments in vivo was the lack of ECs in the cultured vein segments. This endothelial loss was similar to the observation of Clerin et al. and Gusic et al. (5, 11). In these studies, spontaneous endothelium denudation under certain culture conditions during the ex vivo culture of porcine artery and vein segments is described. Further investigations are necessary to determine the cause of endothelial loss and its consequences in the ex vivo culture model.

The value of this ex vivo culture model lies in examining explanted whole-vessel segments under well-defined hemodynamic environments hypothesized to cause NH in vivo. The ex vivo model also provides the opportunity for cell migration and cross-talk within the architectural framework of the native vessel that may be critical for NH development. Finally, this system can be used to assess the responsiveness of the whole-vessel to pharmacological agents.

Antiproliferative, anti-inflammatory and/or antithrombotic agents are logical targets in the development of therapeutic strategies to inhibit NH formation in AVG stenosis (15, 21). In our study, the animals with AVG were maintained on aspirin and clopidogrel to prevent early thrombosis.

Despite successful prevention of early thrombosis, robust NH develops in our porcine model (Figure 2.1). Two antiproliferative agents, paclitaxel and rapamycin, have shown efficacy in inhibiting NH formation in animal AVG models on background aspirin/clopidogrel therapy (17, 21, 22, 34). Paclitaxel and rapamycin directly suppress cell proliferation by stabilizing nuclear mitotic microtubules and inhibiting the mammalian target of rapamycin, respectively (17, 22, 34). The present study explored the potential of targeting different mechanisms of NH formation by exploiting the unique properties of sunitinib. Although sunitinib is known to inhibit the mobility of ECs and certain cancer cells (4, 24, 36, 39), this is the first report that sunitinib inhibits growth factor-stimulated proliferation and migration of normal vascular SMCs (Figures 2.3 and 2.4). We also demonstrated the efficacy of sunitinib in attenuating the formation of venous NH lesions in the ex vivo perfused blood-vessel culture system that reproduces the pathological WSS observed in vivo.

In the context of AVG-induced NH, sunitinib probably exerts multiple effects by antagonizing a variety of RTKs in SMCs and ECs. Major molecular targets of sunitinib include all receptors for PDGF and VEGF, stem-cell factor receptor (KIT), glial cell-derived neurotrophic factor receptor (REarranged during Transfection or RET), colony-stimulating factor 1 receptor (CSF-1R), and Fms-related tyrosine kinase-3 receptor (FLT3), most of which are involved in pro-oncogenic pathways (3, 9, 13, 26). Among these receptors, PDGFRs and VEGFRs, as well as their respective ligand growth factors, are substantially expressed in the NH lesions obtained from the venous anastomotic tissues in our porcine AVG model (Figure 2.2). The expression of other receptors listed above has not been examined in NH. In this study, we demonstrated that sunitinib

blocked signal transduction downstream of RTKs by inhibiting the phosphorylation of key proteins in the MAPK and the PI3K/Akt pathways in SMCs. In addition, we report that sunitinib treatment reversed PDGF-induced changes in the expression of key cell-cycle regulatory proteins. The effects of sunitinib on the MAPK and PI3K/Akt pathways in vascular SMCs, and especially its effects on p70S6k and rpS6, have not been previously reported.

In conclusion, sunitinib was demonstrated to be effective in inhibiting several cellular and intracellular signaling processes associated with NH development in AVGs. Furthermore, sunitinib attenuated NH formation induced by nonphysiological mechanical cues in an ex vivo perfused organ culture system. The long-term efficacy and safety of sunitinib therapy in vivo require further evaluation.

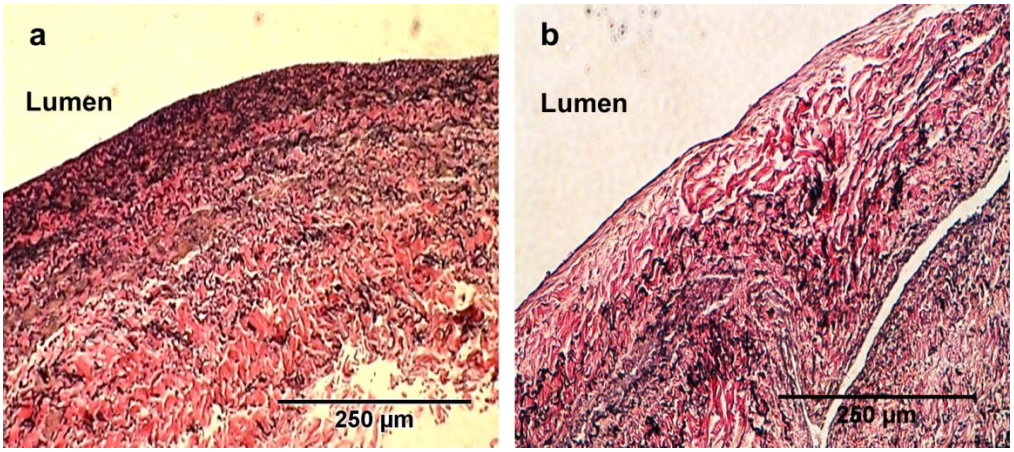

Supplemental Figure 2.1 Vein segments in static culture did not develop NH. Porcine EJV (**a**) and IJV (**b**) segments were cut longitudinally to expose the lumen and cultured in static condition for 14 days in DMEM containing 30% FCS. Cross-sections of cultured vein segments were stained with Van Gieson's stain. No or very little NH lesions were observed under these conditions.

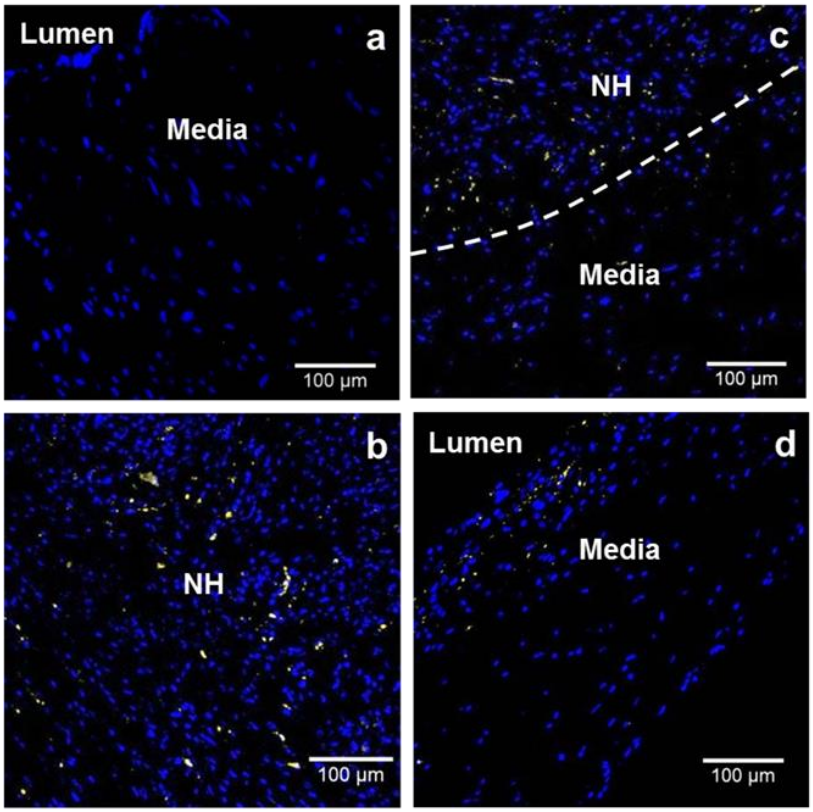

Supplemental Figure 2.2 Low level of apoptotic cell death in porcine jugular veins assessed by the in situ cleaved caspase-3 assay. Apoptotic cells (appearing yellow) in the fresh porcine EJV (panel **a**) were undetectable, in contrast to NH lesions formed in the EJV in a porcine AVG stenosis model (**b**). Both untreated control (panel **c**) and sunitinib-treated (panel **d**) porcine IJV segments perfused ex vivo for 12 days exhibited low levels of apoptosis. Blue staining denotes cell nuclei and the dashed line demarcates the NH lesion from the media.

2.6 References

1. Allon M, Robbin ML. Increasing arteriovenous fistulas in hemodialysis patients: problems and solutions. *Kidney Int* 62: 1109-1124, 2002.

2. Asif A, Gadalean FN, Merrill D, Cherla G, Cipleu CD, Epstein DL, Roth D. Inflow stenosis in arteriovenous fistulas and grafts: a multicenter, prospective study. *Kidney Int* 67: 1986-1992, 2005.

3. Chow LQ, Eckhardt SG. Sunitinib: from rational design to clinical efficacy. *J Clin Oncol* 25: 884-896, 2007.

4. Christensen JG. A preclinical review of sunitinib: a multitargeted receptor tyrosine kinase inhibitor with anti-angiogenic and antitumour activities. *Ann Oncol* 18 (Suppl 10): x3-x10, 2007.

5. Clerin V, Gusic RJ, O'Brien J, Kirshbom PM, Myung RJ, Gaynor JW, Gooch KJ. Mechanical environment, donor age, and presence of endothelium interact to modulate porcine artery viability ex vivo. *Ann Biomed Eng* 30: 1117-1127, 2002.

6. de Boüard S, Herlin P, Christensen JG, Lemoisson E, Gauduchon P, Raymond E, Guillamo JS. Antiangiogenic and anti-invasive effects of sunitinib on experimental human glioblastoma. *Neuro Oncol* 9: 412-423, 2007.

7. Dember LM, Beck GJ, Allon M, Delmez JA, Dixon BS, Greenberg A, Himmelfarb J, Vazquez MA, Gassman JJ, Greene T, Radeva MK, Braden GL, Ikizler TA, Rocco MV, Davidson IJ, Kaufman JS, Meyers CM, Kusek JW, Feldman HI, Dialysis Access Consortium Study Group. Effect of clopidogrel on early failure of arteriovenous fistulas for hemodialysis: a randomized controlled trial. *JAMA* 299: 2164-2171, 2008.

8. Dixon BS, Beck GJ, Vazquez MA, Greenberg A, Delmez JA, Allon M, Dember LM, Himmelfarb J, Gassman JJ, Greene T, Radeva MK, Davidson IJ, Ikizler TA, Braden GL, Fenves AZ, Kaufman JS, Cotton JR Jr, Martin KJ, McNeil JW, Rahman A, Lawson JH, Whiting JF, Hu B, Meyers CM, Kusek JW, Feldman HI; DAC Study Group. Effect of dipyridamole plus aspirin on hemodialysis graft patency. *N Engl J Med* 360: 2191-2201, 2009.

9. Fabian MA, Biggs WH 3rd, Treiber DK, Atteridge CE, Azimioara MD, Benedetti MG, Carter TA, Ciceri P, Edeen PT, Floyd M, Ford JM, Galvin M, Gerlach JL, Grotzfeld RM, Herrgard S, Insko DE, Insko MA, Lai AG, Lélias JM, Mehta SA, Milanov ZV, Velasco AM, Wodicka LM, Patel HK, Zarrinkar PP, Lockhart DJ. A small molecule-kinase interaction map for clinical kinase inhibitors. *Nat Biotechnol* 23: 329-336, 2005.

10. Franke TF, Yang SI, Chan TO, Datta K, Kazlauskas A, Morrison DK, Kaplan DR, Tsichlis PN. The protein kinase encoded by the Akt proto-oncogene is a target of the PDGF-activated phosphatidylinositol 3-kinase. *Cell* 81: 727-736, 1995.

11. Gusic RJ, Myung R, Petko M, Gaynor JW, Gooch KJ. Shear stress and pressure modulate saphenous vein remodeling ex vivo. *J Biomech* 38: 1760-1769, 2005.

12. Joddar B, Shaffer RJ, Reen RK, Gooch KJ. Arterial pO_2 stimulates intimal hyperplasia and serum stimulates inward eutrophic modeling in porcine saphenous veins cultured ex vivo. *Biomech Model Mechanobio.* 10: 161-175, 2011.

13. Karaman MW, Herrgard S, Treiber DK, Gallant P, Atteridge CE, Campbell BT, Chan KW, Ciceri P, Davis MI, Edeen PT, Faraoni R, Floyd M, Hunt JP, Lockhart DJ, Milanov ZV, Morrison MJ, Pallares G, Patel HK, Pritchard S, Wodicka LM, Zarrinkar PP. A quantitative analysis of kinase inhibitor selectivity. *Nat Biotechnol* 26: 127-132, 2008.

14. Kelly BS, Heffelfinger SC, Whiting JF, Miller MA, Reaves A, Armstrong J, Narayana A, Roy-Chaudhury P. Aggressive venous neointimal hyperplasia in a pig model of arteriovenous graft stenosis. *Kidney Int* 62: 2272-2280, 2002.

15. Kent KC, Liu B. Intimal hyperplasia—still there after all these years! *Ann Vasc Surg* 18: 135-137, 2004.

16. Kuji T, Masaki T, Goteti K, Li L, Zhuplatov S, Terry CM, Zhu W, Leypoldt JK, Rathi R, Blumenthal DK, Kern SE, Cheung AK. Efficacy of local dipyridamole therapy in a porcine model of arteriovenous graft stenosis. *Kidney Int* 69: 2179-2185, 2006.

17. Lee BH, Lee JE, Lee KW, Nam HY, Jeon HJ, Sung YJ, Kim JS, Lim HJ, Park JS, Ko JY, Kim DJ. Coating with paclitaxel improves graft survival in a porcine model of haemodialysis graft stenosis. *Nephrol Dial Transplant* 22: 2800-2804, 2007.

18. Li G, Chen SJ, Oparil S, Chen YF, Thompson JA. Direct in vivo evidence demonstrating neointimal migration of adventitial fibroblasts after balloon injury of rat carotid arteries. *Circulation* 101: 1362-1365, 2000.

19. Li L, Blumenthal DK, Terry CM, He Y, Carlson ML, Cheung AK. PDGF-induced proliferation in human arterial and venous smooth muscle cell: Molecular basis for differential effects of PDGF isoforms. *J Cell Biochem* 112: 289-298, 2011.

20. Li L, Terry CM, Blumenthal DK, Kuji T, Masaki T, Kwan BC, Zhuplatov I, Leypoldt JK, Cheung AK. Cellular and morphological changes during neointimal hyperplasia development in a porcine arteriovenous graft model. *Nephrol Dial Transplant* 22: 3139-3146, 2007.

21. Li L, Terry CM, Shiu YE, Cheung AK. Neointimal hyperplasia associated with synthetic hemodialysis grafts. *Kidney Int* 74: 1247-1261, 2008.

22. Masaki T, Rathi R, Zentner G, Leypoldt, JK, Mohammad SF, Burns GL, Li L, Zhuplatov S, Chirananthavat T, Kim SJ, Kern S, Holman J, Kim SW, Cheung AK. Inhibition of neointimal hyperplasia in vascular grafts by sustained perivascular delivery of paclitaxel. *Kidney Int* 66: 2061-2069, 2004.

23. Newby AC, Zaltsman AB. Molecular mechanisms in intimal hyperplasia. *J Pathol* 190: 300-309, 2000.

24. Osusky KL, Hallahan DE, Fu A, Ye F, Shyr Y, Geng L. The receptor tyrosine kinase inhibitor SU11248 impedes endothelial cell migration, tubule formation, and blood vessel formation in vivo, but has little effect on existing tumor vessels. *Angiogenesis* 7: 225-233, 2004.

25. Rekhter M, Nicholls S, Ferguson M, Gordon D. Cell proliferation in human arteriovenous fistulas used for hemodialysis. *Arterioscler Thromb* 13: 609-617, 1993.

26. Roskoski R Jr. Sunitinib: a VEGF and PDGF receptor protein kinase and angiogenesis inhibitor. *Biochem Biophys Res Commun* 356: 323-328, 2007.

27. Rotmans JI, Velema E, Verhagen HJ, Blankensteijn JD, Kastelein JJ, de Kleijn DP, Yo M, PasterKamp G, Stroes ES. Rapid, arteriovenous graft failure due to intimal hyperplasia: a porcine, bilateral, carotid arteriovenous graft model. *J Surg Res* 113: 161-171, 2003.

28. Roy-Chaudhury P, Kelly BS, Melhem M, Zhang J, Li J, Desai P, Munda R, Heffelfinger SC. Vascular access in hemodialysis: issues, management, and emerging concepts. *Cardiol Clin* 23: 249-273, 2005.

29. Roy-Chaudhury P, Kelly BS, Miller MA, Reaves A, Armstrong J, Nanayakkara N, Heffelfinger SC. Venous neointimal hyperplasia in polytetrafluoroethylene dialysis grafts. *Kidney Int* 59: 2325-2334, 2001.

30. Shukla S, Robey RW, Bates SE, Ambudkar SV. Sunitinib (Sutent, SU11248), a small molecule receptor tyrosine kinase inhibitor blocks function of the ATP-binding cassette (ABC) transporters P-glycoprotein (ABCB1) and ABCG2. *Drug Metab Dispos* 37: 359-365, 2009.

31. Singh P, Robbin ML, Lockhart ME, Allon M. Clinically immature arteriovenous hemodialysis fistulas: Effect of US on salvage. *Radiology* 246: 299-305, 2008.

32. Swedberg SH, Brown BG, Sigley R, Wight TN, Gordon D, Nicholls SC. Intimal fibromuscular hyperplasia at the venous anastomosis of PTFE grafts in hemodialysis patients. Clinical, immunocytochemical, light and electron microscopic assessment. *Circulation* 80: 1726-1736, 1989.

33. Terry CM, Blumenthal DK, Sikharam S, Li L, Kuji T, Kern SE, Cheung AK. Evaluation of histological techniques for quantifying hemodialysis arteriovenous (AV) graft hyperplasia. *Nephrol Dial Transplant* 21: 3172-3179, 2006.

34. Terry CM, Li L, Li H, Zhuplatov I, Blumenthal DK, Kim SE, Owen SC, Kholmovski EG, Fowers KD, Rathi R, Cheung AK. In vivo evaluation of the delivery and efficacy of a sirolimus-laden polymer gel for inhibition of hyperplasia in a porcine model of arteriovenous hemodialysis graft stenosis. *J Control Release* 160: 459-467, 2012.

35. Tomas JJ, Stark VE, Kim JL, Wolff RA, Hullett DA, Warner TF, Hoch JR. Beta galactosidase-tagged adventitial myofibroblasts tracked to the neointima in healing rat vein grafts. *J Vasc Res* 40: 266-275, 2003.

36. Tugues S, Fernandez-Varo G, Muñoz-Luque J, Ros J, Arroyo V, Rodés J, Friedman SL, Carmeliet P, Jiménez W, Morales-Ruiz M. Antiangiogenic treatment with sunitinib ameliorates inflammatory infiltrate, fibrosis, and portal pressure in cirrhotic rats. *Hepatology* 46: 1919-1926, 2007.

37. United States Renal Data System, USRDS 2004 Annual Data Report: Atlas of Chronic Kidney Disease and End-Stage Renal Disease in the Unites States, National Institutes of Health, National Institute of Diabetes and Digestive and Kidney Diseases, Bethesda, MD, 2004.

38. van Dijk MC, Hilkmann H, van Blitterswijk WJ. Platelet-derived growth factor activation of mitogen-activated protein kinase depends on the sequential activation of phosphatidylcholine-specific phospholipase C, protein kinase C-zeta and Raf-1. *Biochem J* 325: 303-307, 1997.

39. Xin H, Zhang C, Herrmann A, Du Y, Figlin R, Yu H. Sunitinib inhibition of Stat3 induces renal cell carcinoma tumor cell apoptosis and reduces immunosuppressive cells. *Cancer Res* 69: 2506-2513, 2009.

CHAPTER 3

GENE EXPRESSION ANALYSES OF VEIN REGIONS WITH DIFFERENT SUSCEPTIBILITIES TO NEOINTIMAL HYPERPLASIA IN A PORCINE ARTERIOVENOUS GRAFT STENOSIS MODEL

3.1 Abstract

It is widely accepted that arteriovenous hemodialysis graft (AVG) stenosis develops predominantly as a result of neointimal hyperplasia (NH) formation in susceptible venous anastomotic regions. This important clinical problem has not been resolved due to our limited understanding of the molecular processes involved in the pathophysiology. It is known that the vein regions most susceptible to NH are at the anastomosis, whereas juxta-anastomotic vein regions are relatively resistant to NH. We hypothesize that the gene expression profiles of the NH-prone and nearby NH-resistant vein will be different after graft placement and that these differences could provide important insights into possible therapeutic targets to prevent AVG stenosis. To test this hypothesis, we evaluated the global genomic profiles of NH-prone and NH-resistant vein regions in a porcine model of AVG stenosis. Using a porcine microarray, gene expression changes in these two distinct vein regions were examined at 5 and 14 days following graft placement. Global genomic changes were more dramatic in the NH-prone vein region than in the NH-resistant region at both time points. In the NH-prone region, genes related to regulation of

cell proliferation were most enriched among the significantly up-regulated genes at day 5, while up-regulated genes associated with osteo/chondrogenic vascular remodeling were most enriched at day 14. At both time periods, genes related to muscle phenotype were significantly down-regulated. In the NH-resistant vein region, genomic changes were less prominent. These results provide insights into the spatial and temporal genomic modulation underlying NH formation in AVG, and suggest potential therapeutic strategies to prevent and/or limit AVG stenosis.

3.2 Introduction

Synthetic arteriovenous hemodialysis grafts (AVG) are widely used vascular access conduits for hemodialysis. AVGs are, however, prone to stenosis and subsequent thrombosis and occlusion, leading to primary failure rates that are reported to be 50% and 75% at 1 and 2 years after implantation, respectively (1-4). Localized neointimal hyperplasia (NH) that forms most frequently at the graft-venous anastomosis (hereafter referred to as the venous anastomosis; VA), and less commonly at the graft-arterial anastomosis (arterial anastomosis), is known to be the predominant cause of AVG failure (5). Histological examination of human specimens and tissues from animal AVG stenosis models reveal that the NH lesions are highly cellularized with excessive extracellular matrix (ECM) proteins, inflammatory cells, and micro-neovessels. These changes in the vessel wall can be observed shortly after the AVG placement and progressively increase over time (3, 5, 6). There are currently no therapies to prevent or treat NH formation to achieve long-term AVG patency. Development of effective therapies for NH is impeded largely by our limited understanding of the mechanisms by which the vessel remodels in response to stimuli. It is

postulated that upon graft placement, the venous anastomosis harbors multiple pathogenic components that may play causal roles in the NH formation process, which include enhanced wound healing and inflammatory activities, nonphysiological hemodynamic stress, and the absence of the protective adventitia and endothelium (5, 7-11). As such, venous NH formation may be the result of complex interplay among all residing pathogenic factors, although the precise underlying cellular and molecular events are far from completely understood.

In a porcine model of AVG stenosis that is established in our laboratory, NH formation is localized to the VA and is rarely observed in the distant upstream or downstream vein regions of the VA (i.e., vein region only 1 cm away from the VA, hereafter referred to as the proximal vein (PV)). Because pathogenic factors operating early on in the process of NH formation are expected to trigger a spectrum of gene expression profiles, we hypothesize that the gene expression profiles of the NH-prone (VA) and nearby NH-resistant (PV) vein regions will be different after graft placement and that analysis of the gene expression patterns in the NH-prone region will provide clues regarding potential therapeutic targets to prevent NH. If the VA region is more prone to NH, one possible indication is that there would be a larger number of genes with significantly altered expression compared to the PV region, and that these genes are involved in NH development. To test this hypothesis, we employed a porcine global gene expression microarray to investigate the differential genomic features of the NH-prone vein region and the NH-resistant region relative to a common reference control vein at early time periods following AVG placement. To our knowledge, this is the first investigation of the differential global genomic profiles in these distinct vein regions in a porcine or in other models of AVG.

3.3 Materials and Methods

3.3.1 Materials

All reagents used for RNA isolation including RNA*later* solution, QIAzol Lysis Reagent, and the miRNeasy RNA extraction kit were purchased from Qiagen Inc. (Valencia, CA). Reagents used for microarray labeling and hybridizations were provided by the Microarray Core Facilities at the University of Utah. The porcine 44K (v1) oligonucleotide microarray slides representing 43,803 probes were purchased from Agilent Technologies (Palo Alto, CA). All reagents used for RT-PCR were obtained from Applied Biosystems (Foster City, CA).

3.3.2 Porcine model of AVG stenosis

The porcine AVG stenosis model employed in our laboratory has been previously described (3, 12). Animal surgeries were performed in accordance with a protocol that was approved by the Institutional Animal Care and Use Committees (IACUCs) at the Veterans Affairs Salt Lake City Health Care System and the University of Utah. Female Yorkshire pigs (Sigma Livestock, Salt Lake City, UT) weighing 30-35 kg were used to implant expanded polytetrafluoroethylene (ePTFE) grafts unilaterally between the ipsilateral external jugular vein (EJV) and the common carotid artery (CCA), creating both graft-end-to-vessel-side arterial and venous anastomoses. Sodium heparin was administered during the surgery and aspirin (Pharmaceutical Formulations, Edison, NJ), clopidogrel (Bristol-Myers Squibb, New York, NY), and enrofloxacin (Bayer, Pittsburgh PA) were administered peri-operatively. Graft patency was monitored by Doppler ultrasound until the animals were euthanized at the two indicated time

points, 5 or 14 days post-graft placement. A total of ten operated animals were used to perform gene expression studies. Two animals were subjected to premature euthanasia due to early occlusion of the ePTFE graft, and therefore were not utilized for the microarray experiments. Each time period was N = 4 animals (replication at the level of biology).

Grafted and native vein segments (1 cm each, including a vein segment from the unoperated control EJV on the contralateral side of each operated animal) were retrieved according to the scheme shown in Figure 3.1, and were immediately immersed in RNA*later* solution (Qiagen Inc., Valencia, CA). Immersed vein segments were then kept at 4 °C for no longer than 2 weeks before tissue samples were processed for total mRNA extraction as described below.

3.3.3 RNA extraction, microarray hybridization, and data analysis

Total mRNA was extracted from collected vein sample lysates using the miRNeasy Mini Kit (Qiagen). A small portion (≤ 50 mg) of each vein segment, including the roof and the floor walls as well as any tissue that might have grown inside the lumen, was minced using razor blades. For homogenization, minced samples were further disrupted using a TissueLyser (Qiagen). DNase treatment was included in the extraction procedure to confirm further purification of RNA. RNA concentrations were measured using a spectrophotometer (LAMBDA Bio, PerkinElmer, Waltham, MA). The quality of mRNA was determined using an Agilent Bioanalyzer 2100 (Agilent Technologies) and mRNA integrity was assessed by the RNA integrity number (RIN). If the amount of RNA collected was insufficient or the integrity of RNA was unsatisfactory with an RIN smaller

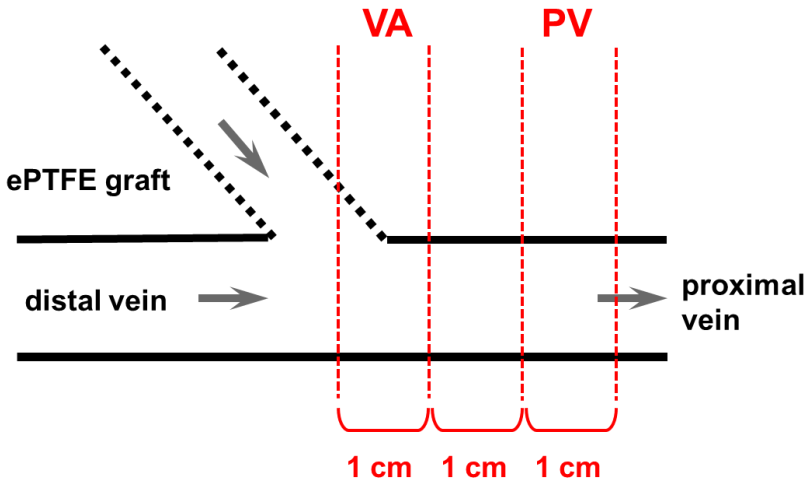

Figure 3.1 Diagrammatic representation of the venous anastomosis (VA) and a vein segment downstream of the VA (PV; proximal vein) of an operated EJV in a porcine AVG stenosis model. NH formation predominantly occurs at the VA and less likely at juxta-anastomotic vein regions, such as in the distal or the proximal EJV segments (distal or proximal relative to the location of the heart). The VA and PV (1 cm length each) segments were collected at day 5 or day 14 following graft placement. An unoperated EJV segment (1 cm length) from the contralaetral side of each animal was also collected as a common reference control sample, which is not shown in the diagram. Samples were immediately immersed in RNA*later* solution upon dissection. Arrows indicate the direction of the blood flow within the AVG.

than 5, RNA extraction was repeated for those specific samples with banked tissue samples.

The Agilent Two-Color Quick Amp Labeling Kit was used to generate fluorescently-labeled complimentary RNA (cRNA) targets. Agilent RNA spike-in controls were combined with input total mRNA samples, which were then primed with oligo (d)T-T7 RNA polymerase promoter oligonucleotide sequences. Complementary DNA (cDNA) synthesis was accomplished through the addition of M-MLV-Reverse Transcriptase. Following cDNA synthesis, T7 RNA polymerase and cyanine 3- or cyanine 5-CTP were combined with the reaction mixtures to simultaneously amplify the materials to generate cRNA targets. Microarray hybridizations were performed using Agilent SureHyb Hybridization chambers according to manufacturer's instructions. Hybridization chambers were loaded onto a rotisserie hybridization oven and were incubated at 65 °C for 17 h, and then washed in Gene Expression Wash Buffer. Microarray slides were briefly dipped in a solution of acetonitrile and then dried. Slides were scanned in an Agilent G2505C Microarray Scanner at 5 μm resolution, which allows simultaneous detection of cyanine 3 and cyanine 5 signals on the hybridized slide. Finally, scanned data were loaded into Agilent Feature Extraction Software (v10.5) for data analysis.

The quality of the microarray data was evaluated by examining the quality control report produced by the Agilent microarray platform. Every array performed passed all eleven quality metrics in Agilent's QC report. Microarray data were filtered to remove values from control features and any features flagged as nonuniform or population outliers. Remaining features from each microarray probe were averaged to yield a single value for each probe. Resulting intensity values were log2-transformed and normalized using median centering.

Normalized data for all probes were clustered in R with the hclust ( ) function, using Euclidean distance and Ward's method. This clustering revealed a batch effect in the data that correlated with the date on which the data were generated. Microarray data were processed in multiple batches over the course of 2 years due to technical and time constraints, and clustering of normalized data revealed a batch effect that correlated with the date on which the data were generated (data not shown). A batch-adjustment analysis was performed using ComBat analysis software (13). Specifically, each microarray was described in a parameter file by the following parameters: sample name, batch number (1 through 4), origin of tissue, and time point of treatment (5 days or 14 days). Given the parameter file and a matrix of normalized microarray data, the ComBat software ComBat estimated factors that correlated with batch number (1 through 4), origin of tissue, and time point of tissue retrieval, and subtracted the batch-related factors while leaving the effects of other covariates. Following batch adjustment, hierarchical clustering revealed that the batch effects were largely controlled, with samples clustering primarily by origin of tissue, and then by time point. Batch-adjusted data were uploaded into GeneSifter® Analysis Edition v3.7 (http://www.genesifter.net, Geospiza, Seattle, WA) for statistical analysis.

Transcripts with mean fold-changes ≥ 4.0 and adjusted ANOVA $p < 0.05$ (Benjamini and Hochberg correction) in either the VA or the PV segment (or both) compared to their corresponding transcripts from common EJV control segments were selected for subsequent analysis. The rather stringent fold-change cut-off with moderate statistical significance across 4 pigs allowed us to efficiently explore the massive microarray data for understanding the most relevant biological significance. Our selection threshold also takes normal gene expression variations reported in the

literature into consideration (14-16). For example, studies report that there can be as much as 4-fold random fluctuations as physiological variance for less tightly regulated genes, such as most of the housekeeping genes, in human tissues. In addition, a threshold of 2-fold or less has been shown to be statistically invalid even for duplicated experiments (15).

After filtering, there were 1392 and 787 transcripts, which included the unannotated transcripts with no accession numbers at day 5 and day 14 post-graft placement, respectively. The Agilent porcine 44K (v1) 60-mer oligonucleotide microarray platform contains 43,803 representing probes. A significant number of probes in this porcine array were unannotated transcripts without accession numbers and could therefore not be utilized for Gene Ontology (GO) studies. These transcripts were only described by the unique Tentative Consensus (TC) identifiers derived from The Institute for Genomic Research (TIGR) Gene Indices, a collection of species-based databases that was constructed for analyzing genes and expressed sequence tag (EST) sequences. Therefore, these transcripts were excluded from further analyses. For incompletely annotated porcine transcripts with accession numbers, we used nucleotide basic local alignment search tool (BLAST) to determine similar sequences in other species using sequence matches above a specified cut-off threshold (≥ 50% matching query-subject coverage and E-value ≤ 10^{-4}). In most cases, the annotated “hit” sequence with the highest total score that fulfilled our specified cut-off threshold criteria was selected. To extract biological information from the patterns of gene expression associated with NH, we used GATHER for identification of enriched biological themes (19). GATHER, a Gene Annotation Tool to Help Explain Relationships, is a web-based ontology algorithm that detects enrichment of GO terms and signatures from high-throughput genomic

experiments. Annotated transcripts significantly altered in each of the two vein regions were separately subjected to GATHER analysis. Also, up- or down-regulated transcripts were separately analyzed. Although there seems to be no gold standard for Bayes Factor cut-offs (a Bayes Factor it is not an absolute decision value as long as it is a positive value), studies have reported that a cut-off of 6 most likely balances false positives and false negatives. A Bayes Factor cut-off of at least 6 was applied to all analyses (19).

3.3.4 Quantitative reverse transcriptase-PCR

Using the same mRNA samples used for microarray studies, we assessed the expression of seven genes of interest by quantitative RT-PCR. Conversion from mRNA to cDNA was conducted using the High Capacity RNA-to-cDNA kit (Applied Biosystems) with a reaction volume of 20 μL. All primer and probe sets were obtained from the inventoried Taqman® Gene Expression Assay for *Sus scrofa* (Applied Biosystems). The PCR reaction in a 20 μL reaction volume was carried out by initializing (50 °C, 2 min followed by 95 °C, 10 min), 40 cycles of denaturation (95 °C, 15 s), and annealing and extension (60 °C, 1 min) using an Applied Biosystems 7300 Real-Time PCR System. PCR amplification efficiencies were similar for all genes tested. Relative gene expression was normalized to the expression of the housekeeping gene, beta-2 microglobulin (B2M), and the comparative C_T method was used to quantify the fold differences in gene expression.

3.4 Results

3.4.1 Spatial and temporal gene expression changes between the VA and PV at day 5 and day 14 post-graft placement

We compared the global gene expression profile changes after filtering the transcripts that satisfied our selection threshold (mean fold-changes ≥ 4.0 and ANOVA $p < 0.05$ in either the VA or the PV segment (or both) compared to the corresponding control EJV samples) at day 5 and day 14 following AVG placement. Our threshold criteria applied to the microarray data identified 1392 and 787 transcripts differentially expressed at day 5 and day 14, respectively, which included the unannotated transcripts with no accession numbers (Figure 3.2; full clustering is shown in Supplemental Figure 3.1). Figure 3.2 illustrates the spatial and temporal global gene expression profiles of the filtered transcripts presented as a microarray heat map (each group N = 4). Clustering of samples showed that the VA and PV are more similar to each other than to the unoperated control EJV segment. At day 14, fewer transcripts were significantly regulated compared to day 5. This temporal difference of the number of significantly altered transcripts may reflect the complexity of very early molecular events (e.g., within a few days) that may contribute to the initial stages of NH development. The unannotated transcripts with no accession numbers were excluded from further data analyses, leaving 801 and 447 filtered transcripts at day 5 and day 14, respectively.

In Figure 3.3, Venn diagrams of the 801 and 447 filtered transcripts at day 5 and day 14, respectively, indicate that a substantial number of significantly regulated transcripts were shared between the two vein regions as well as between the two time points. With only a few exceptions,

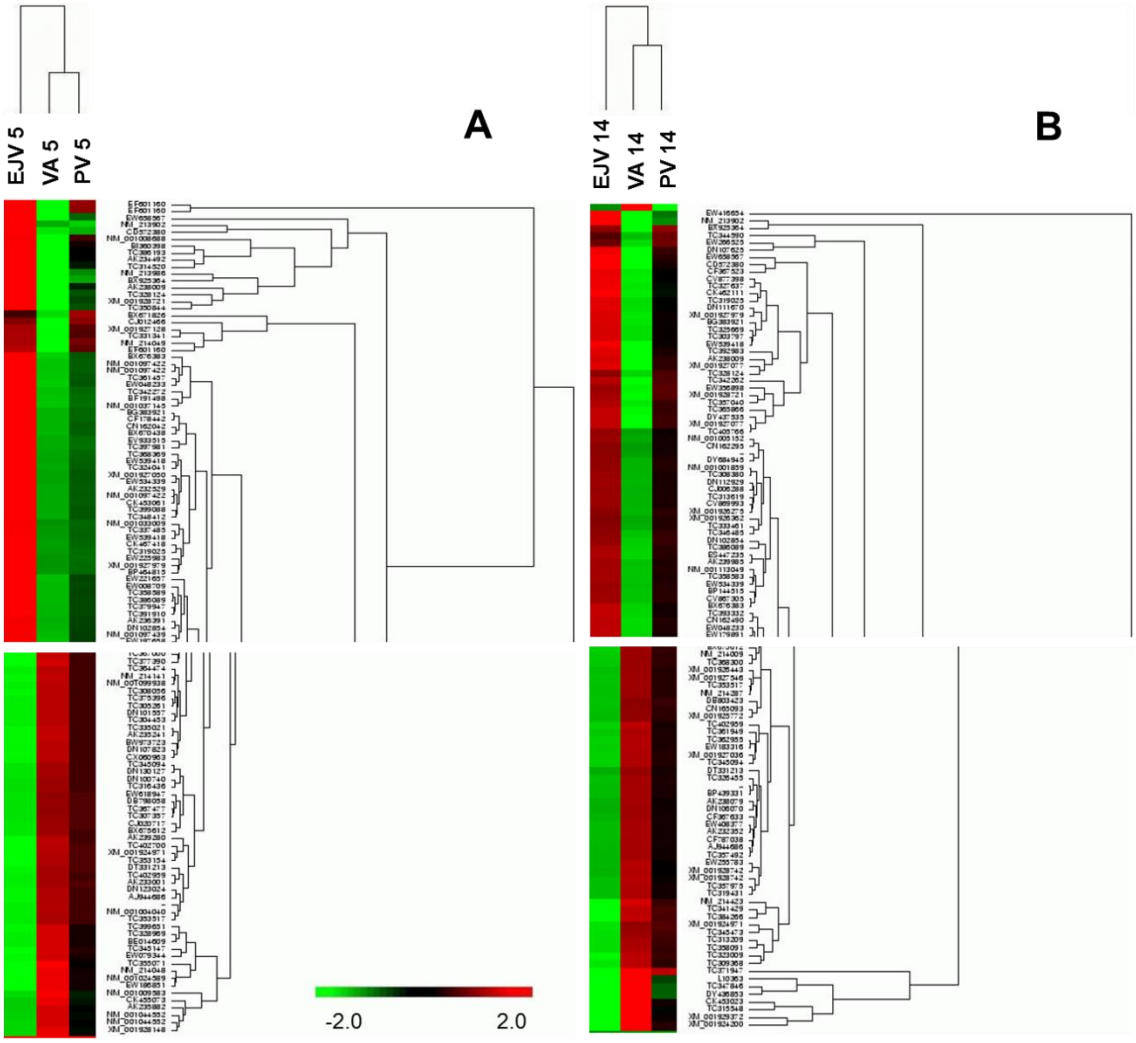

Figure 3.2 The spatial and temporal gene expression profile changes between the VA and PV regions at day 5 (A) and day 14 (B) post-graft placement. GeneSifter identified 1392 and 787 transcripts that met our selection threshold from four independent microarray experiments at day 5 and day 14, respectively. Sample clustering indicates that the VA and PV are more similar to each other than to the unoperated control EJV segment. The microarray heat map shows part of the most greatly regulated portions of the VA and PV cluster analyses. The color-coded scale for log-transformed data is shown at the bottom.

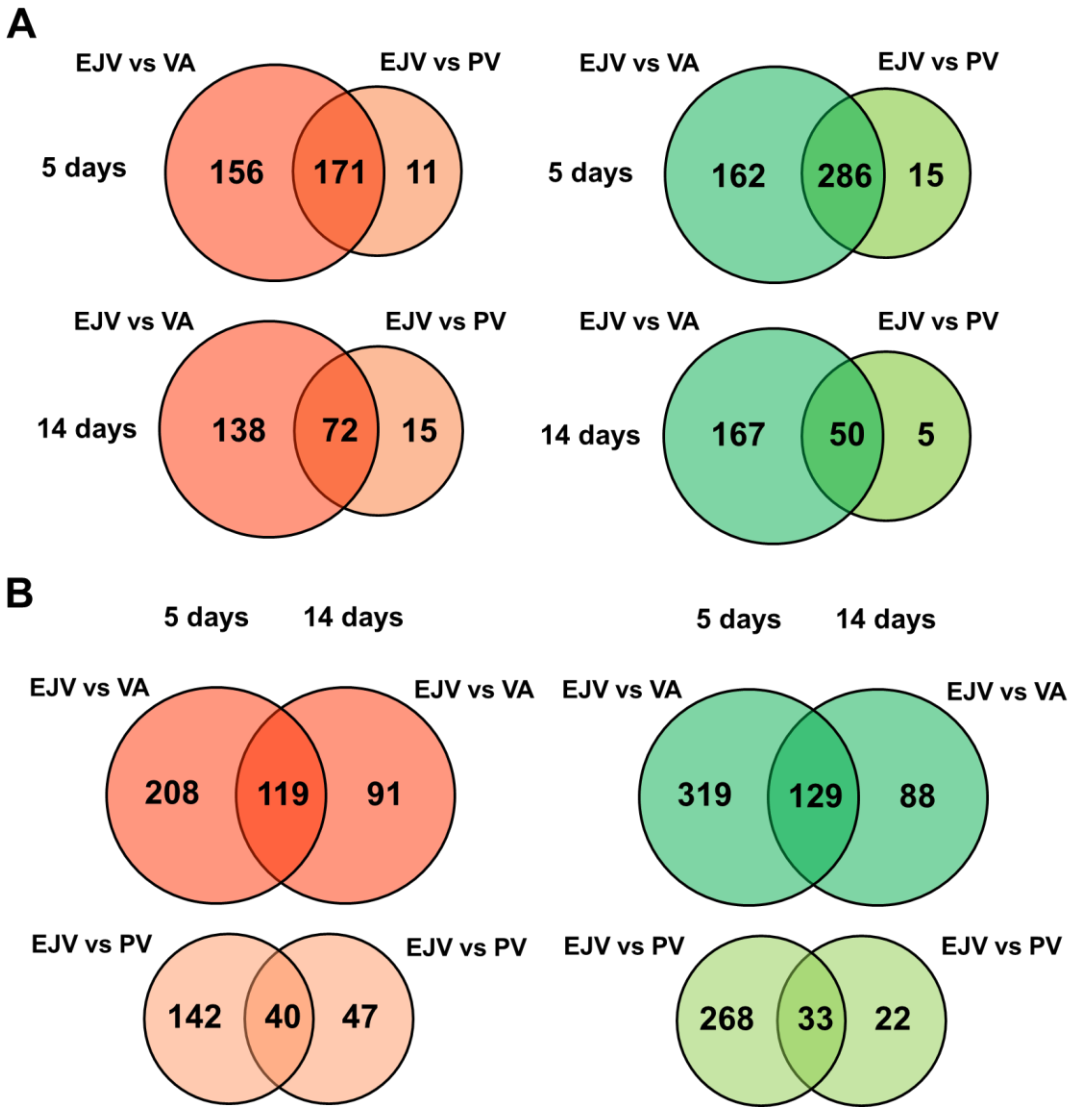

Figure 3.3 Venn diagrams indicating the degree of overlap between the spatially and temporally regulated transcripts in the VA and PV regions. The degree of overlap of 801 and 447 filtered transcripts which are significantly regulated at day 5 and day 14, respectively, is illustrated. **(A)** At both time points following AVG placement, substantial numbers of transcripts whose expressions were up- (red) or down-regulated (green) are regulated in common between the VA and PV. **(B)** The numbers of up- (red) or down-regulated (green) transcripts that temporally overlap between day 5 and day 14 in each vein region are shown. Overall, greater number of transcripts was differentially regulated in the VA than in PV, and at 5 days than at 14 days post-graft placement.

transcripts regulated in one direction in one vein region or time point were regulated in the same direction in the other. Overlapping transcripts satisfied the threshold criteria in both vein regions (Figure 3.3A) or at both time points (Figure 3.3B). These findings suggest that certain molecular events are regulated in common between the two distinct hemodynamic environments. It is also conceivable that there are both early transient gene expression changes as well as early molecular events that were sustained into day 14.

3.4.2 Up-regulated genes with cell proliferation-associated annotations were enriched in the VA and PV at day 5 post-graft placement

We performed GATHER analysis to investigate potential functional relationships of significantly altered transcripts in each of the two vein regions. Because a large number of the gene transcripts selected were incompletely annotated, nucleotide BLAST was used to infer the identity of those porcine transcripts having accession numbers. These incompletely annotated genes were added to those that were fully annotated for subsequent analysis. Among the filtered transcripts described above, incompletely annotated transcripts with no significant BLAST alignments were discarded, and a total of 625 and 387 transcripts for the VA and PV, respectively, were subjected to GATHER analysis for the day 5 time point. Up- or down-regulated transcripts from the microarray data were analyzed separately.

The most significant (Bayes Factor ≥ 6) functional annotations of up-regulated transcripts in the VA represented cell cycle regulation GO terms that putatively participate in the regulation of cell proliferation processes (Table 3.1A). Genes contributing to these terms included cyclins and

Table 3.1 Over-represented Gene Ontology (GO) terms for significantly up-regulated genes at 5 days post-graft placement in the VA (A) and PV (B). (A) At day 5 in the VA, GATHER analysis of the 283 up-regulated transcripts representing 261 genes relative to the control EJV is shown. Significant annotations with Bayes Factor of at least 6 all denote cell cycle-related events. **(B)** At day 5 in PV, GATHER analyzed 162 up-regulated transcripts representing 151 genes relative to the control EJV. A number of significant annotations also displayed association with cell cycle-related events.

A

Gene Ontology ID.	Annotation	p value	Bayes Factor
1. GO:0007067 [8]	Mitosis	< 0.0001	25
2. GO:0000087 [7]	M phase of mitotic cell cycle	< 0.0001	24
3. GO:0000279 [6]	M phase	< 0.0001	24
4. GO:0000278 [6]	Mitotic cell cycle	< 0.0001	23
5. GO:0000280 [7]	Nuclear division	< 0.0001	22
6. GO:0008283 [4]	Cell proliferation	< 0.0001	17
7. GO:0007049 [5]	Cell cycle	< 0.0001	15
8. GO:0000910 [5]	Cytokinesis	< 0.0001	8
9. GO:0000074 [6]	Regulation of cell cycle	0.0001	6
10. GO:0001501 [5]	Skeletal development	0.0001	6
KEGG Pathway	**Annotation**	**p value**	**Bayes Factor**
1. path:hsa04110	Cell cycle	< 0.0001	8
TRANSFAC	**Annotation**	**p value**	**Bayes Factor**
1. V$NFY_01	Nuclear factor Y (Y-box binding factor)	< 0.0001	9

B

Gene Ontology ID.	Annotation	p value	Bayes Factor
1. GO:0007067 [8]	Mitosis	< 0.0001	11
2. GO:0000087 [7]	M phase of mitotic cell cycle	< 0.0001	10
3. GO:0000278 [6]	Mitotic cell cycle	< 0.0001	9
4. GO:0000280 [7]	Nuclear division	< 0.0001	8
5. GO:0000279 [6]	M phase	< 0.0001	8
6. GO:0009628 [5]	Response to abiotic stimulus	0.0001	6

cyclin-dependent kinases (e.g., CCNA2, CCNB1, CCNF, CDC2), nuclear components of mitosis and cytokinesis (e.g., BRRN1, CENPF, KIF23, KNTC2), and transcription factors known to play roles in regulation of cell survival (e.g., E2F8, WT1) (Supplemental Table 3.1). Kyoto Encyclopedia of Genes and Genomes (KEGG) analysis showed that the cell cycle pathway was a significant pathway activated in the VA at day 5, further supporting the GO analysis. Analysis using the TRANSFAC module identified genes with nuclear factor Y (NFY) binding sites as having a meaningful Bayes Factor (Table 3.1A). For up-regulated transcripts in the PV at day 5, a number of the cell cycle regulation terms observed in the VA were also commonly identified as significantly enriched but with lower Bayes Factors (Table 3.1B). These annotations were associated with several of the same genes that contributed to the cell cycle regulation terms in the VA (Supplemental table 3.1). No KEGG pathway terms or TRANSFAC components were identified with a meaningful Bayes Factor in the PV at day 5.

3.4.3 Enrichment of up-regulated genes in the osteo/chondrogenesis pathways in the VA and PV at day 14 post-graft placement

At day 14, progression of venous NH lesions becomes more prominent as the vessels adapt to the new pathological environment. At the molecular level, we expected that the spectrum of expressed genes during this period to be different from that of the earlier 5-day period. A total of 336 and 111 transcripts for the VA and PV, respectively, were subjected to GATHER analysis for the day 14 time point. In the VA, GO analysis of up-regulated transcripts revealed that genes associated with a group of related annotations (*Skeletal Development*, *Ossification*, and *Bone*

Remodeling) were significantly enriched (Table 3.2A). Genes contributing to these terms were also associated with less refined GO classes such as *Morphogenesis*, *Organogenesis*, and *Development* in Table 3.2A. When each gene in these gene sets was explored, we found that several key components of the osteo/chondrogenic pathways (e.g., CDH11, COL11A1, IBSP, SPP1) together with the upstream master transcriptional regulators of bone (RUNX2) and cartilage (SOX9) differentiation were substantially up-regulated in the VA (Supplemental Table 3.1). ECM-receptor interaction was identified as a significant pathway activated in the VA at day 14, and AP-1 transcription factor binding sites were identified in a large number of up-regulated genes. In the PV at day 14, several of the osteo/chondrogenic pathway genes observed in the VA were also significantly up-regulated, and were reflected in the enriched annotations (Table 3.2B). These findings clearly suggest that up-regulation of vascular calcification-related pathways may be important in the pathological development of NH following AVG placement.

3.4.4 Down-regulation of genes associated with muscle physiology in the VA and PV at day 5 post-graft placement

There were also a large number of transcripts down-regulated in both vein regions at day 5. These genes were represented by the *Morphogenesis*, *Organogenesis*, and *Development* terms. GO terms related to muscle contractile phenotype (*Muscle Development* and Muscle *Contraction*) were commonly identified in the VA and PV among the enriched annotations (Table 3.3). Exploration of genes represented by these terms revealed components of muscle cytoskeletal structure and muscle contractile function (e.g., ACTA2, ACTG2, CASQ2, DES, FHL1,

Table 3.2 Over-represented GO terms for significantly up-regulated genes at 14 days post-graft placement in the VA (A) and PV (B). (A) At day 14 in the VA, GATHER analysis of the 171 up-regulated transcripts representing 154 genes relative to the control EJV is shown. Osteo/chondrogenic pathway genes were enriched and were associated with developmental terms. **(B)** At day 14 in the PV, GATHER analyzed 75 up-regulated transcripts representing 70 genes relative to the control EJV. Several of the developmental terms observed in VA were also significantly enriched.

A

Gene Ontology ID.	Annotation	p value	Bayes Factor
1. GO:0001501 [5]	Skeletal development	< 0.0001	10
2. GO:0009653 [3]	Morphogenesis	< 0.0001	10
3. GO:0007155 [4]	Cell adhesion	< 0.0001	10
4. GO:0009887 [4]	Organogenesis	< 0.0001	9
5. GO:0048513 [3]	Organ development	< 0.0001	9
6. GO:0007275 [2]	Development	< 0.0001	8
7. GO:0044237 [4]	Cellular metabolism	< 0.0001	7
8. GO:0001503 [5]	Ossification	< 0.0001	7
9. GO:0046849 [4]	Bone remodeling	< 0.0001	7
10. GO:0030216 [4]	Keratinocyte differentiation	< 0.0001	6
KEGG Pathway	**Annotation**	**p value**	**Bayes Factor**
1. path:hsa04512	ECM-receptor interaction	< 0.0001	8
TRANSFAC	**Annotation**	**p value**	**Bayes Factor**
1. V$AP1_C	AP-1 binding site	< 0.0001	9

B

Gene Ontology ID.	Annotation	p value	Bayes Factor
1. GO:0001501 [5]	Skeletal development	< 0.0001	11
2. GO:0009887 [4]	Organogenesis	0.0001	6
3. GO:0048513 [3]	Organ development	0.0001	6

Table 3.3 Over-represented GO terms for significantly down-regulated genes at 5 days post-graft placement in the VA (A) and PV (B). (A) At day 5 in the VA, GATHER analyzed 342 down-regulated transcripts representing 303 genes relative to the control EJV. Significant occurrences included GO terms related to organ morphogenesis, muscle physiology, and cell adhesion. **(B)** At day 5 in PV, 225 down-regulated transcripts representing 199 genes relative to the control EJV were analyzed. Genes related to organ morphogenesis and muscle contractile phenotype were significantly enriched.

A

Gene Ontology ID.	Annotation	p value	Bayes Factor
1. GO:0007275 [2]	Development	< 0.0001	18
2. GO:0009653 [3]	Morphogenesis	< 0.0001	17
3. GO:0009887 [4]	Organogenesis	< 0.0001	15
4. GO:0048513 [3]	Organ development	< 0.0001	15
5. GO:0007517 [5]	Muscle development	< 0.0001	11
6. GO:0007155 [4]	Cell adhesion	< 0.0001	9
7. GO:0045995 [4]	Regulation of embryonic development	< 0.0001	7
8. GO:0007399 [5]	Neurogenesis	0.0001	6
9. GO:0030155 [4]	Regulation of cell adhesion	0.0001	6
TRANSFAC	**Annotation**	**p value**	**Bayes Factor**
1. V$LDSPOLYA_B	Lentiviral Poly A downstream element	< 0.0001	9
2. V$NRF2_01	Nuclear respiratory factor 2	< 0.0001	8

B

Gene Ontology ID.	Annotation	p value	Bayes Factor
1. GO:0009653 [3]	Morphogenesis	< 0.0001	18
2. GO:0007275 [2]	Development	< 0.0001	18
3. GO:0009887 [4]	Organogenesis	< 0.0001	17
4. GO:0048513 [3]	Organ development	< 0.0001	17
5. GO:0007517 [5]	Muscle development	< 0.0001	15
6. GO:0006936 [3]	Muscle contraction	< 0.0001	7
7. GO:0007399 [5]	Neurogenesis	< 0.0001	7
8. GO:0008016 [5]	Regulation of heart contraction rate	< 0.0001	7

ITGB1BP2, MYOM1, MYH1, MYH11, SGCD), which were also associated with less refined developmental terms described above. *Cell adhesion* was another enriched GO class identified as down-regulated only in the VA, suggesting increased cell motility and plasticity changes during NH pathogenesis. At day 14 in the VA, a few GO terms associated with development were over-represented, as most of the down-regulated transcripts contributing to these terms at day 5 were also significantly down-regulated at day 14 in the VA (Table 3.4). No significant annotations that satisfied our Bayes Factor cut-off were identified at day 14 in the PV.

3.4.5 GO analysis of the genes that are commonly regulated between the VA and the PV

Analysis of the genes that are significantly regulated in both the VA and the PV regions will provide insight into the early molecular and cellular events that broadly impact the damaged venous anastomosis as well as the adjacent vein regions. Up-regulated genes regulating cellular proliferation processes were enriched in these vein regions at day 5, although the relative enrichment of these genes was less significant compared to that in the VA region alone (Table 3.5A). Down-regulated genes were represented by the *Morphogenesis*, *Development*, and *Organogenesis* terms at day 5 (Table 3.5B). Only up-regulated genes displayed a few over-represented GO terms associated with biological development (Table 3.5C) that satisfied the Bayes factor cut-off.

Table 3.4 Over-represented GO terms for significantly down-regulated genes at 14 days post-graft placement in the VA. At day 14 in the VA, GATHER analyzed 165 down-regulated transcripts representing 148 genes relative to the control EJV. No annotations that satisfied our Bayes Factor cut-off were identified at day 14 in the PV.

Gene Ontology ID.	Annotation	p value	Bayes Factor
1. GO:0007275	Development	< 0.0001	9
2. GO:0009653	Morphogenesis	< 0.0001	9
3. GO:0009887	Organogenesis	0.0001	6
4. GO:0048513	Organ development	0.0001	6

Table 3.5 GO analysis of genes that are commonly regulated between the VA and the PV at 5 (A and B) and 14 days (C) post-graft placement. At day 5 in the VA, GATHER analyzed 155 up-regulated transcripts representing 142 genes **(A)** and 215 down-regulated transcripts representing 189 genes **(B)** relative to the control EJV. **(C)** At day 14 in PV, 62 up-regulated transcripts representing 57 genes relative to the control EJV were analyzed.

A

Gene Ontology ID.	Annotation	p value	Bayes Factor
1. GO:0007067 [8]	Mitosis	< 0.0001	11
2. GO:0000087 [7]	M phase of mitotic cell cycle	< 0.0001	11
3. GO:0000278 [6]	Mitotic cell cycle	< 0.0001	9
4. GO:0000280 [7]	Nuclear division	< 0.0001	9
5. GO:0000279 [6]	M phase	< 0.0001	8
6. GO:0007049 [5]	Cell cycle	< 0.0001	6

B

Gene Ontology ID.	Annotation	p value	Bayes Factor
1. GO:0009653 [3]	Morphogenesis	< 0.0001	18
2. GO:0007275 [2]	Development	< 0.0001	17
3. GO:0009887 [4]	Organogenesis	< 0.0001	16
4. GO:0048513 [3]	Organ development	< 0.0001	16
5. GO:0007517 [5]	Muscle development	< 0.0001	13
6. GO:0007399 [5]	Neurogenesis	< 0.0001	8

C

Gene Ontology ID.	Annotation	p value	Bayes Factor
1. GO:0001501 [5]	Skeletal development	< 0.0001	9
2. GO:0009887 [4]	Organogenesis	< 0.0001	7
3. GO:0048513 [3]	Organ development	< 0.0001	7
4. GO:0009628 [5]	Response to abiotic stimulus	< 0.0001	7
5. GO:0009653 [3]	Morphogenesis	< 0.0001	7

3.4.6 Enriched biological properties and functions based on GO classifications in the VA

We assigned each transcript that was either significantly up- or down-regulated in the VA to a biological property provided by the GATHER analysis (Figure 3.4). Since a given gene could be associated with multiple functional descriptors at different level of detail (depth of GO terms), we used the less-refined annotations at the same depth to categorize the transcripts to its key biological property. Functional classification indicated a marked increase in a cluster of up-regulated transcripts involved in *Cell Proliferation* at day 5, which did not persist into day 14. A cluster defined by *Organogenesis* that encompasses the osteo/chondrogenic terms in the up-regulated transcripts was more prominent at day 14. Among the down-regulated transcripts in the VA, the *Metabolism*, *Cell Adhesion/motility*, and *Organogenesis* clusters comprised substantial proportions of down-regulated genes at both time points.

3.4.7 RT-PCR of expression of selected genes

To validate our microarray results, we selected seven genes of interest and performed RT-PCR for the same RNA samples used for our microarray studies. The seven genes are the key components of the osteo/chondrogenic pathways that were significantly up-regulated in the VA (IBSP, SPP1, MMP9), muscle phenotype-specific genes significantly down-regulated in VA (CKM, ACTA2, CNN1), and a gene whose expression in the VA was not significantly altered compared to control EJV in the microarray study (ETS1). Microarray expression profiles of these genes in VA and PV are shown in Supplemental Table 3.1.

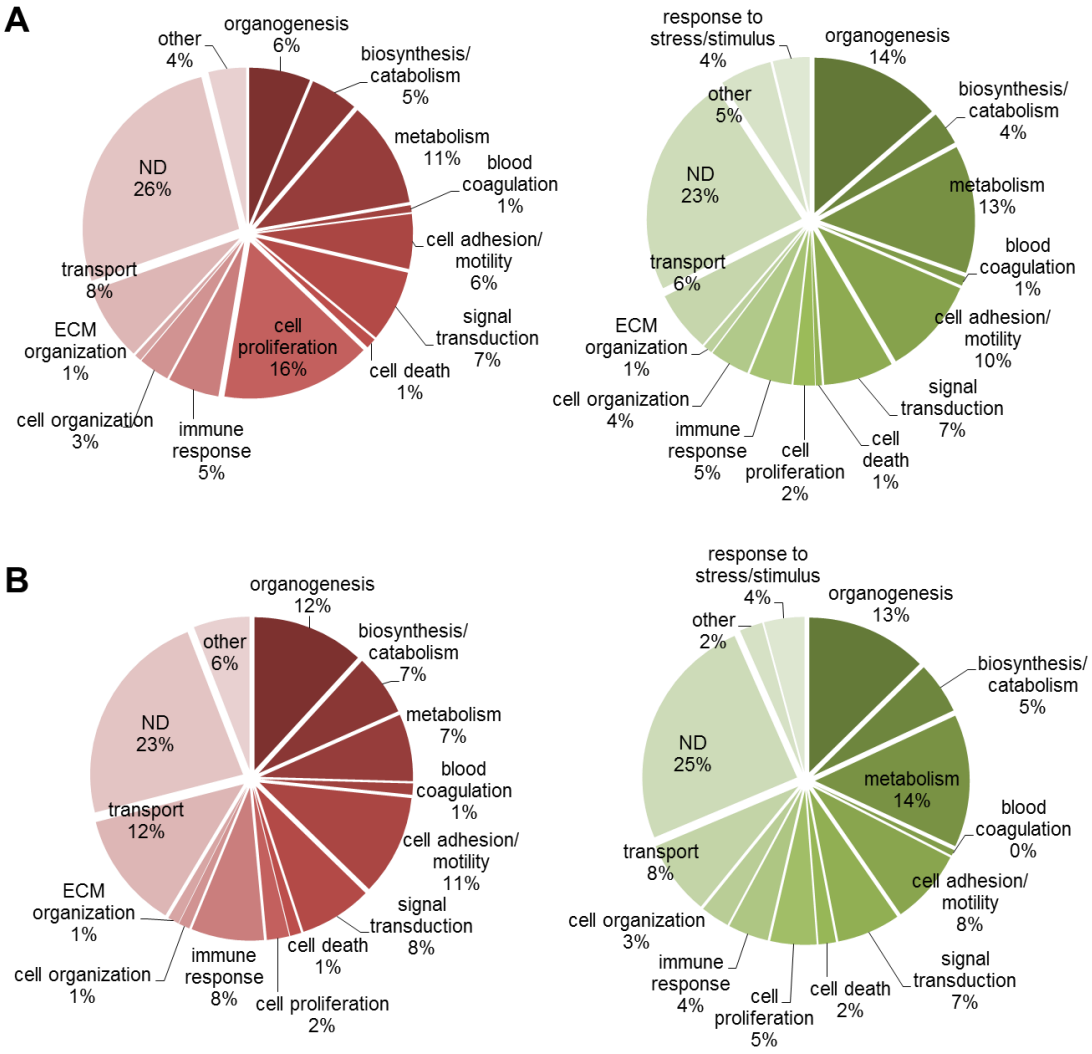

Figure 3.4 Enriched biological properties based on GO analyses in the VA. Each transcript analyzed by GATHER at 5 **(A)** and 14 **(B)** days post-graft placement was assigned to a GO term that describes its key biological properties. Pie charts show the proportion of up- (red circle) or down-regulated (green circle) genes involved in the indicated biological properties. A significant proportion of up-regulated transcripts at day 5 were classified into the *Cell Proliferation* category. At both time points, classification of down-regulated transcripts included substantial proportion of the *Organogenesis* category.

The expression of the housekeeping gene beta2 microglobulin (B2M) was used as a control gene for PCR. Figure 3.5 demonstrates that the PCR results generally agree well with the microarray studies in that IBSP, SPP1, and MMP9 were substantially up-regulated in both the VA and PV, although up-regulation of MMP9 at day 14 was not detected as significantly changed by microarray. There was a trend that CKM, ACTA2, and CNN1 were down-regulated, which was more prominent in the VA at 5 days. Expression of ETS1 was relatively stable at both time points.

3.5 Discussion

Incomplete understanding of the cellular and molecular mechanisms underlying the pathophysiology of venous NH formation in AVG motivated us to investigate the different genomic signatures of NH-prone and NH-resistant vein segments in a porcine model of AVG stenosis. This animal model recapitulates the AVG pathophysiology of humans, and venous NH formation is typically observed as early as a few days after the AVG placement and rapidly progresses over time, eventually resulting in stenosis and occlusion of the graft within several months (3, 5, 6). This accelerated development of NH in pigs enables us to efficiently study the early as well as the later changes in the development of NH. In our present study, examination of the VA and PV regions revealed different gene expression profiles in these vein regions that have different susceptibility to NH. We also demonstrated the differential transcription profiles in these regions at day 5 versus day 14 following AVG placement, a period characterized by early histological evidence of NH development (3).

Genomic studies involving animal models that are relatively less popular have been facing

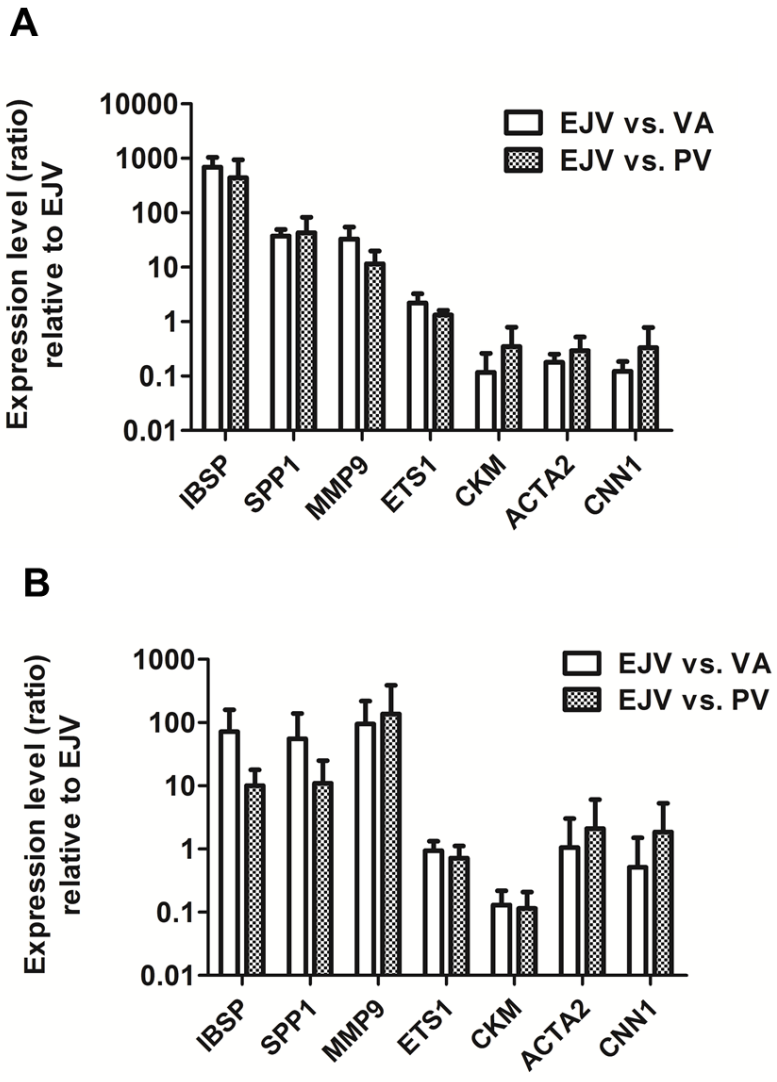

Figure 3.5 Quantitative RT-PCR measurement of seven select genes at 5 (A) and 14 (B) days post-graft placement. To confirm the microarray results of the expression of key genes in the VA and PV relative to the control EJV, RT-PCR was performed to analyze the gene expression levels for the same mRNA samples used for microarray experiments (N=4 for each data point). Error bars indicate standard deviation (SD).

challenges with the incomplete and sometimes incorrect annotation of the genome. The first draft sequencing of the domestic pig (*Sus scrofa*) genome was accomplished by the International Swine Genome Sequencing Consortium (SGSC) in 2009, an effort led by the Wellcome Trust Sanger Institute. A revised and improved annotation was released at the end of 2012 (18, 19). Adding to this work, researchers have been collecting pig-expressed genes by a large-scale expressed sequence tag (EST) analysis and sequencing of entire cDNA clones using full-length-enriched cDNA libraries (20). Although an important advancement for livestock science and biomedical research, it will take time until the pig genome is as fully and accurately annotated as human or other model organisms such as mouse. As such, the current incomplete status of the pig genome annotation has limited our efforts to identify all of the porcine probes of interest in our microarray experiments, among the 43,803 probes represented in the Agilent porcine array.

Analysis of the genomic signatures revealed that the most significant genes up-regulated in the VA and PV at day 5 following AVG placement have strong cell proliferation-associated annotations. These findings coincide with previous studies reporting the highly proliferative early stage of AVG NH development involving proliferation of smooth muscle cells (SMCs) and/or myofibroblasts (2, 3, 5-7, 21, 22). Our present results may also provide insight into which specific genes or pathways are implicated in the cell proliferation processes. Therapeutic strategies targeting cell proliferation at this early stage of NH development, therefore, may be more effective than aiming to inhibit proliferation at a later stage. Figure 3.6 proposes a time-course change in NH formation in the VA, and at least two distinct phases of NH development characterized by an early cellularized growth phase transitioning into a later cell/matrix remodeling phase. It is

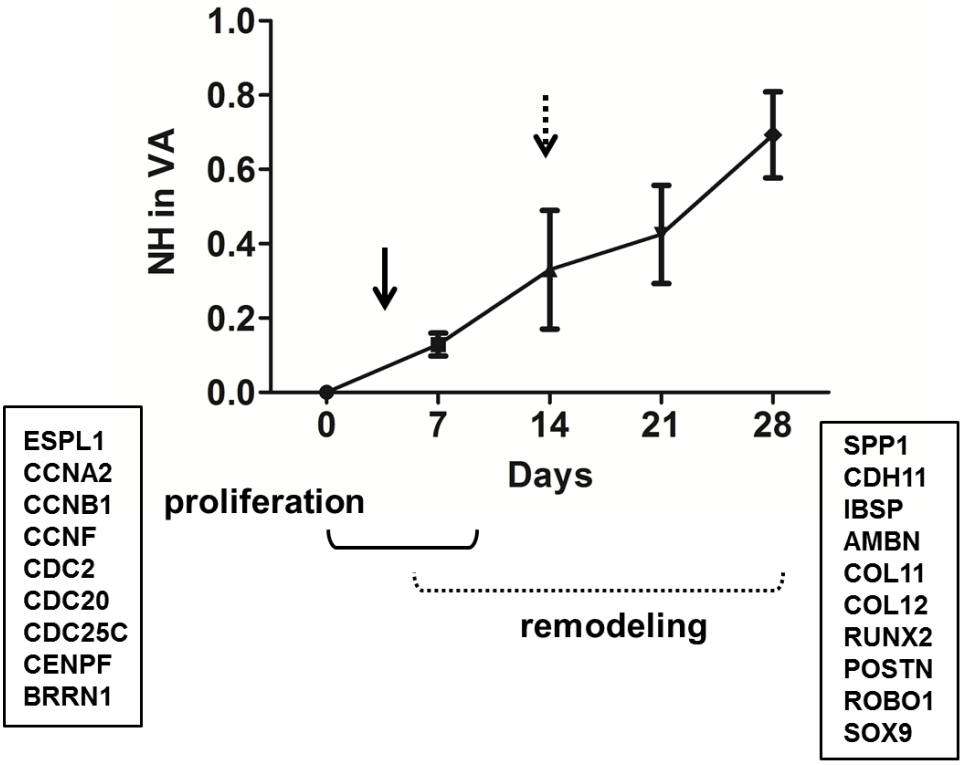

Figure 3.6 Time-course progression of NH index in the VA and early and late pathologic events proposed to contribute to venous NH development. In anastomotic tissue sections obtained from our porcine model of AVG stenosis, NH index in VA increases over time (3). Our current genomic studies suggest that the early phase of NH formation may be characterized by enhanced cellularity driven by highly proliferative vascular cells. The later phase, however, may involve more prevailing cell/matrix remodeling, resulting in neointimal expansion. A list of key genes potentially contributing to each phase based on the microarray data is shown. Arrows indicate day 5 and 14 post-graft placement.

interesting that the PV, a relatively NH-resistant vein region, also demonstrates enrichment of cell proliferation-associated genes at this time point, although such events appeared less prominent in this region compared to the VA.

At day 14, we identified cellular events that have not been extensively reported in NH pathophysiology; *Skeletal Development*, *Ossification*, and *Bone Remodeling*. These events were also detected in the VA at day 5, although the relative importance of this gene set enrichment was diluted by up-regulation of many genes with cell proliferation-associated terms. This suggests that osteo/chondrogenic activities may take place early in NH initiation and is sustained for at least 2 weeks. Tyson et al. demonstrated that vascular SMCs can exhibit osteo/chondrocytic phenotypes that correlated with the enhanced expression of mineralization-regulating proteins in calcified atherosclerotic plaques (23). The markers of calcification they tested included Sox9, Runx2 (Cbfa1), and Ibsp, along with a few other osteo/chondrocyte-specific proteins. We were also able to identify a number of significantly up-regulated genes in the osteo/chondrogenic pathways from our gene set that are transcriptional targets of Sox9 and Runx2. These include SPP1, MMP9, MMP13, COL11A1, and SPARC, which were not directly tested by Tyson et al. The precise nature of vascular mineralization remains under investigation, although a few different hypotheses have attempted to explain its origin in response to pathogenic stimuli in arteries (24). Given the knowledge that calcification is actively suppressed in fully contractile, differentiated arterial SMCs (23, 25, 26), our findings imply that venous NH in AVG may share fundamental similarities with osteo/chondrogenic vascular remodeling that occurs frequently in arterial diseases such as coronary artery disease. In addition, IBSP was shown to be implicated in angiogenesis as a

mediator of endothelial cell adhesion and chemotactic migration (27), and SPP1 may be involved in promoting vascular SMC proliferation (28). Whether these factors play a pivotal causal role in NH formation requires further investigation.

As part of vascular structural remodeling in response to pathogenic cues, SMCs can adapt to perform various functions that are reflected in different SMC phenotypes; specifically contractile and synthetic phenotypes, with a range of intermediate phenotypes (29, 30). Previous studies have proposed that SMCs in NH lesions may dedifferentiate to more efficiently respond to injury and subsequent wound-healing activities, and along with changes in proliferation and migration potentials; the down-regulation of expression of SMC contractile genes would also be expected to occur in the dedifferentiated state (31-33). In fact, many down-regulated genes in our gene sets (e.g., ACTG2, DES, FHL1, MYOM1, MYH11, ITGB1BP2) are putative transcriptional targets of serum response factor (SRF), a master regulator of the SMC contractile apparatus (34). Our data demonstrating the down-regulation of muscle structural components and contractile apparatus support this proposal and point to a strong connection between SMC phenotypic conversion and NH development in AVG. It would be interesting to know whether inhibition of SMC phenotypic plasticity could attenuate the progression of NH lesions in AVG.

We originally hypothesized that the gene expression profiles of the VA and PV will be different after AVG placement as the susceptibility to NH in the two distinct vein regions is different. There are a few factors that could influence this difference; the presence of surgical injuries and the graft material in the VA, and the more disturbed anastomotic hemodynamic environment. Our results suggest that the gene expression profiles did not clearly distinguish the VA from PV as a

number of cellular and molecular events appear to occur in common between the VA and PV. However, a larger number of genes were significantly regulated in the VA, and the relative enrichment of a series of genomic events was more prominent in the VA compared to the PV. A thorough understanding of these underlying molecular changes is expected to provide insight into the rational development of new therapeutic strategies that can improve the long-term performance of AVG. Our findings are also complementary to genomic and proteomic studies investigating hyperplasia-relevant pathways of NH formation in arterial diseases and other types of vein graft conduits (35-37).

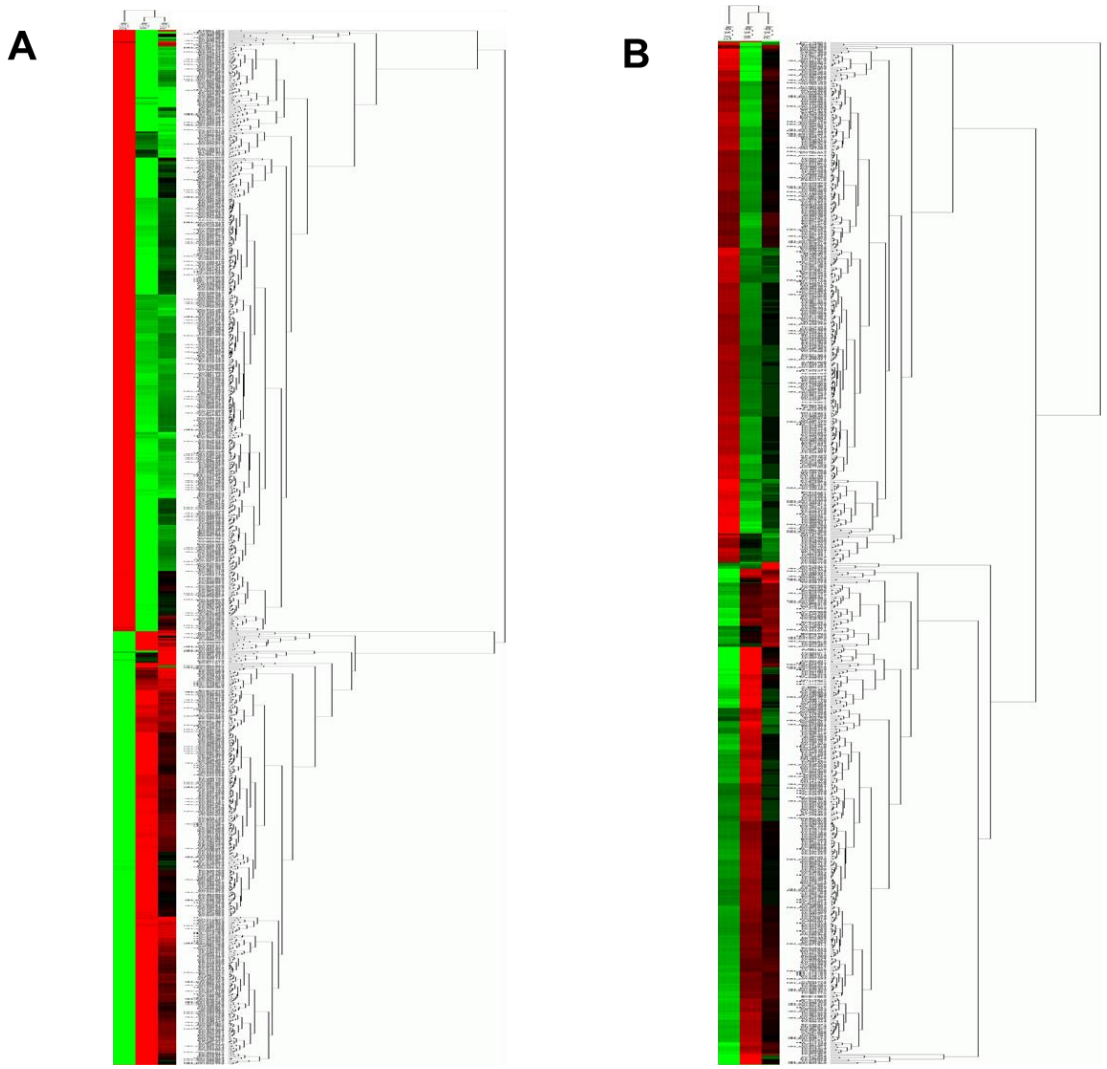

Supplemental Figure 3.1 The spatial and temporal gene expression profile changes between the VA and PV regions at day 5 (A) and day 14 (B) post-graft placement (full clustering).

Supplemental Table 3.1 Differential expression of the key genes between the VA and PV at day 5 and day 14 post-graft placement.

	Day 5				Day 14			
	VA		PV		VA		PV	
Gene Symbol	Log ratio	p Value	Log ratio	p Value	Log ratio	p Value	Log ratio	p Value
ESPL1	2.8	<0.0003	N/S		N/S		N/S	
CCNA2	2.6	<0.0002	N/S		N/S		N/S	
CCNB1	4	<0.0001	2.6	<0.002	N/S		N/S	
CCNF	2.8	<0.003	N/S		N/S		N/S	
CDC2	3.6	<0.0001	2.6	<0.0004	N/S		N/S	
CDC20	3.5	<0.002	2.3	<0.02	N/S		N/S	
CDC25C	2.8	<0.0003	N/S		N/S		N/S	
CENPF	3.5	<0.0002	2.3	<0.003	N/S		N/S	
BRRN1	2.3	<0.002	N/S		N/S		N/S	
KIF23	2.8	<0.0001	N/S		N/S		N/S	
PTTG1	2.8	<0.0002	N/S		N/S		N/S	
KNTC2	3	<0.0002	2	<0.003	N/S		N/S	
SPP1	4.8	<0.0004	4.4	<0.0008	5.4	<0.002	3.6	<0.02
CDH11	2.6	<0.007	N/S		2.3	<0.006	N/S	
IBSP	8	<0.0001	5.8	<0.0001	6.5	<0.002	N/S	
AMBN	N/S		N/S		2.8	<0.003	N/S	
COL11A1	4.5	<0.003	3.3	<0.02	7.3	<0.0001	3.7	<0.0003
COL12A1	2.8	<0.0001	2.8	<0.0001	3	<0.0001	2	<0.0002
RUNX2	4.8	<0.0004	3.5	<0.003	4.2	<0.0001	2.3	<0.004
POSTN	N/S		N/S		3	<0.0003	N/S	
ADAM12	3	<0.0004	2	<0.003	3	<0.0003	N/S	
MATN3	N/S		N/S		2.3	<0.02	2	<0.04
ROBO1	3.8	<0.0003	2.6	<0.004	3.6	<0.0002	N/S	
SOX9	2.8	<0.0002	3.2	<0.0001	3.6	<0.0001	2	<0.0001
LAMA3	-2.3	<0.0004	N/S		N/S		N/S	
ROBO2	-4.5	<0.0001	-2.8	<0.0007	N/S		N/S	
ACTG2	-2.3	<0.005	-2.3	<0.006	N/S		N/S	
CACNA1H	-2.6	<0.0007	-2.3	<0.003	N/S		N/S	
CACNB2	-2.8	<0.001	-2.3	<0.004	N/S		N/S	
CASQ2	-3.6	<0.002	-3	<0.005	-2.3	<0.04	N/S	
DES	-2.6	<0.01	-2.3	<0.02	-2	<0.05	N/S	
FHL1	-2.6	<0.0002	-2	<0.0006	N/S		N/S	
ITGB1BP2	-3.2	<0.003	-2.8	<0.006	-3.2	<0.003	-2.3	<0.02
MYH1	-2.6	<0.003	N/S		-2	<0.02	N/S	
MYH11	-3.3	<0.0009	-3	<0.002	-2.8	<0.006	-2.3	<0.03
MYOM1	-2.6	<0.0005	-2.3	<0.0009	N/S		N/S	

Supplemental Table 3.1 (continued).

	Day 5				Day 14			
	VA		PV		VA		PV	
Gene Symbol	Log ratio	p Value	Log ratio	p Value	Log ratio	p Value	Log ratio	p Value
ODZ1	-2	<0.0005	N/S		N/S		N/S	
SOX6	-2.3	<0.002	N/S		N/S		N/S	
SPOCK2	-2.3	<0.0007	-2	<0.003	N/S		N/S	
ADAM23	-3.2	<0.0001	-3.5	<0.0001	-2.3	<0.02	N/S	
FEZ1	-3.2	<0.0004	-2.6	<0.002	-3.2	<0.0008	N/S	
NTRK2	-5	<0.0001	-2.3	<0.02	-2	<0.008	N/S	
NTRK3	-2.6	<0.0003	-2	<0.001	-2	<0.006	N/S	
SHOX2	-3	<0.0002	-2.6	<0.0005	-2	<0.002	N/S	
SLIT3	N/S		N/S		-2.3	<0.005	N/S	
CALML4	-3	<0.004	-2.6	<0.01	-2.3	<0.007	N/S	
EFNA5	N/S		N/S		-2	<0.0001	N/S	
MMP9	2.6	<0.03	N/S		N/S		N/S	
CKM	2.3	<0.001	N/S		N/S		N/S	
ACTA2	-2.3	<0.0005	-2.3	<0.0003	N/S		N/S	
CNN1	-2.8	<0.002	-2.6	<0.004	-2.6	<0.007	-2.3	<0.02

3.6 References

1. Allon M, Robbin ML. Increasing arteriovenous fistulas in hemodialysis patients: problems and solutions. *Kidney Int* 62: 1109-1124, 2002.

2. Roy-Chaudhury P, Kelly BS, Melhem M, Zhang J, Li J, Desai P, Munda R, Heffelfinger SC. Vascular access in hemodialysis: issues, management, and emerging concepts. *Cardiol Clin* 23: 249-273, 2005.

3. Li L, Terry CM, Blumenthal DK, Kuji T, Masaki T, Kwan BC, Zhuplatov I, Leypoldt JK, Cheung AK. Cellular and morphological changes during neointimal hyperplasia development in a porcine arteriovenous graft model. *Nephrol Dial Transplant* 22: 3139-3146, 2007.

4. United States Renal Data System, USRDS 2012 Annual Data Report: Atlas of Chronic Kidney Disease and End-Stage Renal Disease in the Unites States, National Institutes of Health, National Institute of Diabetes and Digestive and Kidney Diseases, Bethesda, MD, 2012.

5. Li L, Terry CM, Shiu YE, Cheung AK. Neointimal hyperplasia associated with synthetic hemodialysis grafts. *Kidney Int* 74: 1247-1261, 2008.

6. Roy-Chaudhury P, Kelly BS, Miller MA, Reaves A, Armstrong J, Nanayakkara N, Heffelfinger SC. Venous neointimal hyperplasia in polytetrafluoroethylene dialysis grafts. *Kidney Int* 59: 2325-2334, 2001.

7. Mitra AK, Gangahar DM, Agrawal DK. Cellular, molecular and immunological mechanisms in the pathophysiology of vein graft intimal hyperplasia. *Immunol Cell Biol* 84: 115-124, 2006.

8. Haruguchi H, Teraoka S. Intimal hyperplasia and hemodynamic factors in arterial bypass and arteriovenous grafts: a review. *J Artif Organs* 6: 227-235, 2003.

9. Hofer M, Rappitsch G, Perktold K, Trubel W, Schima H. Numerical study of wall mechanics and fluid dynamics in end-to-side anastomoses and correlation to intimal hyperplasia. *J Biomech* 29: 1297-1308, 1996.

10. Radomski MW, Palmer RM, Moncada S. The anti-aggregating properties of vascular endothelium: interactions between prostacyclin and nitric oxide. *Br J Pharmacol* 92: 639-646, 1987.

11. McGeachie JK, Meagher S, Prendergast FJ. Vein-to-artery grafts: the long term development of neointimal hyperplasia and its relationship to vasa vasorum and sympathetic innervation. *Aust N Z J Surg* 59: 59-65, 1989.

12. Kuji T, Masaki T, Goteti K, Li L, Zhuplatov S, Terry CM, Zhu W, Leypoldt JK, Rathi R, Blumenthal DK, Kern SE, Cheung AK. Efficacy of local dipyridamole therapy in a porcine model of arteriovenous graft stenosis. *Kidney Int* 69: 2179-2185, 2006.

13. Johnson WE, Rabinovic A, Li C. Adjusting batch effects in microarray expression data using Empirical Bayes methods. *Biostatistics* 8: 118-127, 2007.

14. King HC, Sinha AA. Gene expression profile analysis by DNA microarrays: promise and pitfalls. *JAMA* 286: 2280-2288, 2001.

15. Claverie JM. Computational methods for the identification of differential and coordinated gene expression. *Hum Mol Genet* 8: 1821-1832, 1999.

16. McCarthy DJ, Smyth GK. Testing significance relative to a fold-change threshold is a TREAT. *Bioinformatics* 25: 765-771, 2009.

17. JT Chang, JR Nevins. GATHER: A Systems Approach to Interpreting Genomic Signatures. *Bioinformatics* 22: 2926-2933, 2006.

18. Archibald AL, Bolund L, Churcher C, Fredholm M, Groenen MA, Harlizius B, Lee KT, Milan D, Rogers J, Rothschild MF, Uenishi H, Wang J, Schook LB; Swine Genome Sequencing Consortium. Pig genome sequence – analysis and publication stratery. *BMC Genomics* 11: 438, 2010.

19. Groenen MA, Archibald AL, Uenishi H, Tuggle CK, Takeuchi Y, Rothschild MF, Rogel-Gaillard C, Park C, Milan D, Megens HJ, Li S, Larkin DM, Kim H, Frantz LA, Caccamo M, Ahn H, Aken BL, Anselmo A, Anthon C, Auvil L, Badaoui B, Beattie CW, Bendixen C, Berman D, Blecha F, Blomberg J, Bolund L, Bosse M, Botti S, Bujie Z, Bystrom M, Capitanu B, Carvalho-Silva D, Chardon P, Chen C, Cheng R, Choi SH, Chow W, Clark RC, Clee C, Crooijmans RP, Dawson HD, Dehais P, De Sapio F, Dibbits B, Drou N, Du ZQ, Eversole K, Fadista J, Fairley S, Faraut T, Faulkner GJ, Fowler KE, Fredholm M, Fritz E, Gilbert JG, Giuffra E, Gorodkin J, Griffin DK, Harrow JL, Hayward A, Howe K, Hu ZL, Humphray SJ, Hunt T, Hornshøj H, Jeon JT, Jern P, Jones M, Jurka J, Kanamori H, Kapetanovic R, Kim J, Kim JH, Kim KW, Kim TH, Larson G, Lee K, Lee KT, Leggett R, Lewin HA, Li Y, Liu W, Loveland JE, Lu Y, Lunney JK, Ma J, Madsen O, Mann K, Matthews L, McLaren S, Morozumi T, Murtaugh MP, Narayan J, Nguyen DT, Ni P, Oh SJ, Onteru S, Panitz F, Park EW, Park HS, Pascal G, Paudel Y, Perez-Enciso M, Ramirez-Gonzalez R, Reecy JM, Rodriguez-Zas S, Rohrer GA, Rund L, Sang Y, Schachtschneider K, Schraiber JG, Schwartz J, Scobie L, Scott C, Searle S, Servin B, Southey BR, Sperber G, Stadler P, Sweedler JV, Tafer H, Thomsen B, Wali R, Wang J, Wang J, White S, Xu X, Yerle M, Zhang G, Zhang J, Zhang J, Zhao S,

Rogers J, Churcher C, Schook LB. Analyses of pig genomes provide insight into porcine demography and evolution. *Nature* 491: 393-398, 2012.

20. Uenishi H, Morozumi T, Toki D, Eguchi-Ogawa T, Rund LA, Schook LB. Large-scale sequencing based on full-length enriched cDNA libraries in pigs: contribution to annotation of the pig genome draft sequence. *BMC Genomics* 13: 581, 2012.

21. Jiang Z, Tao M, Omalley KA, Wang D, Ozaki CK, Berceli SA. Established neointimal hyperplasia in vein grafts expands via TGF-beta-mediated progressive fibrosis. *Am J Physiol Heart Circ Physiol* 297: H1200-H1207, 2009.

22. Kent KC, Liu B. Intimal hyperplasia – still here after all these years! *Ann Vasc Surg* 18: 135-137, 2004.

23. Tyson KL, Reynolds JL, McNair R, Zhang Q, Weissberg PL, Shanahan CM. Osteo/chondrocytic transcription factors and their target genes exhibit distinct patterns of expression in human arterial calcification. *Arterioscler Thromb Vasc Biol* 23: 489-494, 2003.

24. Johnson RC, Leopold JA, Loscalzo J. Vascular calcification: Pathobiological mechanisms and clinical implications. *Circ Res* 99: 1044-1059, 2006.

25. Luo G, Ducy P, McKee MD, Pinero GJ, Loyer E, Behringer RR, Karsenty G. Spontaneous calcification of arteries and cartilage in mice lacking matrix GLA protein. *Nature* 386: 78-81, 1997.

26. Bucay N, Sarosi I, Dunstan CR, Morony S, Tarpley J, Capparelli C, Scully S, Tan HL, Xu W, Lacey DL, Boyle WJ, Simonet WS. Osteoprotegerin-deficient mice develop early onset osteoporosis and arterial calcification. *Genes Dev* 12: 1260-1268, 1998.

27. Dong C, Goldschmidt-Clermont PJ. Bone sialoprotein and the paradox of angiogenesis versus atherosclerosis. *Circ Res* 86: 827-828, 2000.

28. Kang N, Ng CS, Hu J, Qiu ZB, Underwood MJ, Jeremy JY, Wan S. Role of osteopontin in the development of neointimal hyperplasia in vein grafts. *Eur J Cardiothorac Surg* 41: 1384-1389, 2012.

29. Rensen SS, Doevendans PA, van Eys GJ. Regulation and characteristics of vascular smooth muscle cell phenotypic diversity. *Neth Heart J* 15: 100-108, 2007.

30. Hao H, Gabbiani G, Bochaton-Piallat ML. Arterial smooth muscle cell heterogeneity: implications for atherosclerosis and restenosis development. *Arterioscler Thromb Vasc Biol* 23: 1510-1520, 2003.

31. Thyberg J, Blomgren K, Roy J, Tran PK, Hedin U. Phenotypic modulation of smooth muscle cells after arterial injury is associated with changes in the distribution of laminin and fibronectin. *J Histochem Cytochem* 45: 837-846, 1997.

32. Johnson JL, van Eys GJ, Angelini GD, George SJ. Injury induces dedifferentiation of smooth muscle cells and increased matrix-degrading metalloproteinase activity in human saphenous vein. *Arterioscler Thromb Vasc Biol* 21: 1146-1151, 2001.

33. Beamish JA, He P, Kottke-Marchant K, Marchant RE. Molecular regulation of contractile smooth muscle cell phenotype: implications of vascular tissue engineering. *Tissue Eng Part B Rev* 16:467-491, 2010.

34. Miano JM, Long X, Fujiwara K. Serum response factor: master regulator of actin cytoskeleton and contractile apparatus. *Am J Physiol Cell Physiol* 292: C70-C81, 2007.

35. Misra S, Lee N, Fu AA, Raghavakaimal S, Mandrekar J, Bjarnason H, McKusick MA, Iruela-Arispe L, Mukhopadhyay D. Increased expression of a disintegrin and metalloproteinase thrombospondin 1 in thrombosed hemodialysis grafts. *J Vasc Interv Radiol* 19: 111-119, 2008.

36. Misra S, Fu AA, Puggioni A, Glockner JF, McKusick MA, Bjarnason H, Mukhopadhyay D. Proteomic profiling in early venous stenosis formation in a porcine model of hemodialysis graft. *J Vasc Interv Radiol* 20: 241-251, 2009.

37. Li JM, Zhang X, Nelson PR, Odgren PR, Nelson JD, Vasiliu C, Park J, Morris M, Lian J, Cutler BS, Newburger PE. Temporal evolution of gene expression in rat carotid artery following balloon angioplasty. *J Cell Biochem* 101: 399-410, 2007.

CHAPTER 4

GENE EXPRESSION IN PORCINE VENOUS ENDOTHELIAL CELLS IN RESPONSE TO SHEAR STRESS (IN VITRO LAMINAR SHEAR STRESS MODEL)

4.1 Introduction

The pathogenesis of neointimal hyperplasia (NH) associated with hemodialysis arteriovenous grafts (AVG) is incompletely understood to date. The end-products observed are increased smooth muscle cell (SMC) and endothelial cell (EC) proliferation and migration, excessively deposited extracellular matrix (ECM) proteins, and inflammatory activities (1-3). Although multiple factors may contribute to NH development (discussed in section **1.3**), the highly localized nature of NH forming predominantly at the graft-venous anastomosis (hereafter referred to as venous anastomosis) points toward pathophysiological hemodynamic stress as a key contributor (1, 2). Upon creation, AVG shunts arterial blood flow into the venous circulation, causing the vein at the anastomosis to stretch and dilate, which then generates locally aberrant flow patterns such as extremely high and/or low wall shear stress (WSS), WSS gradients, and reversed and/or oscillatory flow (1, 4-6). These drastic changes in the biomechanical environment may trigger the venous cells to physically and biochemically adapt to the new environment. Investigating the association between hemodynamic stress and NH formation (not only in venous

AVG-induced NH, but more extensively studied in the context of arterial NH) has advanced our knowledge of the mechanosensitive properties of vascular cells. A number of early studies demonstrated that aberrantly high WSS can inhibit arterial SMC proliferation while low WSS induces proliferation by modulating the expression of certain growth factors (7-11). Low WSS was also shown to promote the entrapment of platelets and immune cells to NH-prone sites in the artery (1, 12). Enhanced tensile wall stress generally correlates with positive cell proliferation presumably via inducing the prosurvival cellular signaling pathways (1, 13-15). It is thought that cells actively participate in maintaining stress homeostasis by increasing the tissue mass to counteract elevated hemodynamic stress. Turbulent flow also contributed by stimulating the production of growth factors by SMCs, macrophages, and other immune cells within the NH lesions (16).

Thus, to understand the potential underlying mechanisms of NH development in response to hemodynamic stimuli, studying the mechanisms by which vascular cells detect changes in biomechanical forces is important. In this regard, ECs have earned attention due to their unique location at the interface of the blood vessel tissue and the bloodstream. Normally, only ECs are directly exposed to luminal blood flow. Therefore, ECs are thought to be primarily responsible for transmitting biomechanical signals to the rest of the vessel wall. The mechanosensitive machinery in ECs consists of various cell junction molecules, cell surface receptors, effector proteins, and cytoskeletal components, which contribute to changes in EC structure, function, and their interaction with other vascular cell types like SMCs (17, 18). At the molecular level, such adaptation processes are reflected in gene and protein expression profiles that can be

differentially modulated under different biomechanical conditions.

Numerous studies have reported the regulation of endothelial responses to fluid flow, fluid shear stress being the most intensively studied hemodynamic parameter among other types of hemodynamic stimuli. Research by Malek and Izumo showed that shear stress causes differential regulation of arterial EC products in that shear stress increases the expression of vasodilators (nitric oxide; NO) and reduces the production of vasoconstrictors such as PDGF-B and endothelin-1 (19). Chen et al. reported that long-term shear stress regulates the expression of genes related to inflammation and cell proliferation in aortic ECs, suggesting that such stimuli can promote vascular remodeling (20). Many others also reported that shear stress modulates the EC expression of a variety of genes encoding growth factors, chemoattractants, adhesion and coagulation molecules, and proto-oncogenes (21, 22). However, these studies were conducted using arterial ECs, whereas only limited information is available on whether venous ECs respond to shear stress in the same manner as arterial ECs. This is an important question for us, as NH formation occurs more frequently at the venous anastomosis in stenosed AVG. Abnormal changes in physiological shear stress are important in arterial diseases as the absence of or decreased shear stress may cause crucial pathologic situations for arteries (which are otherwise constantly exposed to high WSS). For example, atherosclerotic plaques have greater propensity to develop at arterial bifurcations and regions of high curvature where hemodynamics are complex and low or oscillatory WSS occurs (23, 24).

The vein is normally exposed to much lower WSS (magnitude ranges from 1 to 5 dyne/cm^2) unless manipulated to encounter arterial circulation such as in vein grafts (24).

Therefore, it is likely that the venous ECs may display different biochemical properties from arterial ECs when exposed to nonphysiological shear stress. In our porcine model of AVG stenosis described in the previous chapters of this thesis, the venous anastomosis experiences sustained complex flow pattern changes characterized by extremely high and/or low WSS and WSS gradients compared to the juxta-anastomotic vein segments that are relatively resistant to NH formation (Figure 4.1). Effects of such pathophysiological WSS on venous EC physiology, especially at the molecular level, and their contribution to NH formation have not been defined clearly.

Here we describe an in vitro model of laminar shear stress applied to a monolayer of primary venous ECs isolated from porcine external jugular veins (EJV). Using a porcine microarray, we examined the global gene expression profiles of isolated ECs continuously exposed to two different magnitudes of prolonged shear stress for 24 h: venous-level physiological (low) shear stress or arterial-level high shear stress, relative to gene expression profiles of ECs cultured under static conditions. We hypothesized that the differential gene expression between the static, low, and the high shear stress-exposed venous ECs indicates that pathologic WSS observed at the AVG venous anastomosis in vivo may contribute to the EC biochemical changes underlying NH development. Our findings could provide the first step in understanding the effects of hemodynamic stress on venous NH development associated with AVG stenosis.

In addition, we employ the in vitro laminar shear stress model used in this study to investigate other physiological processes in bovine arterial ECs (BAEC) that are affected by shear stress (25). The in vitro laminar shear stress model was used to examine whether heating

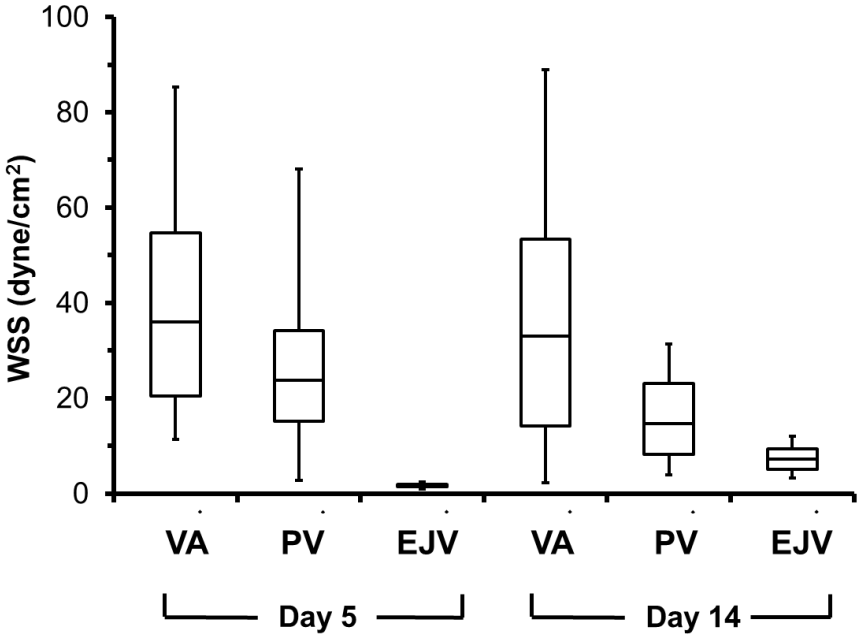

Figure 4.1 Wall shear stress (WSS) profile changes in the venous anastomosis (VA) and in a vein segment slightly downstream of the venous anastomosis (PV; proximal vein) in a porcine AVG model. At day 5 following graft placement, unstable flow characterized by extremely high and/or low WSS is observed in both the VA and PV. Such WSS changes in the VA were sustained into day 14 whereas the magnitude of WSS change was decreased in PV at day 14. EJV indicates a control vein from the unoperated contralateral side of each animal. The average WSS is shown for N = 2 for each group. (Data provided by Daniel B. Pike and Yan-Ting E. Shiu).

sensitizes the NO response in BAECs, resulting in greater eNOS activation and enhanced production of NO. Increased local temperature in human skeletal muscle feed arteries have been shown to reduce alpha1-adrenergic receptor-mediated vasoconstriction; however, the underlying mechanisms have not been elucidated. Ives et al. hypothesized that the thermal effects could be due to the vasodilatory actions of nitric oxide (NO) produced by the endothelium through shear stress stimulation of endothelial NO synthase (eNOS) (25). In this chapter, the laminar shear stress experiments used to evaluate this hypothesis are described, and results and discussions of the results are referred to the published work by Ives et al. (25).

4.2 Materials and Methods

4.2.1 Materials

Cell culture reagents including EBM-2 media and growth supplements for porcine venous ECs were purchased from Lonza (Walkersville, MD). BAECs and Dulbecco's Modified Eagle Medium (DMEM) were purchased from Life Technologies (Grand Island, NY). Collagenase A was obtained from Roche Applied Science (Indianapolis, IN). Antibodies directed against von Willebrand Factor (vWF) were purchased from DAKO Pharmaceuticals (Carpinteria, CA), and smooth muscle alpha-actin antibodies were from Sigma (St. Louis, MO). Porcine anti-CD31 antibodies were obtained from R&D Systems (Minneapolis, MN). Secondary antibodies used for fluorescence microscopy were obtained from Life Technologies. Glass microslides and silicone sheeting for in vitro flow experiments were purchased from Corning (Corning, NY) and Specialty Manufacturing Inc. (Saginaw, MI), respectively. Fibronectin solution from bovine plasma was

purchased from Sigma. All reagents and materials for RNA isolation and microarray experiments are described in in Chapter 3.

4.2.2 Isolation of porcine venous ECs and cell culture

Animal procedures were performed aseptically in accordance with a protocol that was approved by the Institutional Animal Care and Use Committees (IACUCs) at the Veterans Affairs Salt Lake City Health Care System and the University of Utah. Female Yorkshire cross domestic pigs (Sigma Livestock, Salt Lake City, UT) weighing approximately 30 to 35 kg were used to collect venous ECs from the EJV. Preparation of animals including anesthesia is described in detail in Chapter 2.

Primary porcine venous ECs were collected from fresh, unoperated EJVs by collagenase A tissue digestion. Briefly, an EJV segment of about 5 to 7 cm was ligated at both ends, and warm collagenase A solution (1 mg/ml concentration diluted in serum-free cell culture media) was injected directly into the lumen of the ligated EJV segment. After incubation for 5 min, followed by rigorous massaging of the vessel wall using sterile techniques, contents were emptied into a container filled with fetal calf serum (FCS) to inactivate the enzyme reaction. Cells were harvested by gentle centrifugation and cultured in flasks in EBM-2 media in a humidified 37 °C incubator with 5% CO_2 and 95% ambient air. EC cultures were expanded to produce batches of passage number 5 to 6 cells. Cells isolated this way produced a homogenous EC population devoid of other cell types, such as SMCs, at our desired passage number when determined by immunostaining. Before each flow experiment, we confirmed the endothelial nature of these cells by positive vWF

and CD31, and negative smooth muscle α-actin immunostaining (Figure 4.2). Briefly, sampled cells from each EC batch were seeded onto 2-well chamber slides at a density of $1x10^5$ cells/well and grown overnight in a tissue culture incubator. Cells were then fixed in 2% paraformaldehyde, followed by permeabilization in 0.5% Triton X-100 solution. Cells were incubated overnight at 4 °C with primary antibodies specific for the respective proteins. Proteins were visualized by immunofluorescence. Three different animals were used to collect ECs from EJVs, and cell cultures from each animal were maintained separately. For all flow experiments, EC cultures at passage 5 to 6 were used.

Commercially purchased BAECs Life Technologies (Grand Island, NY) were cultured in flasks in DMEM supplemented with 10% FCS. Cultures were maintained in a humidified 37 °C incubator with 5% CO_2 and 95% ambient air. All experiments were conducted with cultures at passage 3 to 6.

4.2.3 Preparation of matrix-coated microslides

Glass microslides (28.5 cm^2, 1 mm thickness) and silicone sheeting with two different thicknesses (0.025 or 0.05 cm) cut to expose the flow channel were cleansed and sterilized before use. The flow channel has a length of 5.5 cm, a width of 2.5 cm, and a height of either 0.025 cm or 0.05 cm, for generation of high or low shear stress, respectively. This channel was created between the microslide and the parallel-plate flow chamber, separated by the silicone gasket. Bovine plasma fibronectin (1 mg/ml), diluted in phosphate-buffered saline (PBS), was coated as a thin film in the flow channel using sterile techniques (5 μg of fibronectin/cm^2). Fibronectin solution

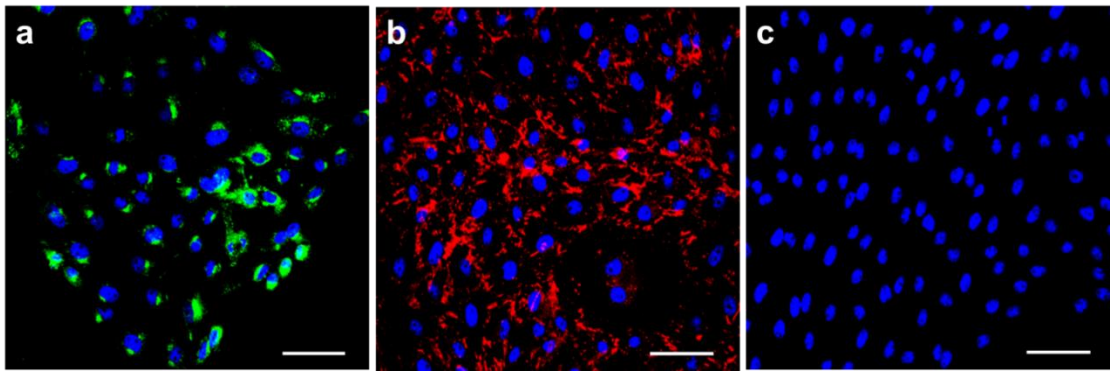

Figure 4.2 Immunostaining of isolated porcine venous ECs with vWF, CD31, and smooth muscle α-actin at passage number 5. Porcine venous ECs were isolated from EJV using collagenase A tissue digestion and EC cultures were expanded. At passage number 5, sampled cells were immunostained for either vWF (cytosolic, appearing green in panel **a**), CD31 (membranous, appearing red in panel **b**) or smooth muscle α-actin (blue staining only in panel **c** denotes nuclei and negative staining for α-actin) to confirm their endothelial nature and to examine any SMC contamination. ECs were positive for vWF and CD31, and negative for smooth muscle α-actin. Blue staining denotes cell nuclei. Scale bar=100 μm.

was incubated on slides for 2 h at room temperature to allow matrix adsorption. Porcine EC cultures at passage 5 to 6 or BAEC cultures at passage 3 to 6 were seeded onto these fibronectin-coated surfaces at a density of $1x10^5$ cells/slide and were grown to approximately 80 to 90% confluence before each shear stress experiment.

4.2.4 In vitro laminar shear stress experiments

The in vitro unidirectional laminar shear stress model was described similarly by Shiu et al. and Albuquerque et al., with modifications to enable application of a wide range of shear stress values (26, 27). The system consists of an upper and a lower reservoir from which the oxygenated culture media continuously recirculates through the flow channel to shear cells at a defined volumetric flow rate calculated to generate specific shear stress values. Volumetric flow rate (Q) was measured manually through a flow meter positioned immediately downstream of the flow chamber. Sterile techniques were maintained in the 37 °C constant-temperature hood throughout the experiment. Shear stress (τ) was calculated using the following equation: $\tau = (6\mu Q)/(wh^2)$, where μ is the viscosity of the culture media containing serum (μ = 0.01 Poise), Q is the volumetric flow rate (determined at the time of each experiment), *w* is the width, and *h* is the height of the flow channel. We conducted 3 sets of independent shear stress experiments with the venous ECs collected from three different animals (N=3 for each group). In each set, cells derived from the same animal were either exposed to continuous low shear stress (2 to 5 dyne/cm^2) or high shear stress (35 to 40 dyne/cm^2) for 24 h, with each condition having a technical replicate. The flow system was maintained at 37 °C and culture media was supplied with 5% CO_2 in balanced air.

Control ECs with the same passage number as with the sheared cells were seeded onto fibronectin-coated microslides in an identical manner and were cultured under a static, undisturbed condition for 24 h in a tissue culture incubator.

The same preparation procedures were conducted for BAECs except that these cells were exposed to only high shear stress (15 to 20 dyne/cm^2) for 1 h. This is within the physiological range of major human arteries and has been documented to activate EC signal transduction (21). The flow system was kept at either 37 °C or 39 °C in a constant-temperature hood. Control ECs with the same passage number as with the sheared cells were seeded onto fibronectin-coated surfaces in an identical manner and were cultured under a static flow, undisturbed condition at either 37 °C or 39 °C for 1 h in a tissue culture incubator. Upon completion of the flow experiments, cell lysates were collected in ice-cold lysis buffer containing detergent, and standard Western blotting procedures were performed (25).

4.2.5 RNA extraction and microarray hybridization

After 24 h of exposure of porcine venous ECs to laminar shear stress, cells were immediately washed with warm PBS. Cells were then directly lysed in 1 ml of QIAzol Lysis Reagent (Qiagen) on the microslides and lysates were collected with a rubber cell scrapper. A separate set of cells were subjected to phase contrast microscopy for morphological examination after exposure to shear stress, and these cells were not used for RNA extraction (Figure 4.3). Extraction of total mRNA, RNA labeling, and microarray hybridization on Agilent porcine 44K (v1) oligonucleotide microarray slides were conducted as described in Chapter 3, except that RNA

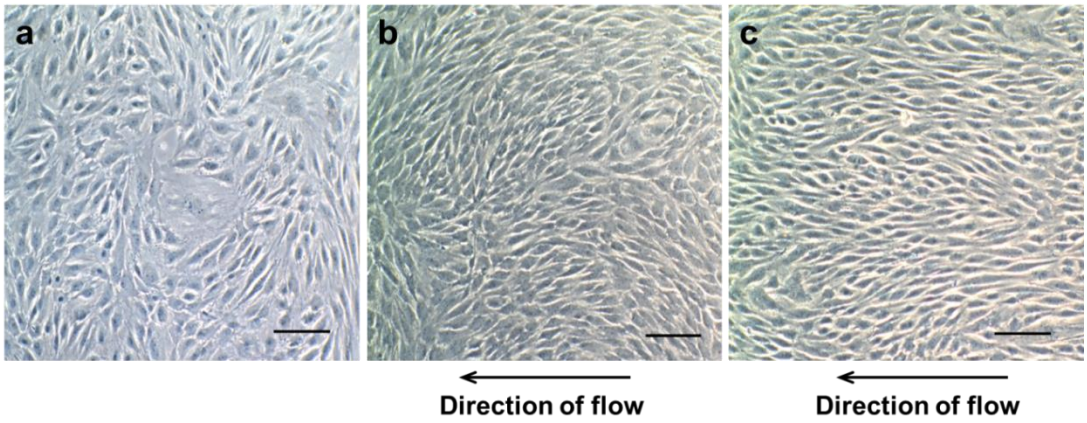

Figure 4.3 Morphological changes of cultured porcine venous ECs exposed to low or high laminar shear stress for 24 h. After exposure to laminar shear stress for 24 h, ECs cultured on fibronectin-coated microslides were washed in warm PBS and their morphological changes in response to shear stress were assessed using phase contrast microscopy. Compared to ECs grown under static condition that remained randomly oriented (**a**), ECs aligned in the direction of flow in both low (**b**) and high (**c**) shear stress-exposed cells. Flow direction was from right to left as indicated by the arrows. Scale bar=100 μm.

extracted this way displayed RNA Integrity Number (RIN) greater than 9 in all samples.

4.2.6 Bioinformatics analyses of gene expression profiles

Data normalization and adjustment of batch effects were conducted as described in Chapter 3, except that microarrays were processed in three batches over the course of several months. Following normalization and batch-adjustment, hierarchical clustering revealed that samples were clustered by shear stress conditions with low and high shear stress-exposed samples being similar. Batch-adjusted data were uploaded into GeneSifter® Analysis Edition v3.7 (http://www.genesifter.net, Geospiza, Seattle, WA) for statistical analysis.

Transcripts with mean fold-changes of ≥ 4.0 and ANOVA $p < 0.05$ (Benjamini and Hochberg correction) in either the low or high shear stress groups (or both) compared to their corresponding transcripts from common static control were first filtered. After filtering, there were 414 transcripts that satisfied our threshold, which included un-annotated transcripts with no accession numbers. These transcripts were excluded for further genomic analyses. For uncharacterized probes with a primary accession number, we used nucleotide basic local alignment search tool (BLAST) to manually determine similar sequences in other species using sequence matches above a specified cut-off threshold (≥ 50% matching query-subject coverage and E-value ≤ 10^{-4}). In most cases, an annotated "hit" with the highest total score that fulfilled our specified threshold criteria was selected as the genes to be used for further analysis. GATHER analysis was performed as described in Chapter 3. Annotated transcripts significantly altered in each of the two shear stress conditions were separately subjected to GATHER analysis. Also, up-

or down-regulated transcripts were separately analyzed.

4.2.7 Quantitative reverse transcriptase-PCR

The same mRNA samples used for microarray studies were subjected to Taqman quantitative RT-PCR. Details of the experiment are described in Chapter 3. We assessed the expression of five key genes selected from the microarray studies (ANGPT2, F2, CIDEC, KLF4, and SELL). PCR amplification efficiencies were similar for all genes tested. Relative gene expression was normalized to the expression of the housekeeping gene, beta-2 microglobulin (B2M), and the comparative C_T method was used to quantify the fold differences in gene expression.

4.3 Results

4.3.1 Morphology of venous ECs in response to shear stress

We examined the morphology of porcine venous ECs exposed to either low (2 to 5 dyne/cm^2) or high (35 to 40 dyne/cm^2) unidirectional laminar shear stress for 24 h. The overall monolayer integrity of the cells and their shapes after the long exposure time in vitro were assessed using phase contrast microscopy. Elongation and alignment of cells in the direction of flow was observed with shear stress (Figure 4.3 panels b and c), whereas the cells cultured under static condition remained randomly oriented (Figure 4.3 panel a). Such observations are consistent with EC cytoskeletal alignment under flow reported in a number of previous studies (28-30). This demonstrates that the level of shear stress, especially the high shear stress, applied to monolayer ECs grown on fibronectin-coated microslides, did not cause damage to the cells nor

detachment of cells from the microslides during the 24 h experiment, and was able to induce morphological changes.

4.3.2 Global gene expression changes in low and high shear stress-exposed venous ECs

We compared the global genomic changes of low and high shear stress-exposed venous ECs relative to the common control ECs grown under static conditions for the same period of time. DNA microarray analysis identified hundreds of transcripts that were significantly regulated in either low shear or high shear environments or both. A threshold (mean fold-changes of ≥ 4.0 and ANOVA $p < 0.05$) was applied to filter transcripts that are significantly regulated in response to shear stress. As discussed in Chapter 3, this criterion takes the magnitude of variations in normal gene expression variations reported in the literature into consideration and allows us to efficiently explore the massive microarray data set for identifying genes with the most relevant biological significance. Analyses of both low and high shear stress-modulated genes showed that 414 transcripts met our threshold and were significantly different between the sheared and static EC cultures. Figure 4.4 illustrates the global gene expression profiles of the filtered transcripts presented as a microarray heat map (each group N = 3). Clustering of samples showed that the two shear stress-exposed groups were more similar to each other than to the static control group. Due to incomplete annotation of many transcripts on the array, un-annotated transcripts with no accession numbers were excluded from further data analyses, leaving 223 filtered transcripts.

In Figure 4.5, Venn diagrams of the 223 filtered transcripts indicate that a substantial

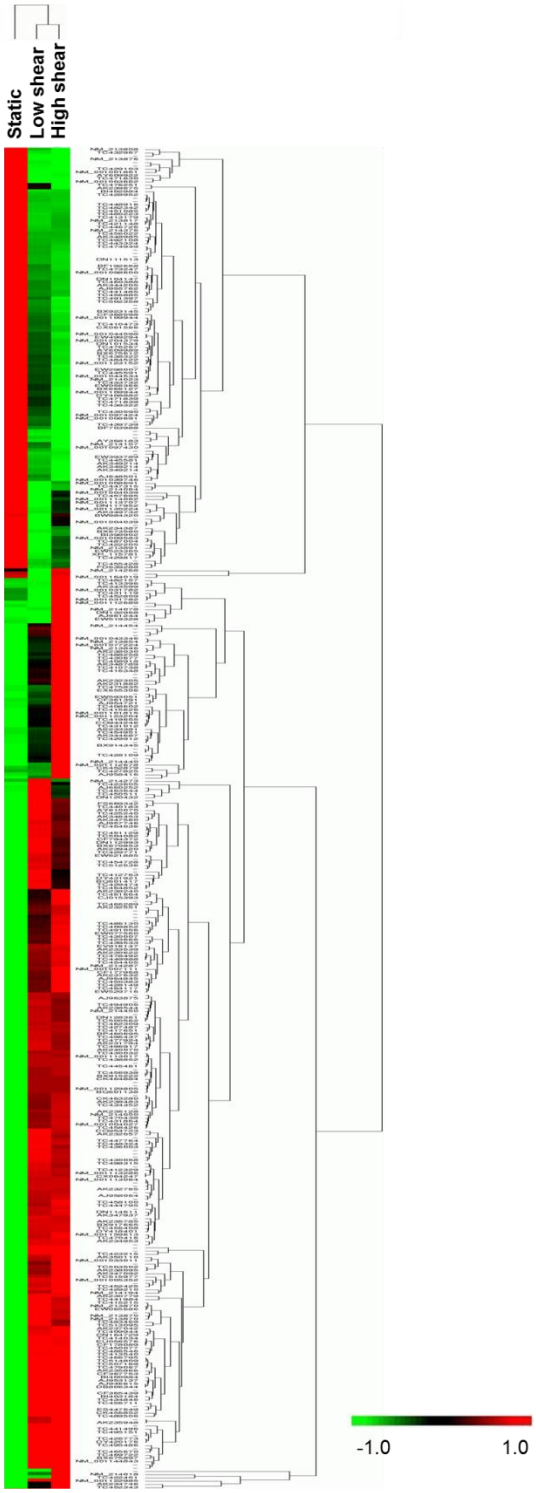

Figure 4.4 Gene expression profile changes of low or high shear stress-exposed venous ECs. GeneSifter identified 414 transcripts that met our selection threshold from three independent microarray experiments. Sample clustering indicates that the two shear stress-exposed groups were similar to each other than to the static control group (each group N=3). The color-coded scale for log-transformed data is shown at the bottom.

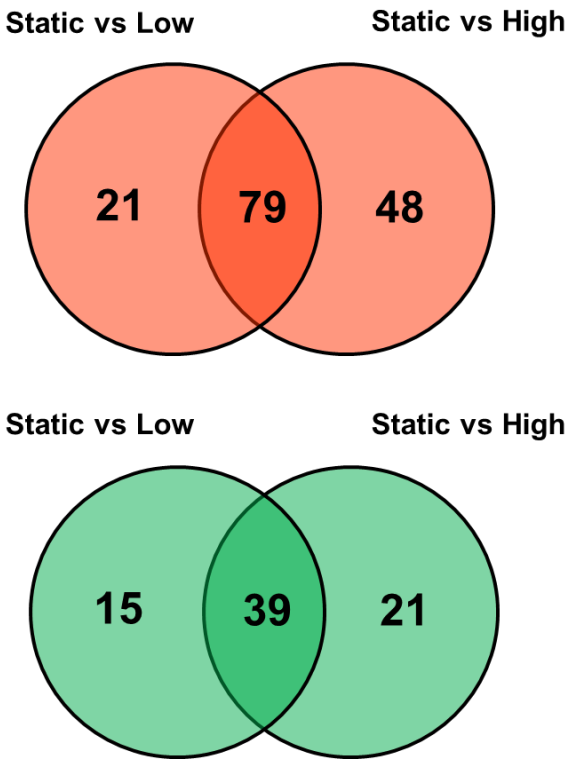

Figure 4.5 Venn diagrams indicating the degree of overlap between low and high shear stress-exposed ECs. A substantial number of the 223 filtered transcripts overlap between the low- and high-shear stress groups. The numbers of up- (red) or down-regulated (green) transcripts are shown. Greater number of transcripts was differentially regulated in high shear stress-exposed ECs compared to low shear stress-exposed ECs.

number of regulated transcripts that satisfied our threshold criteria were shared between the two different shear stress groups, and more transcripts were significantly regulated in the high shear stress group compared to the low shear stress group. These findings suggest that even a physiological level of low shear stress was capable of inducing EC genomic changes similar to those observed with much higher shear stress level.

4.3.3 Gene enrichment of significantly up- or down-regulated transcripts in response to low or high shear stress

A total of 112 and 140 transcripts for low and high shear stress-exposed ECs, respectively, were subjected to GATHER's Gene Ontology (GO) analysis. Analysis of up-regulated genes in each shear stress group revealed that the most significant (Bayes factor ≥ 6) biological process enriched among low shear stress-regulated genes was strongly related to STAT protein nuclear translocation and cell communication (Table 4.1A). The two genes that were associated with both annotations were F2 and F2R, which are thrombin and thrombin receptor, respectively. Significant up-regulation of dopa decarboxylase (DDC) in the high shear stress group was associated with terms related to biosynthesis of dopamine (Table 4.1B). However, all of the significantly identified terms pertaining to dopamine biosynthesis were associated with this one gene (DDC) only, suggesting that there was no meaningful enrichment of dopamine biosynthesis or other gene sets among the high shear stress-modulated genes that were up-regulated.

When down-regulated genes were examined for each shear stress group, annotations strongly related to stress/stimuli response were significantly enriched in both shear stress groups

Table 4.1 Over-represented Gene Ontology (GO) terms for significantly up-regulated genes in the ECs exposed to low (A) or high (B) shear stress for 24 h. (A) GATHER analysis of the 72 up-regulated transcripts representing 70 genes in ECs exposed to low shear stress relative to the static control ECs is shown. Only two annotations were identified with a meaningful Bayes Factor (≥ 6). **(B)** GATHER analyzed 89 up-regulated transcripts representing 86 genes in ECs exposed to high shear stress relative to the static control. Although terms related to dopamine biosynthesis were identified as most significant, only one gene (DDC) contributed to these terms.

A

Gene Ontology ID.	Annotation	p value	Bayes Factor
1. GO:0007262 [8]	STAT protein nuclear translocation	< 0.0001	7
2. GO:0007154 [3]	Cell communication	0.0001	6

B

Gene Ontology ID.	Annotation	p value	Bayes Factor
1. GO:0006585 [8]	Dopamine biosynthesis from tyrosine	< 0.0001	8
2. GO:0042423 [7]	Catecholamine biosynthesis	< 0.0001	8
3. GO:0046219 [7]	Indolakylamine biosynthesis	< 0.0001	8
4. GO:0006587 [8]	Serotonin biosynthesis from tryptophan	< 0.0001	8
5. GO:0042446 [6]	Hormone biosynthesis	0.001	6
6. GO:0007262 [8]	STAT protein nuclear translocation	0.002	6

(Table 4.2A and B). Significantly regulated genes that contributed to these terms included cytokines such as CCRL1, CXCL2, CXCL5, CXCL10, CXCL14, SPP1, and RPS6KA5. Microarray expression profiles of these genes are shown in Table 4.3.

4.3.4 RT-PCR of expression of selected genes

To validate our microarray results, we selected five genes (ANGPT2, CIDEC, F2, KLF4, and SELL) whose expressions were significant and differentially regulated between the low and high shear stress (Table 4.3) and performed RT-PCR for the same RNA samples used for our microarray studies. Studies conducted by others in vascular ECs have shown that ANGPT2 and KLF4 are regulated by laminar shear stress in the same direction as we observed here (31-33). CIDEC, F2, and SELL perform important cellular functions such as focal adhesion (34, 35), cell alignment, and migration and thrombosis, but modulation of these genes by shear stress in ECs has not been reported in the literature. Microarray expression profiles of these genes are shown in Table 4.3. The expression of the housekeeping gene beta2 microglobulin (B2M) was used as a control gene for PCR. Figure 4.6 demonstrates that the PCR results generally agree well with the microarray studies except that F2 expression change was similar between the two shear stress groups when examined by PCR.

4.4 Discussion

Shear stress is a key hemodynamic force that plays a pivotal role in regulating the physiological processes in cells of the blood vessel wall. It is widely appreciated that pathophysiological shear stress, such as extremely high and/or low WSS experienced by cells in

Table 4.2 Over-represented GO terms for significantly down-regulated genes in the ECs exposed to low (A) or high (B) shear stress for 24 h. (A) GATHER analysis of the 40 down-regulated transcripts representing 37 genes in ECs exposed to low shear stress relative to the static control ECs is shown. **(B)** GATHER analyzed 51 down-regulated transcripts representing 47 genes in ECs exposed to high shear stress relative to the static control. Under both conditions, genes associated with response to stress or stimuli were significantly enriched.

A

Gene Ontology ID.	Annotation	p value	Bayes Factor
1. GO:0042221 [6]	Response to chemical substance	< 0.0001	10
2. GO:0009628 [5]	Response to abiotic stimulus	< 0.0001	9
3. GO:0042330 [5]	Taxis	< 0.0001	8
4. GO:0006935 [6]	Chemotaxis	< 0.0001	8
5. GO:0009611 [5]	Response to wounding	< 0.0001	6
6. GO:0009605 [4]	Response to external stimulus	0.0002	6

B

Gene Ontology ID.	Annotation	p value	Bayes Factor
1. GO:0042330 [5]	Taxis	< 0.0001	10
2. GO:0006935 [6]	Chemotaxis	< 0.0001	10
3. GO:0042221 [6]	Response to chemical substance	< 0.0001	9
4. GO:0009611 [8]	Response to wounding	< 0.0001	8
5. GO:0006950 [4]	Response to stress	< 0.0001	8
6. GO:0009628 [5]	Response to abiotic stimulus	0.0001	6
7. GO:0007267 [4]	Cell-cell signaling	0.0001	6
8. GO:0009605 [4]	Response to external stimulus	0.0001	6
9. GO:0050896 [3]	Response to stimulus	0.0001	6

Table 4.3 Differential gene expression in porcine venous ECs in response to 24-h low or high shear stress.

	Low shear		High shear	
Gene Symbol	Log ratio	p Value	Log ratio	p Value
F2	4.3	<0.0001	5.8	<0.0001
F2R	2.8	<0.0001	2.8	<0.0001
DDC	N/S		3.2	<0.0001
CCRL1	-2.3	<0.0001	-3	<0.0001
CXCL2	-3.6	<0.0002	-3.8	<0.0001
CXCL5	-4	<0.0001	-4	<0.0001
CXCL10	-3	<0.02	-2.6	<0.002
CXCL14	-2.8	<0.0001	-2.8	<0.0001
SPP1	N/S		-2	<0.0001
RPS6KA5	-2	<0.0001	-2.3	<0.0001
CIDEC	N/S		6.6	<0.0001
SELL	N/S		3	<0.003
KLF4	N/S		2	<0.0001
ANGPT2	-3.2	<0.0001	-4.2	<0.0001
ADAMTS1	3.8	<0.0001	4.1	<0.0001
KLHL13	3.8	<0.0001	3.9	<0.0001
SLPI	4.1	<0.0002	3.5	<0.0001
CD40	3.2	<0.0001	4	<0.0001
KCNN4	N/S		5.2	<0.0001
PLEK2	2.6	<0.0001	4.2	<0.0001
UGT1A	3.3	<0.0001	3.3	<0.0001
CYP7A1	3	<0.0001	3.3	<0.0001
CUTA	2.3	<0.0001	3.9	<0.0001
ZWILCH	3.3	<0.0001	2.8	<0.0001
BAALC	2.8	<0.0001	3	<0.0001
AQP1	2.8	<0.008	2.8	<0.0001
FCGR1A	2.6	<0.0001	3	<0.0001
GNG2	2.6	<0.0001	2.6	<0.0001
NQO1	2.6	<0.0001	2.8	<0.0001
JAG1	2.6	<0.0001	2.6	<0.0001
CCDC146	2.3	<0.0002	2.8	<0.0001
VEZT	2.6	<0.0001	2.3	<0.0001
NPPB	N/S		3.6	<0.0003
ABCC2	2.6	<0.0001	2.3	<0.0001
RASGEF1B	2.3	<0.0001	2.6	<0.0001
CX3CR1	2.3	<0.0001	2.3	<0.0001
PTGS1	N/S		3	<0.0001
FN1	2.3	<0.0001	2.3	<0.0001
SCGN	N/S		3.3	<0.0001
BDKRB1	2.3	<0.0001	2.3	<0.0001
RNASE1	2	<0.0001	2.6	<0.0001

	Low shear		High shear	
Gene Symbol	Log ratio	p Value	Log ratio	p Value
RAB3C	2.6	<0.0001	2	<0.0001
MUC19	2.3	<0.0001	2.3	<0.0001
HCRTR1	N/S		3.2	<0.0001
ABTB2	2	<0.0001	2.3	<0.0001
PLVAP	2	<0.0001	2.6	<0.0001
EFNA4	2.3	<0.0001	2	<0.0001
CKB	2	<0.0001	2	<0.0001
FBXO43	2	<0.0001	2	<0.0001
ZNF615	2.3	<0.0001	2	<0.0001
HMOX1	2	<0.0001	2	<0.0001
SERPINE2	2	<0.0001	2.3	<0.0001
RGS16	2	<0.0001	2	<0.0001
ADRBK1	2	<0.0002	2	<0.0001
GSTO1	2	<0.0001	2	<0.0002
TNK2	2	<0.0001	2	<0.0001
HIST1H2BD	2.3	<0.0002	N/S	
CPT1A	2	<0.0001	2	<0.0001
SLC39A8	2.3	<0.0001	N/S	
RMB24	2	<0.0001	N/S	
LMO7	2	<0.0001	2	<0.0001
IGFBP4	2	<0.0001	N/S	
FAM110D	N/S		2	<0.0001
FTL	2	<0.0001	N/S	
PR39	2	<0.0001	N/S	
ARMCX2	2.3	<0.0001	N/S	
ASPA	N/S		2	<0.0001
ZNF2	N/S		2	<0.0001
ARL4C	N/S		2	<0.0001
UROC1	N/S		2	<0.0003
TEK	N/S		2.3	<0.0001
HYAL2	N/S		2.3	<0.0001
CLDN11	4	<0.009	N/S	
ANXA13	N/S		4	<0.0001
SELP	N/S		3.2	<0.0001
ADIPOQ	N/S		3	<0.002
PTPRR	N/S		2	<0.0001
GNRHR	2	<0.0003	N/S	
THY1	N/S		2	<0.0001
FAM190A	2	<0.0001	N/S	
P2RX5	N/S		2	<0.0001
FZR1	N/S		2	<0.0001

Table 4.3 (continued).

	Low shear		High shear	
Gene Symbol	Log ratio	p Value	Log ratio	p Value
SLC17A3	N/S		2.3	<0.0001
C2	N/S		2	<0.002
TNXB	N/S		2	<0.0001
EFCAB3	3.7	<0.0001	4	<0.0001
PPP1R14C	3.5	<0.0001	3.7	<0.0001
UGT1A10	3.3	<0.0001	3.8	<0.0001
C7	3	<0.0001	2.6	<0.0001
PDGFD	3	<0.0001	2.6	<0.0001
ELMOD1	2.6	<0.0001	2.6	<0.0001
SOX11	2.3	<0.0002	2.6	<0.0001
HIST1H2AC	3	<0.0001	2	<0.0001
RAP1GAP2	2	<0.0001	2.3	<0.0001
NR2F2	2	<0.0001	2.6	<0.0001
COLEC10	2.6	<0.0001	N/S	
CD83	2	<0.0002	2.3	<0.0001
DDIT4	N/S		2.8	<0.0001
MRAP2	2.6	<0.0003	N/S	
ASS1	N/S		2.3	<0.001
FRMD4B	N/S		2	<0.0001
PGRMC1	2	<0.0001	N/S	
STRA8	2	<0.0009	N/S	
ZFP14	2	<0.0005	N/S	
LHX6	N/S		3.2	<0.0003
TGM2	N/S		2.6	<0.0001
EDNRB	N/S		2.3	<0.004
ENTPD1	N/S		2.3	<0.0001
RET	N/S		2	0.003
KCNJ2	2.3	<0.0001	N/S	
IL13RA2	N/S		2	<0.0001
SMPDL3B	N/S		2.3	<0.0001
HCRTR2	-2.3	<0.0006	N/S	
HTR2B	-2.6	<0.0005	N/S	
HERC6	-2	<0.0001	N/S	
RFPL2	-2	<0.0006	N/S	
MREG	N/S		-2	<0.0002
CDS1	N/S		-2	<0.0001
PDCD1	N/S		-2	<0.0001
NTF3	N/S		-2	<0.007
AP1S3	N/S		-2	<0.0005

	Low shear		High shear	
Gene Symbol	Log ratio	p Value	Log ratio	p Value
TMEFF2	N/S		-2	<0.0001
ANKRD45	N/S		-2	<0.0005
ITGA1	-2	<0.0001	N/S	
MAPK13	N/S		-2	<0.0001
DIRAS3	N/S		-2	<0.0001
SLC16A6	N/S		-2.6	<0.0001
PEG10	N/S		-2	<0.0001
AKAP12	-2	<0.0009	-2.3	<0.0003
EFCAB5	N/S		-2	<0.0001
DTNBP1	-2	<0.0001	-2	<0.0001
SST	-2.3	<0.04	N/S	
ITGB8	N/S		-2.6	<0.0001
VCAM1	-2.3	<0.003	N/S	
IFIT1	-2	<0.0001	-2.3	<0.0001
AREG	-2.3	<0.0001	-2	<0.0001
RSAD2	-2.3	<0.003	-2	<0.004
TBR1	-2.3	<0.0001	-2	<0.0001
UNG	-2.3	<0.0001	-2.3	<0.0001
CC2D2A	-2.3	<0.0001	-2.6	<0.0001
FABP5	-2.3	<0.0001	-2.8	<0.0001
EIF2B5	-2.3	<0.0001	-2.3	<0.0001
ADM	-2	<0.0001	-3	<0.0001
GLMN	-2.6	<0.0001	-3	<0.0001
FMO1	-3.3	<0.0001	-2.8	<0.0004
MRC1	-3	<0.0001	-3.2	<0.0001
FST	-3.5	<0.0001	-3.3	<0.0001
CETN1	-3.2	<0.001	-3.6	<0.0004
QRFPR	-3.7	<0.0001	-3.3	<0.0001
FAM107A	-2.6	<0.0001	-2.8	<0.0001
PARP14	-2.3	<0.0002	-2.3	<0.0001
HOXA1	-2	<0.0001	-2	<0.0001
CIRBP	-2	<0.0001	N/S	
ARID5B	N/S		-2.3	<0.0001
SDPR	N/S		-2	<0.0001
CMET	-2.3	<0.0001	N/S	
BACH1	N/S		-2	<0.0001
CHST1	N/S		-2	<0.0001
NPTX2	N/S		-2	<0.0001
ENDOU	-2	0.0004	N/S	

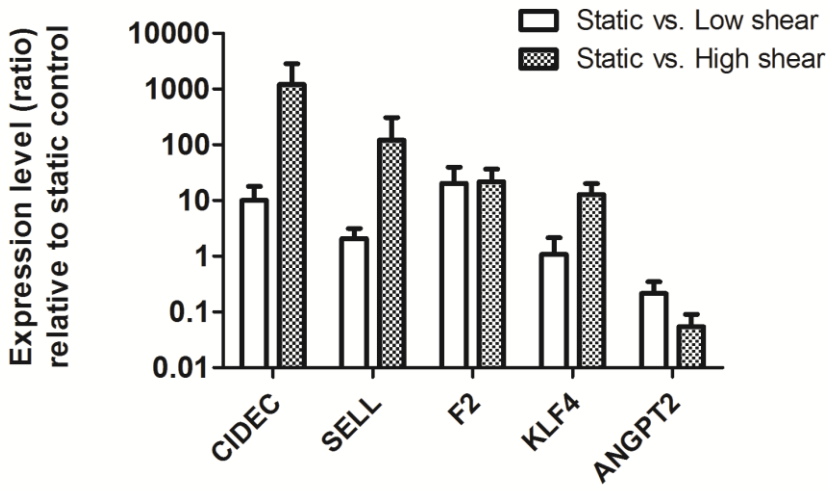

Figure 4.6 Quantitative RT-PCR measurements of five select genes that are differentially regulated between ECs exposed to low and high shear stress from microarray studies. To confirm the microarray results, RT-PCR was performed to analyze the gene expression levels for the same mRNA samples used for microarray experiments (N=3 for each data point). Error bars indicate standard deviation (SD).

the AVG venous anastomosis, can induce a variety of pathogenic events resulting in structural and functional changes in affected cells. In the present study, we investigated the effects of shear stress on gene expression profiles in cultured porcine venous ECs to elucidate genes and/or cellular pathways that may be important mediators of venous NH development associated with AVG stenosis. The in vitro experimental flow system we adopted here does not perfectly recapitulate the in vivo conditions in the venous anastomosis. However, this model addresses several important factors because biological effects of specific hemodynamic parameters (e.g., shear stress) on specific cell types (e.g., ECs or SMCs) can be studied, which cannot be separated from other pathogenic factors in complex in vivo flow environments. This provides us with information on the underlying cellular and molecular events induced by pathophysiological hemodynamics that may potentially be implicated in NH development.

Using this system, porcine venous ECs were exposed to either physiological venous (low) shear stress or arterial (high) shear stress continuously for 24 h, and their gene expression changes relative to statically cultured ECs were assessed. Although we adopted the static value as a reference control to elucidate shear stress-dependent changes, it is important to note that venous ECs are physiologically exposed to low shear stress, and the absence of shear stress may be considered nonphysiological. Previous studies demonstrated that sudden application of shear stress to statically cultured ECs can induce drastic changes in the initial genomic profiles. Many of these immediately responsive genes, however, are thought to be transient and return to baseline level after sustained exposure to shear stress, for example, for 24 h (20). Since prolonged shearing of ECs may be more physiologically relevant to the flow conditions occurring in vivo than

short-term exposure, we examined the gene expression profiles in response to sustained shear stress.

Gene enrichment analysis of significantly regulated genes that satisfied our threshold criteria revealed that a few enrichment terms were associated with up- or down-regulated gene sets from each shear stress group. Among the up-regulated genes in the low shear stress group, F2 and F2R contributed to two terms identified as significant, *STAT protein nuclear translocation* and *Cell communication*. These genes were also significantly up-regulated in the high shear stress group. It is also interesting to note, however, that expression of F2R was down-regulated in response to 24 h arterial shear stress in human umbilical vein ECs (HUVEC) and in microvascular ECs in a study conducted by Nguyen et al. (36). Although ECs of different origins can respond to shear stress differentially, the discrepancy between our study and theirs is not clear. Analysis of significantly down-regulated gene sets in both shear stress groups showed that cytokines related to stress/stimuli response were enriched. Shear stress-mediated modulation of cytokines and chemokines has been previously studied by others (37), although modulation of the specific cytokines that we identified in this current study has not been reported before (CCRL1, CXCL2, CXCL5, CXCL10, CXCL14, and SPP1).

Increasing evidence shows that there is a spectrum of shear stress-modulated genes that are common between a number of different studies of similar or different vascular cell types. In this context, many genes that were significantly regulated in response to shear stress from our venous EC microarray studies have been shown to be regulated in arterial and other ECs. For example, endothelial Krüppel-like factor (KLF) genes are shear stress-responsive transcription factors that

regulate cellular differentiation and tissue development (38), and previous studies showed that a few members of the KLF genes were significantly induced by laminar shear stress in arterial ECs (32, 39, 40). In our microarray study, we identified KLF4 to be differentially up-regulated under high shear stress conditions. In addition, angiopoietin-2 (ANGPT2), a critical regulator of vascular stabilization and maturation, was shown to be down-regulated by high flow in HUVECs in vitro by others, an observation in agreement with ours (41).

We had hypothesized that the gene expression profiles between low and high shear stress-exposed venous ECs would be different as pathologic shear stress can induce a variety of cellular processes which may contribute to venous NH development in AVGs. Results from our current study revealed that many shear stress-responsive genes were differentially regulated between the two groups, and analysis of enriched genes and/or pathways in each group provided us with knowledge of the underlying biological events (Table 4.3). Further investigation on how shear stress-dependent genes act together to alter the endothelial physiology in hemodynamically-adapted venous ECs is necessary. Gene expression data of this in vitro study can also be compared to the whole porcine AVG tissue microarray results discussed in Chapter 3, to determine the shear stress-dependent endothelial genes and/or pathways that are significantly altered in NH lesions.

4.5 References

1. Li L. Terry CM, Shiu YT, Cheung AK. Neointimal hyperplasia associated with synthetic hemodialysis grafts. *Kidney Int* 74: 1247-1261, 2008.

2. Kelly BS, Heffelfinger SC, Whiting JF, Miller MA, Reaves A, Armstrong J, Narayana A, Roy-Chaudhury P. Aggressive venous neointimal hyperplasia in a pig model of arteriovenous graft stenosis. *Kidney Int* 62: 2272-2280, 2002.

3. Roy-Chaudhury P, Kelly BS, Miller MA, Reaves A, Armstrong J, Nanayakkara N, Heffelfinger SC. Venous neointimal hyperplasia in polytetrafluoroethylene dialysis grafts. *Kidney Int* 59: 2325-2334, 2001.

4. Ballyk PD, Walsh C, Butany J, Ojha M. Compliance mismatch may promote graft-artery intimal hyperplasia by altering suture-line stresses. *J Biomech* 31: 229-237, 1998.

5. Haruguchi H, Teraoka S. Intimal hyperplasia and hemodynamic factors in arterial bypass and arteriovenous grafts: a review. *J Artif Organs* 6: 227-235, 2003.

6. Manos TA, Sokolis DP, Giagini AT, Davos CH, Kakisis JD, Kritharis EP, Stergiopulos N, Karayannacos PE, Tsangaris S. Local hemodynamics and intimal hyperplasia at the venous side of a porcine arteriovenous shunt. *IEEE Trans Inf Technol Biomed* 14: 681-690, 2010.

7. Kraiss LW, Geary RL, Mattsson EJ, Vergel S, Au YP, Clowes AW. Acute reductions in blood flow and shear stress induce platelet-derived growth factor-A expression in baboon prosthetic grafts. *Circ Res* 79: 45-53, 1996.

8. Mondy JS, Lindner V, Miyashiro JK, Berk BC, Dean RH, Geary RL. Platelet-derived growth factor ligand and receptor expression in response to altered blood flow in vivo. *Circ Res* 81: 320-327, 1997.

9. Sterpetti AV, Cucina A, D'Angelo LS, Cardillo B, Cavallaro A. Response of arterial smooth muscle cells to laminar flow. *J Cardiovasc Surg* 33: 619-624, 1992.

10. Sterpetti AV, Cucina A, Santoro L, Cardillo B, Cavallaro A. Modulation of arterial smooth muscle cell growth by haemodynamic forces. *Eur J Vasc Surg* 6: 16-20, 1992.

11. Ueba H, Kawakami M, Yaginuma T. Shear stress as an inhibitor of vascular smooth muscle cell proliferation. Role of transforming growth factor-beta 1 and tissue-type plasminogen activator. *Arterioscler Thromb Vasc Biol* 17: 1512-1516, 1997.

12. Tarbell JM, Qui Y. Arterial wall mass transport: the possible role of blood phase resistance in the localization of arterial disease. In: Bronzino, JD., editor. The Biomedical Engineering Handbook: Tissue Engineering and Artificial Organs. 3. CRC Press Taylor & Francis Group, LLC; Boca Raton: 2006. p. 9.1-9.15.

13. Sumpio BE, Banes AJ. Response of porcine aortic smooth muscle cells to cyclic tensional deformation in culture. *J Surg Res* 44: 696-701, 1988.

14. Mills I, Cohen CR, Kamal K, Li G, Shin T, Du W, Sumpio BE. Strain activation of bovine aortic smooth muscle cell proliferation and alignment: study of strain dependency and the role of protein kinase A and C signaling pathways. *J Cell Physiol* 170: 228-234, 1997.

15. Li Q, Muragaki Y, Ueno H, Ooshima A. Stretch-induced proliferation of cultured vascular smooth muscle cells and a possible involvement of local renin-angiotensin system and platelet-derived growth factor (PDGF). *Hypertens Res* 20: 217-223, 1997.

16. Budu-Grajdeanu P, Schugart RC, Friedman A, Valentine C, Agarwal AK, Rovin BH. A mathematical model of venous neointimal hyperplasia formation. *Theor Biol Med Model* 5: 2, 2008.

17. Chien S. Mechanotransduction and endothelial cell homeostasis: the wisdom of the cell. *Am J Physiol Heart Circ Physiol* 292: H1209-1224, 2007.

18. Ishida T, Takahashi M, Corson MA, Berk BC. Fluid shear stress-mediated signal transduction: how do endothelial cells transduce mechanical force into biological responses? *Ann N Y Acad Sci* 811: 12-23, 1997.

19. Malek AM, Izumo S. Molecular aspects of signal transduction of shear stress in the endothelial cell. *J Hypertens* 12: 989-999, 1994.

20. Chen BP, Li YS, Zhao Y, Chen KD, Li S, Lao J, Yuan S, Shyy JY, Chien S. DNA microarray analysis of gene expression in endothelial cells in response to 24-h shear stress. *Physiol Genomics* 7: 55-63, 2001.

21. Chien S, Li S, Shyy YJ. Effects of mechanical forces on signal transduction and gene expression in endothelial cells. *Hypertension* 31: 162-169, 1998.

22. Davies PF. Flow-mediated endothelial mechanotransduction. *Physiol. Rev* 75: 519-560, 1995.

23. Warboys CM, Amini N, de Luca A, Evans PC. The role of blood flow in determining the sites of atherosclerotic plaques. *F1000 Med Rep* 3: 5, 2011.

24. Chiu JJ, Chien S. Effects of disturbed flow on vascular endothelium: pathophysiological basis and clinical perspectives. *Physiol Rev* 91: 327-387, 2011.

25. Ives SJ, Andtbacka RH, Kwon SH, Shiu YT, Ruan T, Noyes RD, Zhang QJ, Symons JD, Richardson RS. Heat and α1-adrenergic responsiveness in human skeletal muscle feed arteries: the role of nitric oxide. *J Appl Physiol* 113: 1690-1698, 2012.

26. Shiu YT, Li S, Marganski WA, Usami S, Schwartz MA, Wang YL, Dembo M, Chien S. Rho mediates the shear-enhancement of endothelial cell migration and traction force generation. *Biophys J* 86: 2558-2565, 2004.

27. Albuquerque ML, Waters CM, Savla U, Schnaper HW, Flozak AS. Shear stress enhances human endothelial cell wound closure in vitro. *Am J Physiol Heart Circ Physiol* 279: H293-H302, 2000.

28. Malek AM, Izumo S. Mechanism of endothelial cell shape change and cytoskeletal remodeling in response to fluid shear stress. *J Cell Sci* 109: 713-726, 1996.

29. Hahn C, Wang C, Orr AW, Coon BG, Schwartz MA. JNK2 promotes endothelial cell alignment under flow. *PLoS One* 6(8): e24338, 2011. doi:10.1371/journal.pone.0024338

30. van der Meer AD, Poot AA, Feijen J, Vermes I. Analyzing shear stress-induced alignment of actin filaments in endothelial cells with a microfluidic assay. *Biomicrofluidics* 4(1): 11103, 2010. doi:10.1063/1.3366720.

31. Bongrazio M, Baumann C, Zakrzewicz A, Pries AR, Gaehtgens P. Evidence for modulation of genes involved in vascular adaptation by prolonged exposure of endothelial cells to shear stress. *Cardiovasc Res* 47: 384-393, 2000.

32. Mun GI, Boo YC. A regulatory role of Krüppel-like factor 4 in endothelial argininosuccinate synthetase 1 expression in response to laminar shear stress. *Biochem Biophys Res Commun* 420: 450-455, 2012.

33. McCormick SM, Eskin SG, McIntire LV, Teng CL, Lu CM, Russell CG, Chittur KK. DNA microarray reveals changes in gene expression of shear stressed human umbilical vein endothelial cells. *Proc Natl Acad Sci U S A* 98: 8955-8960, 2001.

34. Haralabopoulos GC, Grant DS, Kleinman HK, Maragoudakis ME. Thrombin promotes endothelial cell alignment in Matrigel in vitro and angiogenesis in vivo. *Am J Physiol* 273: C239-245,1997.

35. Subramanian H, Grailer JJ, Ohlrich KC, Rymaszewski AL, Loppnow JJ, Kodera M, Conway RM, Steeber DA. Signaling through L-selectin mediates enhanced chemotaxis of lymphocyte subsets to secondary lymphoid tissue chemokine. *J Immunol* 188: 3223-3236, 2012.

36. Nguyen KT, Eskin SG, Patterson C, Runge MS, McIntire LV. Shear stress reduces protease activated receptor-1 expression in human endothelial cells. *Ann Biomed Eng* 29: 145-152, 2001.

37. Urschel K, Cicha I, Daniel WG, Garlichs CD. Shear stress patterns affect the secreted chemokine profile in endothelial cells. *Clin Hemorheol Microcirc* 50: 143-152, 2012.

38. Atkins GB, Jain MK. Role of Krüppel-like transcription factors in endothelial biology. *Circ Res* 100: 1686-1695, 2007.

39. Dekker RJ, van Soest S, Fontijn RD, Salamanca S, de Groot PG, VanBavel E, Pannekoek H, Horrevoets AJ. Prolonged fluid shear stress induces a distinct set of endothelial cell genes, most specifically lung Krüppel-like factor (KLF2). *Blood* 100: 1689-1698, 2002.

40. Clark PR, Jensen TJ, Kluger MS, Morelock M, Hanidu A, Qi Z, Tatake RJ, Pober JS. MEK5 is activated by shear stress, activates ERK5 and induces KLF4 to modulate TNF responses in human dermal microvascular endothelial cells. *Microcirculation* 18: 102-117, 2011.

41. Goettsch W, Gryczka C, Korff T, Ernst E, Goettsch C, Seebach J, Schnittler HJ, Augustin HG, Morawietz H. Flow-dependent regulation of angiopoietin-2. *J Cell Physiol* 214: 491-503, 2008.

CHAPTER 5

SUMMARY AND FUTURE DIRECTIONS

5.1 Summary

In the United States, more than 20% of all hospitalizations in hemodialysis population and up to 50% of the first year hemodialysis costs are associated with vascular access complications (1). The complexity of the pathophysiology underlying AVG and AVF vascular access failures has largely obstructed our efforts to resolve this important clinical problem. Focusing on the pathophysiology of the AVG stenosis, the major goal of our study is to propose that improved understanding of the complex cellular and molecular mechanisms contributing to early NH development is essential in devising future therapeutic strategies aimed at preventing and/or treating AVG stenosis and failure.

Among the multiple pathogenic factors contributing to the venous NH pathogenesis, pathophysiological hemodynamics is thought to play an important role in localized NH development (2, 3). Based on this notion, we employed an ex vivo perfused vein culture model to investigate the therapeutic potential of an antineoplastic agent, sunitinib, in inhibiting venous NH formation under aberrant hemodynamic conditions. In in vitro experiments, sunitinib inhibited growth factor-stimulated proliferation and migration of human vascular cells, and the intracellular signaling components implicated in its inhibitory mechanism were revealed. Sunitinib then

significantly attenuated the formation of venous NH lesions in the vein culture model that reproduces the pathogenic WSS observed in vivo. We also highlighted the utility of this ex vivo culture model for evaluating potential NH-preventive agents. Our findings have led us to suggest that sunitinib may be an effective pharmacological inhibitor of NH.

We employed a porcine global gene expression microarray analysis to investigate the genomic changes underlying venous NH development in a porcine AVG stenosis model. We demonstrated that a number of genomic events were regulated in common between the NH-prone VA and the NH-resistant PV regions. However, a larger number of genes were significantly regulated in the VA, and the relative enrichment of a series of genomic events was more prominent in the VA compared to the PV. Among these genomic events, we identified the osteo/chondrogenic processes to be up-regulated, which has not been extensively reported in NH pathophysiology, and genes related to muscle contractile phenotype to be down-regulated in the VA.

We next explored the genomic responses of porcine venous ECs exposed to physiological and pathophysiological shear stress in an in vitro laminar flow system. We found that many shear stress-responsive genes were differentially regulated between ECs exposed to prolonged low and high shear stress; however, how shear stress-dependent genes act together to alter the endothelial physiology in the context of venous NH requires further investigation.

5.2 Future Directions

5.2.1 Chapter 2

Our findings encourage future investigations into whether sunitinib demonstrates NH-preventive efficacy in vivo, such as in a porcine AVG stenosis model. In order to locally administer sunitinib to the desired site of action (i.e., venous anastomosis), an appropriate means of drug delivery should be devised. Our laboratory recently developed a polymer-based perivascular wrap system for controlled and directed delivery of sunitinib as a model drug. In porcine in vivo release studies using this wrap, sustained release of sunitinib at efficacious levels around the wrapped external jugular vein was accomplished for at least 4 weeks (4). In vivo efficacy studies of sunitinib with positive results will complement our current in vitro and ex vivo studies, and therefore will corroborate the therapeutic potential of sunitinib as an NH-preventive agent for the treatment of hemodialysis AVG stenosis.

5.2.2 Chapter 3

The global gene expression profiles of the NH-susceptible vein region in our porcine AVG model suggested that a variety of genomic events may be implicated in venous NH development. Future studies can be directed towards exploring each of these altered processes and determining their potential role in NH development. Especially the osteo/chondrogenic pathways that were significantly altered in our microarray results may be of particular interest. Although a few components in these pathways have been shown to be implicated in cellular events strongly associated with hyperplasia formation (5, 6), much more research needs to be done on

characterizing vascular calcification and its potential involvement in NH formation in the vein.

5.2.3 Chapter 4

Since NH development occurs predominantly at the venous anastomosis, it is important to understand how vascular cells of the vein respond to putative pathogenic factors that are responsible for NH formation. Exploring the gene expression changes in response to abnormal shear stress in porcine venous ECs provided us with some knowledge of the cellular and molecular processes that may be involved in NH development. However, ECs are one of the three major cell types that constitute the blood vessel wall; thus, it would also be interesting to examine the shear stress-induced genomic changes in SMCs, fibroblasts as well as in co-culture models of two or more of the above cell types. Future work may also consider comparing genomic profiles of in vivo NH lesions and vascular cells subjected to in vitro flow studies to determine any shear stress-dependent events that may be hyperplasia-relevant.

5.3 References

1. Lok CE, Bhola C, Croxford R, Richardson RM. Reducing vascular access morbidity: comparative trial of two vascular access monitoring strategies. *Nephrol Dial Transplant* 18: 1174-1180, 2003.

2. Li L. Terry CM, Shiu YT, Cheung AK. Neointimal hyperplasia associated with synthetic hemodialysis grafts. *Kidney Int* 74: 1247-1261, 2008.

3. Manos TA, Sokolis DP, Giagini AT, Davos CH, Kakisis JD, Kritharis EP, Stergiopulos N, Karayannacos PE, Tsangaris S. Local hemodynamics and intimal hyperplasia at the venous side of a porcine arteriovenous shunt. *IEEE Trans Inf Technol Biomed* 14: 681-690, 2010.

4. Sanders WG, Hogrebe PC, Grainger DW, Cheung AK, Terry CM. A biodegradable perivascular wrap for controlled, local and directed drug delivery. *J Control Release* 161: 81-89, 2012.

5. Dong C, Goldschmidt-Clermont PJ. Bone sialoprotein and the paradox of angiogenesis versus atherosclerosis. *Circ Res* 86: 827-828, 2000.

6. Kang N, Ng CS, Hu J, Qiu ZB, Underwood MJ, Jeremy JY, Wan S. Role of osteopontin in the development of neointimal hyperplasia in vein grafts. *Eur J Cardiothorac Surg* 41: 1384-1389, 2012.

APPENDIX A

EX VIVO PERFUSED ORGAN CULTURE SYSTEM AND FLOW EXPERIMENTS TO STUDY THE EFFECTS OF SUNITINIB ON VENOUS NH FORMATION

A.1 Introduction

The perfusion of blood vessel segments ex vivo offers significant advantages over static vessel culture models by allowing for exposure to dynamic and more physiologically relevant culture environment. Therefore, the ex vivo perfusion systems, such as the ex vivo system described in Chapter 2, have been a useful tool in the investigation of short-term and/or long-term physiological or pathophysiological effects on explanted vessel segments. In Chapter 2, a laminar flow ex vivo perfusion system was employed to evaluate the antihyperplastic properties of sunitinib on flow-induced venous NH formation. A detailed description of the construction of this perfusion system, including all materials, and the procedures of the flow experiments are provided in this Appendix. Application of this unique perfusion system may include studies of other common venous and/or arterial pathophysiology that require more physiologically-relevant models than monolayer cell cultures.

A.2 Materials and Methods

A.2.1 Materials

Tissue culture-grade silicone (Masterflex PharMed BPT®) and Tygon tubing, tubing connectors, fittings, and all other accessories were purchased from Cole-Parmer (Vernon Hills, IL). Tubing with various inside diameters were used which approximately ranged from 0.5 mm to 10 mm. The peristaltic pump and all pump accessories were also obtained from Cole-Parmer. All glassware was custom-made in the research glassblowing shop and the vessel chamber in the mechanical shop from the Department of Chemistry at the University of Utah. 5% CO_2 compressed balance air was purchased from the General Stores and Receiving at the University of Utah. All tissue culture reagents were purchased as described in Chapter 2.

A.2.2 Methods

A.2.2.1 Sterilization. Sterilization of all parts and accessories including the vessel chamber before each and every experiment is important as bacterial contamination of explanted tissues can produce unreliable experimental results. If bacterial contamination is present during explant and/or during placement in the vessel chamber, obvious bacterial growth may be observed within 24 h (e.g., media color change and odor), and tissues are immediately discarded.

All glassware (the two culture media reservoirs and a water chamber), tubing, and tubing accessories (connectors, fittings, adapters, and flow valve) were washed and autoclaved under dry cycle for at least 30 min prior to each experiment. The vessel chamber was disassembled and all metal accessories were also washed and autoclaved. After connecting the glassware and

tubing, the entire flow system was placed in a tissue culture hood and inner surface was washed twice with 70% ethanol using a peristaltic pump, followed by rinsing with sterile distilled water for at least three times to completely remove ethanol. The flow system was allowed to dry in clean air overnight in the culture hood.

A.2.2.2 Vessel explant. On the day of perfusion experiment, the vessel chamber tub and cover was soaked in 70% ethanol for at least 10 min prior to placement of vein segments and then completely dried in clean air. The flow system was rinsed once more with DMEM without serum in order to remove residual water inside the tubing. Using sterile techniques in the surgery suite, vein segments (3 to 5 cm in length) freshly harvested from pig internal jugular veins were fixed onto the metal adapters and collected in DMEM containing 30% serum and two time's concentrated antibiotics (gentamicin and amphotericin B). Upon transfer to the tissue culture room, vein segments were kept in the same media and placed in a tissue culture incubator until ready for placement. This time period usually did not exceed 2 h from beginning of vessel explant and tissues were managed as quickly as possible.

A.2.2.3 Flow system assembly. In the tissue culture hood, the vein segment was placed in the vessel chamber at its in vivo length (using the grid inscribed on the bottom of the vessel chamber tub) and the metal adapters were connected to the tubing using sterile gloves (Figure A.1). Before adding media that fills the chamber tub, the vein was checked for any leakage by flowing media through the vessel for 5 to 10 min. Any vessels that showed leakage due to incomplete ligation of small branches or holes were discarded. Finally, the entire flow system was transferred from the tissue culture hood to the flow hood. The two glass reservoirs were connected to gas

A

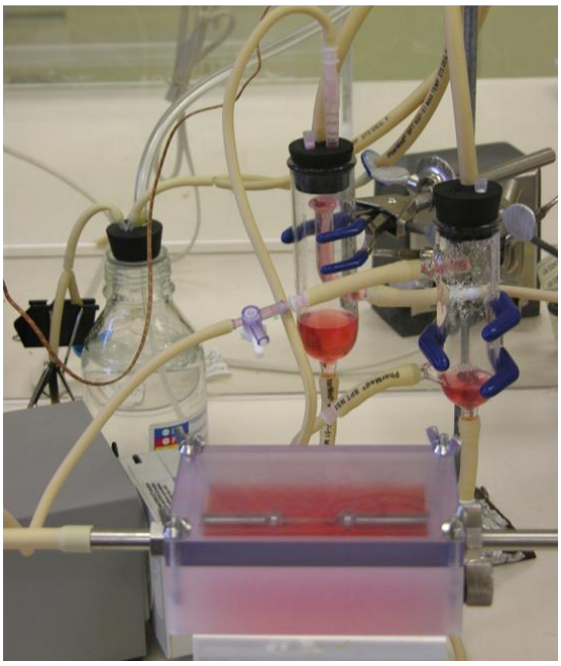

B

Figure A.1 The ex vivo perfused blood vessel organ culture model. (A) The flow system consists of a peristaltic pump, two reservoirs that hold the culture media and a blood vessel chamber. The system is aerated with moist 5% CO_2 balance air and the temperature is controlled at constant 37 °C. **(B)** Explanted vein segments were fixed onto the metal tubes at their in vivo length using sterile techniques and checked for any leakage before each flow experiment.

tubing that flows sterile 5% CO_2 balance air (air passes a syringe filter to maintain sterility), and the flow hood was set to 37 °C. Volumetric flow rate was measured manually through a flow valve positioned immediately downstream of the vessel chamber. A detailed description of how WSS was calculated is stated in Chapter 2.

A.2.2.4 Flow experiments. Fresh media was supplied every 2 to 3 days and the vein segments were cultured for 12 consecutive days with media flowing continuously. When changing old media, the entire system was transferred into the tissue culture hood to prevent contamination due to exposure of vessels to open air. Sunitinib was added to the media on the second day of culture and throughout 12 days. Bacterial contamination was determined by microscopic visual examination of the culture media. If strong odor and obvious color change in media developed, vessels were immediately discarded. In some cases, bacterial contamination could only be observed microscopically without changes in media color and odor. These vessels were closely monitored and fresh media was supplied every 1 to 2 days, and vessels were utilized for data if still no change in media color occurs. At the end of experiments, vessels were fixed in 10% neutral buffered formalin for 24 to 48 h as described in Chapter 2, without removing from the vessel chamber. After each and every experiment, the flow system was disassembled, washed with mild detergent, and completely dried in air.

A.3 Conclusion

The ex vivo perfusion system we employed is a unique tissue culture model of venous NH that can be used to rapidly screen potential pharmacological inhibitors of NH. Careful preparation

of the flow experiments is important to prevent bacterial contamination of the explanted tissues. The above procedures, if properly followed, have proven to reduce contamination problems associated with mishandling of the tissues and the flow system.